Application of Carbonaceous Material for Remediation of Oil Sands Process Water: Adsorption and Development of Nanocomposite Membranes with Enhanced Properties

by

Chelsea Benally

A thesis submitted in partial fulfillment of the requirements for the degree of

Doctor of Philosophy
in
Environmental Engineering

Department of Civil and Environmental Engineering
University of Alberta

ABSTRACT

Oil sands process water (OSPW) is a highly complex mixture that contains sand, silt, clay, dissolved salts, heavy metals and a wide range of organic compounds such as naphthenic acids (NAs) and polyaromatic hydrocarbons (PAHs). To effectively manage water during operations and support reclamation efforts, there is a need to release the treated OSPW back into the environment. This thesis presents the results of two different treatment options for OSPW: membrane filtration and adsorption.

Ultrafiltration nanocomposite polysulfone (PSU) membranes containing 0 to 5 wt.% carboxyl (-COOH) modified multiwalled carbon nanotubes (mMWNT) were fabricated and used to treat OSPW. Addition of mMWNT to PSU resulted in increased membrane surface hydrophilicity. Small additions of mMWNT (up to 1 wt.%) resulted in decreased average pore size on the selective membrane surface. Pure water and OSPW flux followed the same trend, decreasing with small mMWNT additions (up to 0.5 wt. %), followed by an increasing flux with higher mMWNT additions. All nanocomposite membranes had a higher rejection of polyethylene glycol (PEG) (76.5%-92.3%) than plain PSU membranes (65.5%). Membranes containing 2 wt.% mMWNT had the highest polyethylene glycol (PEG) flux and rejection of 83.1%. Addition of mMWNT reduced the tendency for membrane fouling to occur, indicated by a decrease in fouling ratios and increased flux recovery ratios for nanocomposite membranes as compared with those obtained for plain PSU. The dominant fouling mechanisms during OSPW filtration were standard blocking and cake filtration. Additions of 0.2 wt.% and 2 wt.% mMWNT resulted in permeates with SDI_{15} values lower than 1.0 and increased acid-extractable fraction (AEF) removal (11.9% and 13.9%, respectively) as compared with AEF removal by plain PSU membrane.

Adsorption results demonstrated that mesoporous carbonaceous material can successfully be used to adsorb persistent and toxic organic contaminants from OSPW. Carbon xerogel (CX) made at pH 5.5 removed a larger amount of AEF than CX made at pH 6.9. The adsorption equilibrium was reached by about 12 hours for both AEF and total classical naphthenic acids (NAs). 74.6% of AEF was removed and 88.8% of total classical NAs were removed during 24 hours adsorption. With respect to classical NAs removal, a larger carbon number resulted in higher NAs removal. Carbon number had more influence on NAs removal when compared with hydrogen deficiency resulting from rings or unsaturated bonding formation (–Z number). For a 3 g/L dose of CX 5.5, the equilibrium adsorption capacity was found to be 15 mg AEF/g CX5.5 and 7.8 mg NAs/g CX5.5. Adsorption of AEF and total classical NAs onto CX5.5 followed pseudo-second order kinetics. With respect to diffusion of AEF and NAs, there were three distinct regions: bulk diffusion, film diffusion and pore diffusion. Pore diffusion had the lowest rate constant in all cases analyzed and was thus the rate limiting diffusion step. The results of this study showed that a mesoporous carbonaceous material such as CX may have the potential to be utilized in a fixed bed adsorption column for continuous treatment of OSPW or as a semi-passive treatment method in pit lakes for the removal of organic constituents from OSPW.

PREFACE

All research completed for this thesis was designed and planned by myself in conjunction with my supervisor, Dr. Mohamed Gamal El-Din. I attempted to conduct a majority of the experiments as well as the interpretation/analysis of the data and the preparation of the manuscripts under the supervision of Dr. Mohamed Gamal El-Din. Post-doctoral members of Dr. Gamal El-Din's research group also contributed to manuscript edits, sample analysis, and some of them were co-authors of the manuscripts submitted or prepared for submission for publication. Other analyses were performed in other departments at the University of Alberta. Contributions to each chapter are seen below:

- Dr. Mingyu Li, post-doctoral fellow in Dr. Gamal El-Din's research group, edited the membrane literature review manuscript (Chapter 2).
- Dr. Selamawit Messele, post-doctoral fellow in Dr. Gamal El-Din's research group, edited the adsorption literature review manuscript (Chapter 3).
- A version of Chapter 4 was included in the publication: Benally, C., Li, M., and Gamal El-Din, M. 2018. "The effect of carboxyl multiwalled carbon nanotubes content on the structure and performance of polysulfone membranes for oil sands process-affected water treatment." Separation and Purification Technology, **199**: 170-181. I prepared the membranes, performed a majority of the membrane characterization and membrane performance experiments discussed in Chapter 4, as well as composition of the manuscript. Dr. Gamal El-Din contributed to the research, planning, final editing and approval of the manuscript. Dr. Alla Alpatova helped me in the early stages of the membrane development. Ms. Shimiao Dong installed the software and programmed the balance used to weigh the water (permeate). Dr. Mingyu Li contributed to the research planning, data analysis and interpretation, and manuscript editing. Dr. Pamela Chelme-Ayala contributed to the manuscript editing. High resolution scanning electron microscope (SEM) analysis of the selective side of membrane samples was conducted by the University of Alberta Department of Earth and Atmospheric Sciences Scanning Electron Microscope Laboratory.
- A version of Chapter 5 was included in the publication: Benally, C., Li, M., and Gamal El-Din, M. 2018. "The effect of carboxyl multiwalled carbon nanotubes content on the

structure and performance of polysulfone membranes for oil sands process-affected water treatment." Separation and Purification Technology, **199**: 170-181. I prepared the membranes, performed the membrane filtration experiments, performed water quality analysis, performed analysis of resulting flux data, and wrote the manuscript. Dr. Gamal El-Din contributed to the research planning and final editing and approval of the manuscript. Dr. Mingyu Li contributed to the research planning, data analysis interpretation, and manuscript editing. Dr. Pamela Chelme-Ayala contributed to the manuscript editing. Dr. Mohamed Meshref provided training and general guidance for acid-extractable fraction (AEF) extraction and for analysis of AEF by Fourier transform infrared (FT-IR) spectroscopy. Analysis of membrane samples by X-ray photoelectron spectroscopy (XPS) was conducted by the University of Alberta nanoFAB. Analysis of membrane samples by scanning electron microscopy/energy-dispersive X-ray spectroscopy (SEM-EDS) was conducted by the University of Alberta Department of Earth and Atmospheric Sciences Scanning Electron Microscope Laboratory.

- A version of Chapter 6 will be submitted to the Water Research as: Benally, C., Messele, S., and Gamal El-Din, M. "Adsorption of organic matter in oil sands process water by carbon xerogel." I performed the effect of dose, equilibrium time and kinetics adsorption experiments. I analyzed the oil sands process water (OSPW) pre and post adsorption via extraction of AEF and analysis by FT-IR. I analyzed resulting AEF and naphthenic acids (NA) concentration data to determine the kinetics of adsorption, diffusion mechanism and rate-determining steps during adsorption. Dr. Gamal El-Din contributed to the research planning and final editing and approval of the manuscript. Dr. Selamawit Messele contributed to the research planning, preparation and characterization of carbon xerogel samples used for the adsorption studies, aided in data analysis interpretation, and manuscript editing. Dr. Pamela Chelme-Ayala contributed to the manuscript editing. Dr. Rongfu Huang in Dr. Gamal El-Din's research group conducted the NA quantification by UPLC-TOF-MS. Ms. Shimiao Dong performed the UPLC-TOF-MS data mining to obtain the NAs concentrations.

DEDICATION

This thesis work is dedicated to all of my loving family and friends, but especially:

- To my son, Alexan Cardinal. You motivate me beyond belief just by being here. You have a wonderful soul and I am happy to be your mother.
- To my mother and father who continue to work very hard in life in order to help their children, grandchildren, and great grandchildren. Your efforts do not go unnoticed and your love and support help me each day.
- To all of my ancestors who survived many hardships so that my generation and younger generations could be here today.

ACKNOWLEDGEMENTS

I would like to express sincere appreciation and gratitude to my supervisor, Dr. Mohamed Gamal El-Din, for his guidance and support during my time in his research group. I am very thankful to have been a part of his research group where I had the opportunity to learn about many important aspects of water. He provided many insights into the work that was conducted and gave motivation to myself and the group in many different ways. I hope that I can one day come to have the knowledge base that Dr. Gamal El-Din has with respect to water and water treatment.

I also would like to thank Dr. Pamela Chelme-Ayala in Dr. Gamal El-Din's research group for her gentle support and help. I appreciate all of her efforts in editing the chapters and manuscripts and for being there to help with many other tasks that helped things to flow nicely in our research group. Thank you for the endless reminders and sharing of information.

My sincere gratitude also goes to the postdoctoral fellows in Dr. Gamal El-Din's research group who helped to revise conference posters, presentations, and manuscripts. They also helped me to gain a better understanding of certain aspects of the work being conducted, and helped me with analysis of OSPW samples. They are Dr. Mingyu Li, Dr. Selamawit Ashagre Messele, and Dr. Rongfu Huang.

Finally, I would like to acknowledge my family for their endless love and support on my school endeavors. Thank you to my parents. Thank you to my son who has been very patient with me while I've been in school again. Thank you to my friends who help me each day with encouragement.

TABLE OF CONTENTS

LIST OF TABLES

LIST OF FIGURES

1. INTRODUCTION AND RESEARCH OBJECTIVES

1.1 Background and Motivation

1.1.1 Alberta oil sands operations

The Alberta oil sands hold an estimated 2.5 trillion barrels of bitumen within three major oil deposits covering an area of approximately 140000 km^2 in the northern part of the province (Allen 2008a; Penner and Foght 2010). The oil sands are composed of approximately 10% bitumen mixed with 5 % water and 85% mineral solids comprised of sand, clay and silt (Zubot et al. 2012). Before bitumen can be upgraded to produce synthetic crude oil, it must first be extracted from the oil sands by the Clark caustic hot water extraction process that uses approximately 3 m^3 of water for every m^3 of oil sands processed (Klamerth et al. 2015). Bitumen mining, extraction, ore processing and upgrading operations consume large amounts of fresh water and generate large amounts of water that has come into contact with oil sands, also known as oil sands process water (OSPW) (Allen 2008a; Zubot et al. 2012).

1.1.2 Oil Sands Process Water (OSPW)

There are approximately 720 million m^3 of OSPW contained in tailings ponds covering a land area roughly 180 km^2 in the Alberta oil sands region (Parajulee and Wania 2014; Zhu et al. 2017). To decrease the fresh water intake requirement for bitumen extraction processes, OSPW may be recycled but the result of reusing the process water over and over is further decrease of OSPW quality (Allen 2008a). All OSPW is stored on-site in tailings ponds due to Alberta's zero discharge approach (Allen 2008a). Environmental impacts attributed to the storage of OSPW in tailings ponds can be seen in the surrounding land, air and water. Impacts include destruction of

natural habitats, emissions of chemical and greenhouse gases, and depletion and contamination of surrounding water resources (Frank et al. 2014; Hodson 2013).

The composition of OSPW can vary drastically due to the broad range of water types (fresh OSPW in tailings ponds or active settling basins, dyke drainage water from surrounding active settling basins, water from wetlands or reclamations ponds that consists of treated or aged OSPW, and consolidated tailings released water) that have come into contact with oil sands, and are thus considered OSPW (Li et al. 2017). OSPW can contain elevated concentrations of salts, naphthenic acids (NAs), polycyclic aromatic hydrocarbons (PAHs), trace heavy metals, BTEX (benzene, toluene, ethyl benzene, and xylenes), and phenols and other inorganic and organic compounds (Gamal El-Din et al. 2011; Li et al. 2017). Studies have shown that NAs contribute to the toxicity in OSPW that affects aquatic life (Allen 2008b).

1.1.3 Naphthenic acids and their quantification

NAs is a broad term that is used to describe a family of saturated aliphatic and alicyclic carboxylic acids that are naturally present within the oil sands and other crude oil deposits (Quinlan and Tam 2015). Carboxylic acids are organic compounds that contain a carboxyl group (-COOH) (Sawyer et al. 2003). Aliphatic compounds are organic compounds in which the characteristic group, in this case the carboxyl group, is linked to a straight or branched carbon chain, whereas alicyclic compounds are aliphatic compounds that contain one or more rings. It is hypothesized that NAs originate within petroleum deposits due to two natural phenomena. Either the deposit has not undergone complete catagenesis or the deposit has undergone aerobic biodegradation which results in the formation of significant amounts of carboxylic acids (Watson et al. 2002; Clemente and Fedorak 2005). During the Clark caustic hot water extraction of bitumen from oil sands, NAs can dissolve into the slightly alkaline OSPW because the pH is

greater than the pKa value of NAs, which range from 5 to 6. Above pH 6, NAs are soluble in the water phase since a portion of the NAs will become deprotonated when the pH is above the pKa value (Quinlan and Tam 2015).

Structurally, NAs can be described by the general empirical formula $C_nH_{2n+Z}O_x$ where "n" is the carbon number ($7 < n < 26$), "Z" is zero or a negative even integer ($0 < |Z| < 18$) representing the hydrogen deficiency resulting from rings or unsaturated bonding formation, and x represents the number of oxygen atoms, where x is 2 for classical NAs or $x \geq 3$ for oxy-NAs (Bertheussen et al. 2017). NAs account for less than 50% of the organic fraction of OSPW (Li et al. 2017). A portion of the organic fraction of OSPW can be extracted in acidic conditions (low pH), and is therefore known as the acid-extractable fraction (AEF). AEF is thought to contribute to toxicity found in OSPW, therefore much research has focused on removal of AEF (Kim et al. 2013). Some studies have shown that NAs are contributors to the acute and chronic toxicity in OSPW to selected tests organisms (Klamerth et al. 2015; Li et al. 2017; MacKinnon and Boerger 1986). In addition to being a contributor to toxicity in OSPW, NAs are also one of the primary causes of corrosion to the equipment used during bitumen extraction; however they are essential during the extraction of bitumen from the sand (Derungs 1956; Fan 1991; Quinlan and Tam 2015).

In order to quantify the amount of AEF and NAs in OSPW, the AEF, which includes the NAs, is first extracted from the OSPW. The protocol developed by Syncrude Canada is utilized for the extraction of AEF and involves the acidification of OSPW to a pH of 2.2 (Jivraj et al. 1995, Rogers et al. 2002). Protonation of the carboxylic acids in the OSPW will occur at pH 2.2 because this pH is less than the range of pKa values (5 to 6) for NAs (Young et al. 2008). Organic solvents such as dichloromethane (DCM), toluene, hexane, ethyl

acetate/dicholoromethane, chloroform, and ethyl acetate can be used to extract NAs from OSPW (Headley et al. 2013a). In many studies involving OSPW, the solvent of choice was DCM for extraction of NAs from OSPW (Headley et al. 2013, Huang et al. 2015, Rogers et al. 2002, Young et al. 2008).

Once the NAs have been extracted from OSPW, then analysis of either the AEF or NAs is performed. One method used to roughly quantify AEF concentration after extraction has been performed is Fourier transform infrared spectroscopy (FT-IR). The FT-IR method gives an overall estimation of AEF and the main advantage of this method is the short time needed for analysis (Gamal El-Din 2011). Some analytical methods that have been used for analysis of NAs in OSPW have been ion mobility spectrometry (IMS), ultraperformance liquid chromatography time-of-flight mass spectrometry (UPLC-TOF-MS) and Fourier transform ion cyclotron resonance mass spectrometry (FTICR-MS) (Sun et al. 2014). As indicated by Sun et al. (2014) IMS gives qualitative information about the distribution of organics in a sample. But in combination with quantitative methods, UPLC-TOF-MS and FTICR-MS, this can prove to be useful semiquantitative method. Although UPLC-TOF-MS has lower resolution than FTICR-MS, it has comparable levels of precision and reliability afforded by the FTICR-MS.

1.1.4 OSPW treatment

Research on treatment of OSPW started as early as the 1970s and initially focused on solid-liquid separation aimed at enhancing settling rates of tailings and recovery of process water by methods such as adsorption, coagulation and flocculation, membrane filtration, pre-coat filtration, electrophoresis-assisted gravity settling, pH adjustment, and freeze-thawing (Allen 2008b). Currently, research for treatment of OSPW includes methods that can be classified as physical, chemical, physicochemical, biological, and combinations of those as seen in wetlands

construction and membrane bioreactors (Alpatova et al. 2014; Allen 2008b). Due to the complexity of OSPW, remediation typically involves several steps (Gamal El-Din et al. 2012).

Removal of suspended solids by methods such as coagulation-flocculation-sedimentation (CFS), gravity separation, granular media filtration, and membrane filtration, is usually the first step in remediation of OSPW. This is because suspended solids can hinder the effectiveness of other treatment options that include high pressure membrane filtration and advanced oxidation/disinfection (Zaidi et al. 1992). Low pressure membrane filtration, like microfiltration (MF) and ultrafiltration (UF), can help reduce suspended solids with no prior pre-treatment processes necessary at a lower cost and lower energy consumption than high pressure membrane filtration (Dong et al. 2014; Zaidi et al. 1992). Dong et al. (2014) and Alpatova et al. (2014) investigated the use of ceramic MF and UF membranes for OSPW treatment. Kim et al. (2013) fabricated nanocomposite polysulfone (PSU) UF membranes as pre-treatment for high pressure membrane filtration of OSPW.

Polysulfone (PSU) is a polymer commonly used to form membranes for wastewater treatment due to its chemical and structural stability combined with mechanical robustness (Richards et al. 2012). To reduce the hydrophobic nature of PSU and the occurrence of membrane fouling, hydrophilic nanoparticles can be incorporated within the polymer matrix to increase surface hydrophilicity and permeate flux (Blanco et al. 2006; Kim et al. 2013). Carbon nanotubes are the most widely used nanoparticle in membranes due to their excellent mechanical, electrical, thermal, and antibacterial properties, as well as the ability to adsorb organic compounds (Kim et al. 2013). A study by Kim et al. (2013) focused on the use PSU/multi-walled carbon nanotube (MWNT) membranes to pre-treat OSPW prior to high pressure membrane filtration. The study investigated the combined effect of low pressure

membrane filtration with PSU membrane containing 0 or 10 wt. % MWNT followed by high pressure membrane filtration. The combination of membranes with MWNTs resulted in the reduction of hydrophobic pollutants and membrane fouling, increased permeate flux, and high removal of organic pollutants. The effect of varying the casting components was not a major factor in the study. Other literature suggests that an optimum loading of MWNT in PSU should lie below 4 wt. % (Choi et al. 2006; Qui et al. 2009). While the low pressure membranes in the above study contained 10 wt.% MWNT, it is plausible that low pressure membranes containing a smaller wt.% of MWNT could actually achieve better results with respect to membrane rejection, flux, reduction of suspended solids and turbidity, and possibly organic pollutants.

After removal of suspended solids, secondary and tertiary treatment technologies have been employed to remove organic material in OSPW. These include treatment methods such as adsorption (Gamal El-Din et al. 2011; Pourrezaei et al. 2014), high pressure membrane filtration (Kim et al. 2011; Kim et al. 2012; Kim et al. 2013), advanced oxidation processes (AOP) (Drzewicz et al. 2010; Klamerth et al. 2015; Wang et al. 2016a; Wang et al. 2016b), and biological treatments (Zhang et al. 2016)

Adsorption is an effective method that can be used to remove organic contaminants from an aqueous solution (Zubot et al. 2012). The use of adsorbents for treatment of OSPW initially focused on removal of oil and other organic foulants from the water for eventual recycled use (Allen 2008b). Reclamation of OSPW in tailings ponds has shifted this use of adsorbents to focus on removal of NAs in OSPW (Allen 2008b; Islam et al. 2014). Activated carbon (AC) and petroleum coke are two adsorbents that have been used to treat OSPW for removal of organic material, namely NAs (Islam et al. 2014; Zubot et al. 2012). More recently biochar was used as an adsorbent to remove NAs from OSPW (Bhuiyan et al. 2016; Frankel et al. 2016). One study

produced a biomass based AC from biochar in order to reduce the overall CO_2 footprint but still obtain an adsorbent that could function well (Iranmanesh et al. 2014).

The performance of the adsorbents depends largely on their surface chemistry and their texture (Carabineiro et al. 2012). While AC is a well-known adsorbent that can be used for removal of organic material, it tends to have a highly microporous structure that is not easily manipulated to suit larger sized adsorbates, as a result some bulkier adsorbate molecules may not have easy access to the pores (Bansal and Goyal 2005). Carbon xerogels (CXs) are polymer derived mesoporous carbonaceous materials that can be modified to change the porous texture or the surface chemistry in order to accommodate a larger range of adsorbates or specific conditions (Mahata et al. 2007). In addition, CX can have high surface area (400-1200 m^2/g), controllable pore size, and high adsorption capacity. These attributes make CX an interesting potential adsorbent material for the removal of NAs in OSPW.

1.2 Research scope and objectives

This research will focus on two physical processes to treat OSPW: 1) the development and use of nanocomposite UF membranes for treatment of OSPW; and 2) adsorption using carbon xerogel for treatment of OSPW. Nanocomposite PSU membranes were made by combining -COOH modified MWNT (mMWNT) to PSU. The effect of varying the casting components is studied, especially as it pertains to the membrane morphology and basic filtration performance. The sole effect of varying mMWNT content is investigated by omitting pore forming agent polyvinylpyrrolidone (PVP). Acid modification of MWNT is by-passed by procuring -COOH modified MWNT (mMWNT) for incorporation into PSU membranes. The objectives of the membrane study were to: (1) fabricate polymeric nanocomposite membranes using polysulfone (PSU) and varying amounts of -COOH modified multi-walled carbon nanotubes (mMWNT); (2)

evaluate the effect of casting mixture composition on resulting membrane morphology and pore structure; (3) evaluate the effect of casting mixture composition on membrane pure water flux and rejection; (4) evaluate how variation of mMWNT content in fabricated membranes affects OSPW filtration performance and resulting permeate water quality; (5) evaluate how mMWNT content in fabricated membranes affects membrane fouling resistance during OSPW filtration; and (6) determine the dominant fouling mechanism(s) during filtration of OSPW.

Carbon xerogel materials were evaluated as a mesoporous carbonaceous adsorbent material used for the removal of organic material (AEF and NAs) in OSPW. The objectives of the adsorption study were to: (1) determine the equilibrium time needed for adsorption of AEF by CX; (2) gain an understanding of the effect of CX dose on adsorption of AEF of OSPW; (3) determine the AEF and NAs adsorption capacity for CX; (4) gain an understanding of the kinetics for the removal of AEF and NAs by CX; and (5) gain an understanding of the types of diffusion involved in the adsorption of AEF and NAs by CX using a diffusion model.

1.3 Hypotheses

With respect to membrane filtration, it was hypothesized that adding hydrophilic nanoparticles within the polymer matrix would affect membrane performance by increasing permeate flux, changing the internal membrane morphology and reducing membrane fouling. With respect to adsorption, it was hypothesized that use of a carbonaceous adsorbent with average surface area but increased mesoporosity and wider pore diameter (carbon xerogel) could effectively remove NAs from OSPW by minimizing the diffusion limitation.

1.4 Thesis organization

This is the first chapter that gives a general introduction and background information, as well as the research objectives. More specifically, Chapter 1 gives a brief background regarding the extraction of oil sands and resulting OSPW tailing pond water. Additionally, OSPW treatment methods are briefly mentioned along with motivation for the current research, which includes membrane filtration and adsorption. The research objectives for the membrane filtration and adsorption work are listed, along with hypotheses. Lastly, the thesis organization is broken down for the reader.

Chapter 2 is the literature review for membrane filtration. The fundamentals of membrane filtration are presented. Membrane classification is discussed and the focus of the literature review then turns to ultrafiltration membranes. Chapter 2 highlights literature pertaining to membranes containing carbon nanotubes and ends with focus on literature about different membrane filtration studies in which OSPW is treated.

Chapter 3 is the literature review for adsorption. The fundamentals of adsorption are presented. These include the following topics: types of adsorption, factors that affect adsorption, steps in adsorption, adsorption isotherms, and diffusion and adsorption kinetics models. Lastly, Chapter 3 highlights literature involving the treatment of OSPW by adsorbents such as activated carbon, petroleum coke, and biochar.

Chapter 4 presents the effects of carboxyl multiwalled carbon nanotubes on the structure and performance of polysulfone composite membranes. The fabrication of the membranes is discussed. The fabricated membranes were characterized by contact angle and SEM imaging. In addition, the results of the fabricated membrane permeability and rejection of PEG are discussed.

Chapter 5 presents the effects of carboxyl multiwalled carbon nanotubes on the performance of polysulfone composite membranes for OSPW treatment. Chapter 5 presents the resulting OSPW flux and flux recovery after simulated membrane cleaning. The fouling analysis of OSPW filtration and the dominant fouling mechanisms were discussed. Lastly, the permeate water quality is presented.

Chapter 6 presents the results of the use of mesoporous carbonaceous materials (carbon xerogel) as adsorbent material for the removal of AEF and NAs in OSPW. For AEF, the results of the equilibrium time experiments, kinetics experiments, effect of adsorbent dose experiments, and adsorption capacity of CX5.5 are discussed. For classical NAs, removal, adsorption capacity for CX5.5, and the diffusion and kinetics of adsorption are presented.

Chapter 7 gives a general overview of the entire thesis and summarizes the major conclusions from previous chapters. Lastly, future recommendations for further research are also presented in this chapter.

1.5 References

Allen, E.W. 2008a. Process water treatment in Canada's oil sands industry: I. Target pollutants and treatment objectives. Journal of Environmental Engineering and Science, **7**: 123-138.

Allen, E.W. 2008b. Process water treatment in Canada's oil sands industry: II. A review of emerging technologies. Journal of Environmental Engineering and Science: **7**: 499-524.

Alpatova, A., Kim, E-S, Dong, S., Sun, N., and Chelme-Ayala, P. 2014. Treatment of oil sands process-affected water with ceramic ultrafiltration membrane: Effects of operating conditions on membrane performance. Separation and Purification Technology, **122**: 170-182.

Bansal and Goyal. 2005. Activated Carbon Adsorption. Taylor & Francis Group. New York, NY.

Bertheussen, A., Simon, S., and Sjöblom, J. 2017. Equilibrium partitioning of naphthenic acids and bases and their consequences on interfacial properties. Colloids and Surfaces A, **529**: 45-56.

Bhuiyan, T.I., Tak, J.K., Sessarego, S., Harfield, D., and Hill, J.M. 2017. Adsorption of acid-extractable organics from oil sands process-affected water onto biomass-based biochar: Metal content matters. Chemosphere, **168**; 1337-1344.

Blanco, J-F., Sublet, J., Nguyen, Q.T., and Schaetzel, P. 2006. Formation and morphology studies of different polysulfones-based membranes made by wet phase inversion process. Journal of Membrane Science, **283**: 27-37.

Carabineiro, S.A.C., Thavorn-amornsri, T., Periera, M.F.R., Serp, P., and Figueiredo, J.L. 2012. Comparison between activated carbon, carbon xerogel and carbon nanotubes for the adsorption of the antibiotic ciprofloxacin. Catalysis Today, **186**: 29-34.

Choi, J-H., Jegal, J., and Kim, W-N. 2006. Fabrication and characterization of multi-walled carbon nanotubes/polymer blend membranes. Journal of Membrane Science, **284**: 406-415.

Clemente, J.S., and Fedorak, P.M. 2005. A review of the occurrence, analysis, toxicity, and biodegradation of naphthenic acids. Chemosphere, **60**: 585-600.

Derungs, W.A. 1956. Naphthenic Acid Corrosion – An Old Energy of the Petroleum Industry. Corrosion, **12**: 41-46.

Dong, S., Kim, E-S, Alpatova, A., Noguchi, H. Liu, Y., and Gamal El-Din, M. 2014. Treatment of oil sands process-affected water by submerged ceramic membrane microfiltration system. Separation and Purification Technology, **138**: 198-209.

Drzewicz, P., Afzal, A., Gamal El-Din, M., Martin, J.W. 2010. Degradation of a Model Naphthenic Acid, Cyclohexanoic Acid, by Vacuum UV (172 nm) and UV (254 nm)/H2O2. Journal of Physical Chemistry A, **114**: 12067-12074.

Fan, T-P. 1991. Characterization of Naphthenic Acids in Petroleum by Fast Atom Bombardment Mass Spectrometry. Energy and Fuels, **5**(3): 371-375.

Frank, R.A., Roy, J.W., Bickerton, G., Rowland, S.J., Headley, J.V., Scarlett, A.G., West, C.E., Peru, K.M., Parrot, J.L., Conly, F.M., and Hewitt, L. M. 2014. Profiling Oil Sands Mixtures from Industrial Developments and Natural Groundwaters for Source Identification. Environmental Science and Technology, **48**: 2660-2670.

Frankel, M.L., Bhuiyan, T.I., Veksha, A., Demeter, M.A., Layzell, D.B., Helleur, R.J., Hill, J.M., and Turner, R.J. 2016. Removal and biodegradation of naphthenic acids by biochar and attached environmental biofilms in the presence of co-contamination metals. Bioresource Technology, **216**: 352-361.

Gamal El-Din, M., Fu, H., Wan, N., Chelme-Ayala, P., Perez-Estrada, L., Drzewicz, P., Martin, J.W., Zubot, W., and Smith, D.W. 2011. Naphthenic acids speciation and removal during petroleum-coke adsorption and ozonation of oil sands process-affected water. Science of the Total Environment, **409**: 5119-5125.

Headley, J.V., Peru, K.M., Fahlman, B., Colodey, A. and McMartin, D.W. 2013. Selective solvent extraction and characterization of the acid extractable fraction of Athabasca oils sands process waters by Orbitrap mass spectrometry. International Journal of Mass Spectrometry **345-347**: 104-108.

Hodson, P.V. 2013. History of environmental contamination by oil sands extraction. Proceedings of the National Academy of Sciences, **111**(5): 1569-1570.

Huang, R., Sun, N., Chelme-Ayala, P., McPhedran, K.N., Changalov, M., and Gamal El-Din, M. 2015. Fractionation of oil sands-process affected water using pH-dependent extractions: A study of dissociation constants for naphthenic acids species. Chemosphere, **127**: 291-296.

Iranmanesh, S., Harding, T., Abedi, J., Seyedeyn-Azad, F., and Layzell, D.B. 2014. Adsorption of naphthenic acids on high surface area activated carbons. Journal of Environmental Science and Health, Part A, **49**(8): 913-922.

Islam, M.S., Dong, T., Sheng, Z., Zhang, Y., Liu, Y., and Gamal El-Din, M. 2014. Microbial community structure and operational performance of a fluidized bed biofilm reactor treating oil sands process-affected water. International Biodeterioration & Biodegradation, **91**:111-118.

Jivraj, M.N., MacKinnon, M., and Fung, B. 1995. Naphthenic acid extraction and quantitative analysis with FT-IR spectroscopy. Syncrude Internal Report, Syncrude Canada Ltd, Edmonton, Alberta, Canada.

Kim, E-S, Liu, Y., and Gamal El-Din, M. 2011. The effects of pretreament on nanofiltration and reverse osmosis membrane filtration for desalination of oil sands process-affected water. Separation and Purification Technology, **81**: 418-428.

Kim, E-S, Liu, Y., and Gamal El-Din, M. 2012. Evaluation of Membrane Fouling for In-Line Filtration of Oil Sands Process-Affected Water: The Effects of Pretreatment Conditions. Environmental Science and Technology, **46**: 2877-2884.

Kim, E-S, Liu, Y., and Gamal El-Din, M. 2013. An in-situ integrated system of carbon nanotubes nanocomposite membrane for oil sands process-affected water treatment. Journal of Membrane Science, **29**: 418-427.

Klamerth, N., Moreira, J., Li, C., Singh, A., McPhedran, K.N., Chelme-Ayala, P., Belosevic, M., and Gamal El-Din, M. 2015. Effect of ozonation on the naphthenic acids' speciation and toxicity of pH-dependent organic extracts of oil sands process-affected water. Science of the Total Environment, **506-507**: 66-75.

Li, C., Fu, L., Stafford, J., Belosevic, M., and Gamal El-Din, M. 2017. The toxicity of oil sands process-affected water (OSPW): A critical review. Science of the Total Environment, **601-602**: 1785-1802.

MacKinnon, M.D., and Boerger, H. 1986. Description of two treatment methods for detoxifying oil sands process water. Water Pollution Research Journal of Canada, **21**: 496–512.

Mahata, N., Silva, A.R., Pereira, M.F.R., Freire, C., de Castro, B., and Figueiredo, J.L. 2007. Anchoring of a [Mn(*salen*)Cl] complex onto mesoporous carbon xerogels. Journal of Colloid and Interface Science, **311**: 152-158.

Parajulee, A. and Wania, F. 2014. Evaluating officially reported polycyclic aromatic hydrocarbon emissions in the Athabasca oil sands region with a multimedia fate model. Proceedings of the National Academy of Sciences, **111**(9): 3344-3349. doi: 10.7073/pnas.1319780111.

Penner, T.J. and Foght, J.M. 2010. Mature fine tailings from oil sands processing harbour diverse methanogenic communities. Canadian Journal of Microbiology, **56**(6): 459-470.

Pourrezaei, P., Alpatova, A., Chelme-Ayala, P., Perez-Estrada, L.A., Jensen-Fontaine, M., Le, X.C., and Gamal El-Din, M. 2014. Impact of petroleum coke characteristics on the adsorption of the organic fractions from oil sands process-affected water. International Journal of Environmental Science and Technology, **11**: 2037-2050.

Qui, S., Wu, L., Pan, X., Zhang, L., Chen, H., and Gao, C. 2009. Preparation and properties of functionalized carbon nanotube/PSF blend ultrafiltration membranes. Journal of Membrane Science, **342**: 165-172.

Quinlan, P.J., Tam, K.C. 2015. Water treatment technologies for the remediation of naphthenic acids in oil sands process-affected water. Chemical Engineering Journal, **279**: 696-714.

Richards, H.L., Baker, P., and Iwuoha, E. 2012, Metal nanoparticle modifie polysulfone membranes for use in wastewater treatment: a critical review. Journal of Surface Engineered Materials and Advanced Technology, **2**: 183-193.

Rogers, V.V., Liber, K., and MacKinnon, M. 2002. Isolation and characterization of naphthenic acids from Athabasca oil sands tailing pond water. Chemosphere, **48**: 519-527.

Sawyer, C.N., McCarty, P.L., and Parkin, G.F. 2003. Chemistry for Environmental Engineering and Science, 5th Edition. McGraw-Hill, New York, N.Y.

Sun, N. Chelme-Ayala, P., Klamerth, N., McPhedran, K., Islam, M.S., Perez-Estrada, L., Drzewicz, P., Blunt, B., Reichert, M., Hagen, M., Tierney, K., Belosevic, M., and Gamal El-Din, M. 2014. Advanced Analytical Mass Spectrometric Techniques and Bioassays to Characterize Untreated and Ozonated Oil Sands Process-Affected Water. Environmental Science and Technology, **48**: 11090-11099.

Wang, C., Klamerth, N., Huang, R., Elnakar, H., and Gamal El-Din, M. 2016a. Oxidation of oil sands process-affected water by potassium ferrate (VI). Environmental Science and Technology, **50** (8): 4238-4247.

Wang, C., Klamerth, N., Messele, S.A., Singh, A., Belosevic, M., and Gamal El-Din, M. 2016b. Comparison of UV/hydrogen peroxide, potassium ferrate (VI), and ozone in oxidizing the organic fraction of oil sands process-affected water (OSPW). Water Research, **100**: 476-485.

Watson, J.S., Jones, D.M., Swannell, R.P.J., and van Duin, A.C.T. 2002. Formation of carboxylic acids during aerobic biodegradation of crude oil and evidence of microbial oxidation of hopanes. Organic Geochemistry, **33**: 1153-1169.

Young, R.F., Wismer, W.V. and Fedorak, P.M. 2008. Estimating naphthenic acids concentrations in laboratory-exposed fish and in fish from the wild. Chemosphere **73**(4), 498-505.

Zaidi, A., Simms, K., and Kok, S. 1992. The use of micro/ultrafiltration for the removal of oil and suspended solids from oilfield brines. Water Science & Technology, **25**(10): 163-176.

Zhang, Y., Xue, J., Liu, Y. and El-Din, M.G. 2016. Treatment of oil sands process-affected water using membrane bioreactor coupled with ozonation: A comparative study. Chemical Engineering Journal, **302**: 485-497.

Zhu, S., Li, M., and Gamal El-Din, M. 2017. Forward osmosis as an approach to manage oil sands tailings water and on-site basal depressurization water. Journal of Hazardous Materials, **327**: 18-27.

Zubot, W., MacKinnon, M.D., Chelme-Ayala, P., Smith, D.W., and Gamal El-Din, M. 2012. Petroleum coke adsorption as a water management option for oil sands process-affected water. Science of the Total Environment, **427-428**: 364-372.

2. MEMBRANE LITERATURE REVIEW

2.1 Membrane fundamentals

Membranes are physical barriers that separate two phases but can allow or restrict the passage of certain substances through the membrane (Mandaeni 1999). The use of membranes was initially classified as a purely physical process (Lewis et al. 2011). There are four different driving forces that set membrane operations apart: electrical, thermal, pressure, and concentration (Cheryan 1998). This literature review focuses on the use of pressure driven membranes for water treatment. With respect to water treatment, there are very few contaminants that cannot be removed by the use of a membrane process if cost is not an issue (Taylor and Wiesner 1999).

A general and simplified schematic of a membrane process for water treatment is shown in Figure 2.1. The feed stream (f) enters into the membrane module. Q_f is the feed stream flowrate. C_f is the feed stream concentration. P_f is the feed stream pressure. The membrane is seen as the diagonal line traversing the membrane module represented as the rectangle. The membrane surface area is given by A_m. Certain feed stream components are able to permeate the membrane, while other components are not able to cross through the membrane; hence the membrane is semipermeable. The portion of the feed stream that has passed through the membrane is shown as permeate stream (p) with flowrate (Q_p), concentration (C_p), and pressure (P_p). The rate that the permeate flows through the membrane is given by the flux, J. The portion of the feed stream that does not pass though the membrane is shown by the concentrate stream (c) with flowrate (Q_c), concentration (C_c), and pressure (P_c). The concentrate stream is also known as the reject, retentate, or waste stream. In general, the concentrate stream, as indicated by the name of the

stream, will be more concentrated in the impermeable components of the feed stream (Crittenden 2005).

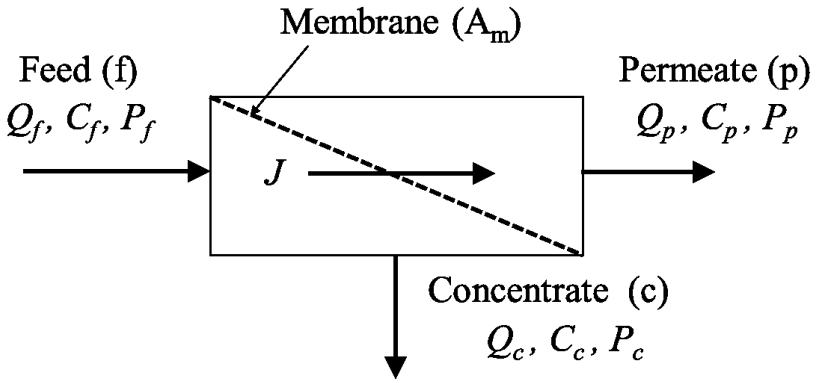

Figure 2.1 Simplified membrane process for water treatment (adapted from Metcalf & Eddy 2003)

There are many ways to classify membranes. Membranes can be classified based upon: 1) material used for fabrication, 2) membrane driving force, 3) membrane pore size or solute exclusion size, and 4) separation mechanism (Metcalf & Eddy 2003).

Benefits of using membranes include having a relatively small footprint, low operational costs, operation at lower temperatures, easier up or down-scaling, and easier integration with other existing processes as compared with conventional counterpart technologies (Ng et al. 2013). Despite having many benefits, one the greatest constraints preventing effective utilization of membrane technology in treatment of OSPW or wastewater treatment has been fouling (You et al. 2012; Dhakras 2011; Zodrow et al. 2009). Membrane fouling occurs when particulate matter found in the feed stream begins to build up onto the surface of the membrane resulting in decreased membrane performance (AWWA 1999). Membrane fouling can lead to a reduction in permeate flux and an increase in the transmembrane pressure (TMP) which results in higher operation and maintenance costs (Kim et al. 2013; Zodrow et al. 2009).

Membrane fouling can occur by four accepted mechanisms: 1) complete pore blocking, 2) pore constriction or narrowing (also known as standard pore blocking), 3) intermediate pore blocking, and 4) cake formation (Crittenden 2005; Iritani 2013). Figure 2.2 shows the four fouling mechanisms. Complete pore blocking occurs when particles in the feed water completely block pore openings on the surface of the membrane without superimposing on other particles, this is shown in Figure 2.2 a (Crittenden 2005; Iritani 2013). The pore blocking occurs only if the material can enter the membrane pore but is large enough to eventually block the whole pore (Metcalf and Eddy 2003). Pore constriction or narrowing (also known as standard pore blocking) occurs when small particulate matter in the feed water adsorbs onto the membrane pore walls, resulting in reduced pore size as shown in Figure 2.2 b (Crittenden 2005; Iritani 2013). Intermediate pore blocking, shown in Figure 2.2 c, takes into account the probability of each particle landing upon already deposited particles, in addition to the possibility of blocking a pore as in complete pore blocking (Iritani 2013). Cake formation (Figure 2.2 d) occurs when particles in the feed water begin to collect on the membrane surface forming a layer of foulant and thus increasing resistance to the oncoming flow of water (Crittenden 2005; Iritani 2013).

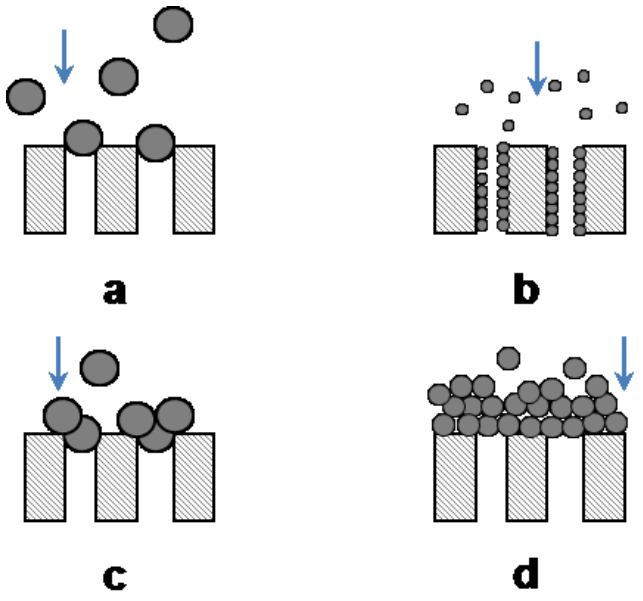

Figure 2.2 Membrane fouling mechanisms: (a) complete pore blocking, (b) pore narrowing (standard pore blocking), (c) intermediate pore blocking, and (d) cake formation. The patterned boxes represent the membranes and the spaces between represent the membrane pores and the dark circles are the particles. (Adapted from Iritani 2013; Metcalf and Eddy 2003).

Alpatova et al. (2013) discuss three types of membrane fouling: inorganic, organic and biofouling. Inorganic fouling is caused by colloidal and particulate material present in the water of interest. Organic fouling is caused by humic acids, proteins, and oils. Biofouling is caused by the attachment of microorganisms to the membrane surface. Fouling can also be reversible or irreversible (Crittenden 2005). Reversible fouling results in recoverable flux decline due to fouling buildup that can be removed during a backwash cycle, or chemically cleaned (Crittenden 2005). Irreversible fouling results in permanent flux decline which is due to membrane fouling that no amount of backwash and chemical cleaning remove (Crittenden 2005).

2.2 Membrane classification

In terms of driving force, membranes can be separated into the following classes: microfiltration (MF), ultrafiltration (UF), nanofiltration (NF) and reverse osmosis (RO) (Lee et al. 2007; Peng et al. 2004). For MF, UF, NF, and RO membranes, hydraulic pressure is applied to force the untreated water through the membrane thereby inducing separation (Taylor and Wiesner 1999). MF and UF are considered low pressure driven processes, while the high pressure driven processes include NF and RO. The amount of pressure required to get the feed water through the membranes is related in part to the average pore size for each membrane type. The transmembrane pressure (TMP) is the pressure drop across the membrane (AWWA 1999).

For each membrane type the average pore size is as follows: MF > UF > NF > RO. This means that MF membranes tend to have the largest average pore size and will likely reject fewer particles than a NF or RO membrane, and the particles rejected by the MF membrane will be larger in size than those rejected by NF or RO membranes. This concept is illustrated in Figure 2.3. MF membranes generally have pores in the macropore size range, greater than 50 nm (Metcalf and Eddy 2003). MF membranes have a minimum solute rejection size of 0.10 μm (AWWA 1999). Common solutes rejected by a MF membrane include sediment, algae, protozoa, and bacteria (Crittenden 2005). UF membranes have pores in the mesopore size range, 2 to 50 nm (Metcalf and Eddy 2003). UF membranes have a minimum solute rejection size of 0.01 μm (AWWA 1999). Common solutes rejected by UF membranes include those mentioned previously for MF membrane and small colloids and viruses (Crittenden 2005). NF membranes have pores in the micropore size range, less than 2 nm (Metcalf and Eddy 2003). NF membranes can reject solutes as small as 0.001 μm (AWWA 1999). Common solutes rejected by a NF membrane include those mentioned previously for UF membranes and dissolved organic matter

and divalent ions, like Ca^{2+} and Mg^{2+} (Crittenden 2005). RO membranes have pores that are less than 2 nm as but are considered as being a dense material, or having no pores (Metcalf and Eddy 2003). RO membranes can reject solutes as small as 0.0001 μm (AWWA 1999). Common solutes rejected by RO membranes include those mentioned for NF membranes in addition to monovalent ions, like Na^{+} (Crittenden 2005).

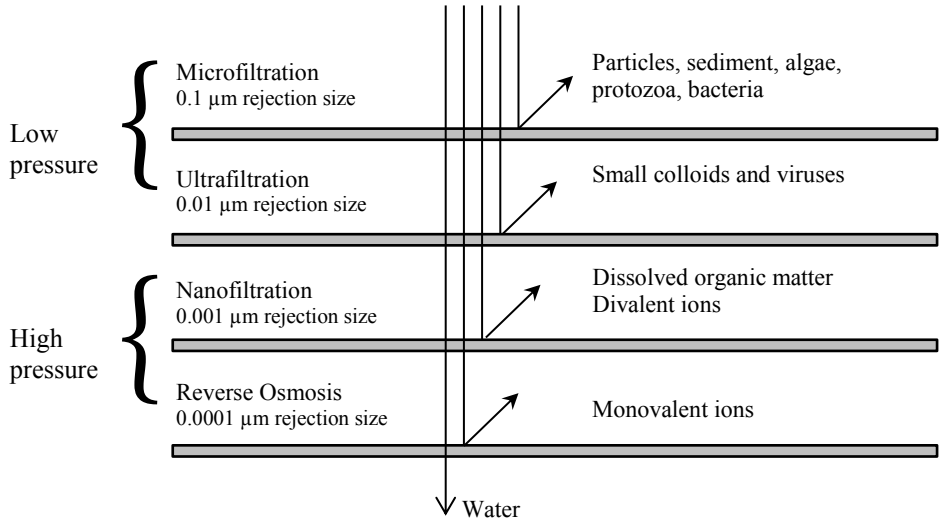

Figure 2.3 Rejection size for low and high pressure driven membranes (adapted from Crittenden 2005).

As discussed by Metcalf and Eddy (2003) the separation mechanism for MF and UF membranes is straining. It is also indicated that in straining, or size exclusion, the particles that are larger than the membrane pore size are not able to permeate the membrane and are rejected. These are the particles that accumulate in the concentrate feed stream. The separation mechanism for NF is a combination of straining and diffusion. Ionic species in the water layer closest to the membrane surface diffuse through the pores of the membrane macromolecules. Lastly, the separation mechanism for RO is only by diffusion.

In terms of low pressure membrane processes, MF and UF membranes are both comprised of porous material. Although current MF and UF membranes are closely related in terms of technology, they were each developed by very different routes (Eykamp 1995). MF membrane technology was developed much earlier than UF membrane technology. Its origins began with the development of nitrocellulose in 1846 and cellulose nitrate membranes in 1855. In MF membrane technology, there is an issue when one attempts to shrink the pore size to that of UF membranes. This problem is one of throughput, which means that the amount of liquid that is able to pass through pores decreases as the pore size shrinks. If MF technology is used to make membranes with UF sized pores (2-50 nm), then the amount of liquid that can pass though the membranes will be greatly decreased. For this reason, UF membrane technology was not developed from MF membrane technology.

UF membrane technology was developed based upon RO membrane technology. In 1959, RO membrane technology was introduced to the world with the formation of the Loeb-Sourirajan membrane at University of California Los Angeles (UCLA) (Eykam 1995). This was the first instance of membranes being asymmetric. Asymmetric membranes have a thin skin on one surface of the membrane a top a thicker supportive membrane layer that may contain large voids (Cheryan 1998). It is the skin layer that is selective. The asymmetric membrane structure solved the issue of throughput that was found in MF membrane technology. It became possible to have a dense membrane that had substantial throughput. This breakthrough in RO membrane technology led to the formation of UF membranes at Massachusetts Institute of Technology (MIT), which spurred the UF membrane research explosion during the 1960s.

Microfiltration membranes are the second most widely used membranes, overshadowed only by membranes used for hemodialysis (Eykamp 1995). They have found use in many

different technological areas. Some of these areas include the pharmaceutical industry, sterile filtration, gas phase applications, wine industry, semiconductor industry, replacement for diatomaceous earth, and most recently in the treatment of wastewater, more specifically the treatment of municipal sewage.

Ultrafiltration membranes have a smaller market than MF membranes (Eykamp 1995). One area of application has been in the replacement of MF. These include the filtration of juices and the recovery of electrocoat paint. MF membranes contain pores that are not much smaller than the particles they are retaining and this has led to major plugging issues, especially with particles that are easily deformed. UF membranes are used in the fractionation of whey and in cheese production. As well UF membranes are used in textile sizing solution recovery, in the pulp and paper industry, and in treatment of oily wasterwaters (Eykamp 1995). Ultrafiltration membranes can be used in place of conventional water treatment methods. Most often UF membranes are used to pre-treat water or wastewater prior to high pressure membrane filtration, such as NF or RO (Kramer et al. 2015). Ultrafiltration membranes have the advantage of being a low-pressure driven process but with more selectivity than microfiltration membranes.

2.3 Types of ultrafiltration membranes

With respect to materials, UF membranes can be comprised of different types of materials, which include inorganic materials (oxides, metals, and ceramics), organic polymers, composite materials (mixed matrix). In addition, these materials can be naturally occurring or synthetic in nature (Mulder 1997).

2.3.1 Inorganic membranes

Inorganic substances that can be used to form membranes include ceramics, oxides, and metals (Ng et al. 2013). The advantages of inorganic membranes that are often stated include: higher chemical stability, longer lifespan, higher mechanical strength, ease of cleaning, higher hydrophilicity, and relatively narrow pore size distribution and higher porosity resulting in higher flux and better separation. Unfortunately, inorganic membranes are more expensive to fabricate and are more susceptible to breakage even though they have superior mechanical strength than polymeric membranes (Hofs et al. 2011; Le and Nunes 2016).

2.3.2 Polymeric membranes

Organic polymers are commonly used to fabricate membranes and include polysulfone, polyvinylidene fluoride (PVDF), polyethersulfone (PES), and many others (Mulder 1997). Polymeric membranes have the advantages of being less expensive and easier to form than other types of membranes. Below are very brief descriptions of some common polymer materials used for membrane fabrication. This is not meant to be an in-depth look at polymer materials.

Cellulose acetate (CA) is a natural plastic material that was used in the development of early membrane technology (Mulder 1997). It is prepared from cellulose by acetylation, a reaction that introduces acetyl functional group (CH_3CO) into the cellulose structure. The advantages of using CA include its hydrophilicity, the ability to produce membranes with a large range of pore sizes (RO sized pores up to MF sized pores), and easy to manufacture membranes. CA use in membranes is limited by low temperature and pH ranges, poor resistance to chlorine, and its biodegradable nature which makes it very susceptible to microbial attack.

Polyamide (PA) is a polymer that consists of macromolecules linked by the amide bond (-CONH-) (Mulder 1997). PA forms the selective skin layer for many composite membranes. While this material overcame some limitations that CA experienced, namely the low pH range, PA has a much lower tolerance for chloride. This is not good when many types of water that may need to be filtered contain some level of chloride. As well, PA has a higher tendency for biofouling to occur.

Polysulfone (PSU) and polyethersufone (PES) are related polymers that contain repeating units of diphenyl sulfone, $(C_6H_5)_2SO_2$. These polymers exhibit high temperature stability during use as a result of the presence of phenyl ether and phenyl sulfone groups (Deanin 1972). These polymers are widely used today as a result of the following characteristics: wide temperature ranges (as high as 125°C for PES), wide pH range tolerance (1 to 13), good chloride resistance (200 mg/L for cleaning and 50 mg/L for short term storage), good chemical resistance to acids, alcohols, aliphatic hydrocarbons, and fully halogenated hydrocarbons. The downfalls of these polymers for use in membranes are high hydrophobicity and low pressure limits (Cheryan 1998).

Poly(vinylidene fluoride) (PVDF) has been used for membrane formation due to the following characteristics: high mechanical strength, and high thermal and chemical stability. The major drawback of using PVDF is its high hydrophobicity (Alpatova et al. 2015).

2.3.3 Composite membranes

Recent research has shown that incorporation of nano-sized inorganics into polymeric membranes can create new materials with enhanced properties such as increased permselectivity, increased hydrophilicity, increased permeate flux, increased mechanical strength, and reduced fouling (Kim et al. 2013; Kim and Deng 2011; Yang 2007). The physicochemical properties of a membrane (i.e., hydrophobicity) can be manipulated by altering the type of nanomaterial

incorporated into a membrane (Kim et al. 2013). For example, the incorporation of antimicrobial or photoreactive nanomaterials into the membrane matrix can take the functionality of membranes beyond a purely physical process by making them reactive (Li et al. 2008).

One method by which composite membranes can be made is by immersion precipitation phase inversion. It involves the casting of a thin film of polymer/solvent solution onto a support, which is then placed into a non-solvent bath where simultaneous diffusion of solvent into the non-solvent bath, and diffusion of non-solvent into the polymer/solvent film will lead to thermodynamic instability and instant liquid-liquid demixing whereby the membrane is formed (Mulder 2000).

Some nanomaterials that have been incorporated into nanocomposite membranes include titanium dioxide (TiO_2) (Bak and Tak 2005; You et al. 2012), silver nanoparticles (Zodrow et al. 2009; Lee et al. 2007), zeolites (Lind et al. 2009), and carbon nanotubes (Kim et al. 2013; Kim et al. 2012a; Celik et al. 2011).

Bae and Tak (2005) compared UF polymeric composite membranes containing TiO_2 to UF polymeric membranes with TiO_2 merely deposited onto the surface in terms of fouling mitigation for use in a membrane bioreactor (MBR). The composite membranes were made by the phase inversion casting method using TiO_2 mixed within PSU, PVDF, or polyacrylonitrile (PAN) membrane materials. The polymeric membranes with TiO_2 deposited onto the UF membrane surfaces were prepared by dipping the membranes into a TiO_2 aqueous suspension and then pressurizing with nitrogen gas. Regardless of polymer type, all membranes with TiO_2 showed increased fouling mitigation and slower flux decline when compared with neat membranes. However the membranes with TiO_2 deposited onto the membrane surface demonstrated greater fouling mitigation when compared with composite membranes.

Shi et al. (2012) prepared and characterized PVDF/TiO_2 composite MF membranes using thermally induced phase separation (TIPS) method. Addition of TiO_2 affected the cyrstallization temperature and crystallization formation but did not affect the PVDF crystal formed (α phase). Addition of TiO_2 up to maximum dose of 0.45 wt.% increased pure water flux, porosity, contact angle, and elongation at break, after which further TiO_2 addition led to the decrease of all the mentioned parameters. A similar trend was seen for tensile strength, however the maximum TiO_2 dose was found to be 0.3 wt.% for that parameter.

Lee et al. (2007) immobilized silver nanoparticles onto thin film composite PA membranes via *in situ* interfacial polymerization in order to mitigate biofouling. Hybrid membranes containing silver particles showed a strong antibiofouling effect on *Pseudomonas*, which were shown to be dead with SEM imaging. The addition of silver nanoparticles had little effect on membrane performance such as water flux and rejection.

Zodrow et al. (2009) incorporated silver nanoparticles into UF PSU membranes by phase inversion method in an effort to mitigate biofouling during water treatment. The composite membranes showed antibacterial properties toward *Escherichi coli* K12, *Pseudomonas mendocina* KR1, and MS2 bacteriophage. Adding silver nanoparticles showed an increase in membrane hydrophilicity but the silver began to leach from the membrane after short filtration time. This is problematic because the benefits of adding the silver nanoparticles into the membrane matrix were not long lasting since the silver nanoparticles were depleted from the surface of the membrane. This is the area where the particles provided the most benefit (antimicrobial and antiviral properties) to inhibit biofouling on the membrane.

Lind et al. (2009) prepared zeolite-polyamide thin film nanocomposite UF membranes to improve membrane characteristics. Zeolites are natural or synthetic hydrated aluminum silicates.

The membranes were prepared by interfacial polymerization of acid chloride and amine monomers in the presence of zeolite nanocrystals. Three different interfacial polymerization chemistries and three different sized zeolites were used to produce different nanocomposite films. In general, smaller sized zeolite crystals resulted in the best permeability enhancements which mean higher flux and higher rejection. Larger sized zeolites resulted in membranes with more favorable surface properties.

2.4 Membranes and carbon nanotubes

Many studies involving the use of carbon nanotubes in membranes have been conducted. This is mainly due to the fact that carbon nanotubes exhibit rapid mass transfer, and have good mechanical, thermal and electrical properties (Wu et al. 2013; Coleman et al. 2006). Kang et al. (2008) have also indicated that carbon nanotubes possess antibacterial effects. Two types of carbon nanotubes exist. Single walled nanotubes (SWNT) are seamless cylinders that are fabricated from one layer of graphene. Multiwalled nanotubes (MWNT) are formed from an array of graphene cylinders arranged concentrically around the center (Coleman et al. 2006).

In 2004, Ballinas et al. developed an inversion casting method for the fabrication of composite membranes which incorporated fine particles of activated carbon into a polysulfone (PSU) polymer matrix. Choi et al. (2006) utilized the method developed by Ballinas et al. to fabricate nanocomposite membranes comprised of multiwalled carbon nanotubes (MWNTs) and PSU. Prior to incorporation of the MWNTs into PSU, the MWNTs were first treated with strong acid in order to change the surface of the MWNTs by introducing oxygen containing groups (-COOH and –OH) which could be deprotonated for good dispersion in polar organic solents (Banerjee et al. 2005). Choi et al. (2006) found that while hydrophilicity of the resulting membrane increased with increased loading of MWNTs, the same was not true for the

permeation properties of the membrane. The nanocomposite membranes with 1.5 wt. % MWNTs had the highest pure water flux and those with 0.5 wt. % MWNTs had the highest poly(ethylene oxide) flux. There was an optimal amount of MWNTs that could be added, after which point the permeation properties saw a decline.

Qui et al. (2009) fabricated functionalized MWNTs PSU membranes by the phase inversion method. The MWNTs were functionalized with isocyanate and isophthaloyl chloride groups by first acidifying using H_2SO_4/HNO_3 and then reacting with excess 5-isocyanoto-isophthaloyl chloride (ICIC). Addition of these groups introduced a mutually interactive functional group between the PSU and the MWNTs that would enhance the compatibility and decrease the occurrence of voids in the membrane. It was found that hydrophilicity increased with increasing amount of MWNTs. Pure water flux and pore size increased with increasing MWNTs up to 0.19 wt.% and then a decrease in each was noted. Decreased protein adsorption in the MWNTs PSU membranes was also observed.

In 2011, Celik et al. conducted a similar study to Choi et al. (2006) and Qui et al. (2009) except that MWNTs were blended with polyethersulfone (PES) to fabricate nanocomposite membranes that were used to filter surface water. The loading of MWNTs was varied to study how this affected the morphology and permeation properties of the membrane. It was found that inclusion of the MWNTs in the membrane did increase the pure water flux, hydrophilicity, roughness and porosity. MWNTs nanocomposite membranes demonstrated 42% less flux decline when compared with the unmodified PES membranes during surface water filtration. Additionally, higher flux recoveries after caustic cleaning were achieved by the MWNTs membranes.

Kim et al. (2012a) conducted a study that evaluated a thin film nanocomposite membrane system comprised of a PSU support layer containing MWNTs topped by a thin polyamide layer containing nanosilver (nAg). The MWNTs loading in the PSU polymer matrix was one parameter that was varied (0, 1, 3, and 5% by weight) and the other was the nAg loading in the thin film topping the support layer. Results indicate that both hydrophilicity and permeation properties increased with increased loading of MWNTs up to 5% by weight. These results do not concur with previous studies conducted on the PSU/MWNTs system which indicate that an optimal amount of MWNTs should occur below 5 wt. % (Choi et al. 2006; Qui et al. 2009). Possible reasons for variation in results may be attributed to the difference in materials used for the fabrication of the membrane. Choi et al. (2006) used *N*-methyl-2-pyrrolidone (NMP) as the organic solvent of choice while Kim et al. (2012) used *N,N*-dimethylformamide (DMF). Qui et al. (2006) used MWNTs that were functionalized by isocyanate and isophthaloyl chloride groups, while Kim et al. (2012) introduced carboxyl groups on the surfaces of MWNTs by acid modification. Additionally, Kim et al. (2012a) added 1% by weight polyvinylpyrrolidone (PVP) to the support PSU membrane. It has been shown that increasing amounts of PVP added to PSU membranes results in increased pore size, formation of a thinner skin layer and macrovoid suppression (Alpatova et al. 2013).

2.5 Membrane filtration of OSPW

Remediation of OSPW is a relatively new subject. The following will give a brief summary and review of the membrane filtration studies that have been published with respect to treatment of OSPW.

Peng et al. (2004) investigated the filtration of OSPW using three different commercially available polymeric flat sheet NF membranes. The membranes used were Desal 5

(Osmonics/Desal), NF 45 (Dow Chemical) and NF 90 (Dow Chemical). The main objectives for the study were to reduce water hardness, caused by divalent cations, and to reduce the toxicity of the water by removing NAs from the OSPW. The produced waters could then be recycled back into extraction and upgrading processes in the oil sands industry. It should be noted that the OSPW samples obtained for this study had total suspended solids content that was less than 25 mg/L and were suitable for NF filtration without clarification (i.e., coagulation/flocculation). Despite this, minimal pretreatment of the OSPW was performed by filtering the water through filter paper with pore size of 11 μm for large debris removal. It was found that NF removed divalent ions with average rejection efficiency greater than 95%. NF effectively removed total organic carbon (TOC), more specifically NAs, with rejection efficiency usually greater than 95%. It was stated that NF should be effective in removing acute toxicity; however no toxicity tests were performed.

Kim et al. (2011) established that pretreatment (coagulation and flocculation) of OSPW can enhance the effectiveness of NF and RO as a viable treatment option for desalination of OSPW. Raw OPSW was pretreated by three different methods: 1) gravity settling with no chemical agents to reduce solid particulate matter in the water, 2) coagulation/flocculation/sedimentation (CFS) using alum as the coagulant, and 3) CFS with alum as the coagulant and coagulant aid - cationic polymer, polydimethyldiallylammonium chloride (poly-DADMAC). Commercial flat sheet NF and RO membranes were used in the lab-scale high pressure cross-flow membrane filtration module. The optimum alum dose was determined to be 30 g/L alum. Pretreatment options involving CFS with coagulant and coagulant aid resulted in enhanced membrane permeability. All pretreatment methods reduced solids in OSPW that form a hydrophobic foulant layer on the membrane surface. Regardless of pretreatment method, all

OSPW filtrations resulted in membrane fouling, resulting in reduced permeate flux and salt rejection. Back washing and physical cleaning resulted in a low recovery of permeate flux. Chemical cleaning with 1 mM HCL resulted in the highest flux recovery ratio (81.2%) for NF membranes tested. RO resulted in 98.5% desalination of OSPW with CFS pretreatment with alum only.

Kim et al. (2012b) further investigated coagulation and flocculation only as a pretreatment step prior to NF and RO filtration of OSPW. Sedimentation was eliminated as a process in order to reduce costs associated with the sedimentation process. The coagulant, alum, was added in the optimal dose of 30 g/L as determined previously by Kim et al. (2011). In this study three different types of coagulant aid (anionic, cationic, and nonionic polymers) were used in addition to the alum. CF treatment of raw OSPW was found to enhance NF and RO membrane permeability and salt rejection. Addition of charged coagulant aids increased membrane permeability by reduction of raw water turbidity. The cationic coagulant aid resulted in the formation of a dense fouling layer on the membrane because the negatively charged membrane surface attracted the positively charged flocs that formed. The anionic coagulant aid resulted in the formation of a course fouling layer on the membrane. The negatively charged membrane electrostatically repelled the negatively charged flocs formed by the anionic coagulant.

Kim et al. (2013) evaluated a system of MWNTs nanocomposite low pressure-driven membrane (LPM) and high-pressure driven membrane (HPM) modules used for the removal of EOF (extractable organic fraction, also known as acid-extractable fraction currently) and ionic species from OSPW. Low pressure PSU membranes with and without 10 wt. % acidified MWNTs were fabricated by the phase inversion casting method. LPMs were used for in-situ pretreatment of OSPW. The high pressure thin-film composite (TFC) membranes were

fabricated by polyamide (PA) interfacial polymerization on the surface of a phase inversion casted PSU membrane. The PA active layer was made with and without 5 wt. % acidified MWNTs. A series of combinations of LPM (with and without MWNTs) and HPM (with and without MNWTs) filtrations experiments were conducted with raw OSPW. LPM with MWNTs had increased normalized flux, increased permeate flux recovery after OSPW filtration and backwash, lower total fouling ratio (R_t) and irreversible fouling ratio (R_{ir}) during OSPW filtration when compared to LPM with no MWNTs. LPM with MWNTs in combination with HPM with MWNTs achieved the highest permeate flux/TMP ratio (5.39 ± 0.757 L/m^2h/bar) and the greatest AEF removal (95.7 ± 2.8%) and ionic species removal (90.6 ± 1.65%) when compared to the results from other combinations involving membranes without MWNTs. This study demonstrated that addition of acidified-MWNTs to the PSU casting solution did have direct effects on membrane morphology, permeate flux, hydrophilicity, and anti-fouling properties of the resulting membranes. However, this study did not examine effects of varying the amount of MWNTs to a finer degree on the membrane properties and performance. LPM had either 0 or 10 wt. % MWNTs added, while the HPM had either 0 or 5 wt. % MWNTs. Other research has shown that an optimal amount of MWNTs can be added, after which a decline in permeation will result (Choi et al. 2006; Qui et al. 2009).

Alpatova et al. (2014) brought the focus solely to ultrafiltration of OSPW. Ceramic in-series UF of OPSW was examined to gain an understanding how transmembrane pressure (TMP) and cross-flow velocity (CFV) can affect the membrane performance, specifically the separation properties and permeate quality. In addition, membrane fouling analysis by resistance in-series model and determination of the fouling mechanisms were also investigated. OSPW feed water was pretreated with alum for both coagulation/flocculation/sedimentation (CFS) and

coagulation/flocculation (CF). Pretreatment by CFS followed by filtration was denoted as CFS-filtration, whereas pretreatment with CF followed by filtration was denoted as direct filtration. While higher TMP resulted in increased permeation, greater flux decline occurred at the higher TMP. This was thought to be caused by the formation of a cake layer on the membrane surface for filtration at the highest TMP, 3.5 bar. At TMP of 2.1 bar, direct filtration (no sedimentation step) led to severe membrane fouling when compared with CFS-filtration. The lowest CFV (0.2 L/min) led to the lowest permeate flux due to membrane fouling. Results of the resistance in-series model indicate with CFS-filtration, no irreversible membrane fouling occurred. The reversible fouling present was dominated by resistance caused by cake formation and a smaller fraction was due to resistance caused by pore blocking. The fouling of the membranes can be attributed in large part to the total internal membrane fouling, which was due to pore blocking and contaminant adsorption onto the membrane surface. The results of the fouling mechanism analysis suggest that initial stages of OPSW filtration were dominated by fouling due to cake layer formation and pore blocking. As the filtration progressed, the main fouling mechanism was cake layer formation only. Chemical oxygen demand (COD) removal efficiency of the produced waters ranged from 24.8 ± 2.7 % to 38.6 ± 2.7%. Acid extractable fraction (AEF) removal efficiency ranged from 1.1 ± 0.7% to 13.0 ± 0.9%. While COD removal decreased with increase of TMP from 1.4 to 3.5 bar, the same was not true of AEF removal. Removal of NAs was minimal. No removal of NAs was observed after CFS treatment with alum dose of 30 mg/L. After CFS-filtration, there was a removal of 12.4% NAs when compared with raw OSPW. Results are to be expected as UF membranes have pore sizes that are larger than the average size of organic species, such as NAs.

Initial research in the area of membrane filtration for treatment of OSPW focused on high pressure NF and RO systems. Alpatova et al. (2014) moved the focus to UF membranes. In 2015, Dong et al. published the first paper on the treatment of OSPW by ceramic MF membranes. The study investigated OSPW treatment by coagulation-flocculation (CF) followed by MF filtration as a method to remove suspended solids and organic material in OSPW. In one treatment train, CF-MF were followed by RO to simulate complete OSPW treatment. The ceramic MF membranes used were made of Al_2O_3 and modified with SiO_2 or TiO_2 nanoparticles in a proprietary process completed by Meidensha Corporation. The RO membrane used was a flat sheet polymeric membrane manufactured by GE Osmonics. It was found that MF removed very little of the organic material (10% and 17% COD and TOC, respectively) but effectively removed 93% of TSS. MF decreased silt density index (SDI_5) enough to allow the treated OSPW to serve as feed water for high pressure membrane filtration (RO). CF combined with MF achieved higher turbidity reduction than CFS. MF-RO treatment train can produce high quality permeate.

2.6 References

Alpatova, A., Kim, E-S., Sun, X., Hwang, G., Liu, Y. and Gamal El-Din, M. 2013. Fabrication of porous polymeric nanocomposite membranes with enhanced anti-fouling properties: Effect of casting composition. Journal of Membrane Science, **444**: 449-460.

Alpatova, A., Kim, E-S., Dong, S., Sun, N., Chelme-Ayala, P., and Gamal El-Din, M. 2014. Treatment of oil sands process-affected water with ceramic ultrafiltration membrane: Effects of operating conditions on membrane performance. Separation and Purification Technology. **122**: 170-182.

Alpatova, A., Meshref, M., McPhedran, K., and Gamal El-Din, M. 2015. Composite polyvinylidene fluoride (PVDF) membrane impregnated with Fe_2O_3 nanoparticles and multiwalled carbon nanotubes for catalytic degradation of organic contaminants. Journal of Membrane Science, **490**: 227-235.

AWWA. 1999. Water Quality and Treatment: A Handbook of Community Water Supplies, 5th edition. McGraw-Hill, New York, NY.

Ballinas, L., Torras, C., Fierro, V., and Garcia-Valls, R. 2004. Factors influencing activated carbon polymeric composite membrane structure and performance. Journal of Physics and Chemistry of Solids, **65**: 633-637.

Banerjee, S., Hemraj-Benny, T., and Wong, S.S. 2005. Covalent surface chemistry of single-walled carbon nanotubes. Advanced Materials, **17**(1): 17-29.

Celik, E., Park, H., Choi, H., and Choi, H. 2011. Carbon nanotube blended polyethersulfone membranes for fouling control in water treatment. Water Research, **45**: 274-282.

Cheryan, M. 1998. Ultrafiltration and Microfiltration Handbook. Technomic Publishing Company, Lancaster, P.A.

Choi, J-H., Jegal, J., and Kim, W-N. 2006. Fabrication and characterization of multi-walled carbon nanotubes/polymer blend membranes. Journal of Membrane Science, **284**: 406-415.

Coleman, J., Khan, U., Blau, W., and Gun'ko, Y. 2006. Small but strong: a review of mechanical properties of carbon nanotube-polymer composites. Carbon, **44**: 1624-1652.

Crittenden, J.C. 2005. MWH's water treatment: principles and design, 2nd edition. John Wiley & Sons, Hoboken, N.J.

Deanin, R.D. 1972. Polymer structure, properties, and applications. Cahners Books, Boston, M.A.

Dhakras, P.A. 2011. Nanotechnology applications in water purification and waste water treatment: a review. *In* Proceedings of the International Conference on Nanoscience, Engineering and Technology (ICONSET), Calicut, India. November 28-30, 2011, pp. 285-291.

Eykamp, W. 1995. Microfiltration and ultrafiltration. *In* Membrane Separations and Technology, Principles and Applications. *Edited by* R.D. Noble and S.A. Stern. Elsevier Science B.V., Amsterdam.

Hofs, B., Ogier, J., Vries, D., Beerendonk, E.F., and Cornelissen, E.R. 2011. Comparison of ceramic and polymeric membrane permeability and fouling using surface water. Separation and Purification Technology, **79**: 365-374.

Iritani, E. 2013. A review on modeling of pore-blocking behaviors of membranes during pressurized membrane filtration. Drying Technology, **31**: 146-162.

Kang, S., Herzberg, M., Rodrigues, D., and Elimelech, M. 2008. Antibacterial effects of carbon nanotubes: size does matter. Langmuir, **24**: 6409-6413.

Kim, E-S., and Deng, B. 2011. Fabrication of polyamide thin-film nano-composite (PA-TFN) membrane with hydrophilized ordered mesoporous carbon (H-OMC) for water purifications. Journal of Membrane Science, **375**(1-2): 46-54.

Kim, E-S., Liu, Y., and Gamal El-Din, M. 2011. The effects of pretreatment on nanofiltration and reverse osmosis membrane filtration for desalination of oil sands process-affected water. Separation and Purification Technology, **81**: 418-428.

Kim, E-S., Hwang, G., Gamal El-Din, M., and Liu, Y. 2012a. Development of nanosilver and multi-walled carbon nanotubes thin-film nanocomposite membrane for enhanced surface water treatement. Journal of Membrane Science, **394-395**: 37-48.

Kim, E-S., Liu, Y., Gamal El-Din M. 2012b. Evaluation of Membrane Fouling for In-Line Filtration of Oil Sands Process-Affected Water: The Effects of Pretreatment Conditions. Environmental Science & Technology, **46**: 2877-2884.

Kim, E-S., Liu, Y., and El-Din, M. 2013. An in-situ integrated system of carbon nanotubes nanocomposite membrane for oil sands process-affected water treatment. Journal of Membrane Science, **429**: 418-427.

Kramer, F.C., Shang, R., Heijman, S.G.J., Scherrenberg, S.M., van Lier, J.B., and Rietveld, L.C. 2015. Direct water reclamation from sewage using ceramic ultra- and nanofiltration. Separation and Purification Technology, **147**: 329-336.

Le, N.L., and Nunes, S.P. 2016. Materials and membrane technologies for water and energy sustainability. Sustainable Materials and Technologies, **7**: 1-28.

Lee, S.Y., Kim, H.J., Patel, R., Im, S.J, Kim, J.H., and Min, B.R. 2007. Silver nanoparticles immobilized on thin film composite polyamide membrane: chacterization, nanofiltration, antifouling properties. Polymers for Advanced Technologies, **18**(7): 562-568.

Lewis, S.R., Datta, S., Gui, M., Coker, E.L., Huggins, F.E., Daunert, S., Bachas, L., and Bhattacharyya, D. 2011. Reactive nanostructured membranes for water purification. PNAS, **108**(21): 8577-8582.

Li, Q., Mahendra, S., Lyon, D.Y., Brunet, L., Liga, M.V., Li, D., and Alvarez, P.J.J. 2008. Antimicrobial nanomaterials for water disinfection and microbial control: Potential applications and implications. Water Research, **42**(18): 4591-4602.

Lind, M.L., Ghosh, A.K., Jawor, A., Huang, X., Hou, W., Yang, Y., and Hoek, E.M.V. 2009. Influence of zeolite crystal size on zeolite-polyamide thin film nanocomposite membranes. Langmuir, **25**(17): 10130-10145.

Mandaeni, S.S. 1999. The Application of Membrane Technology for Water Disinfection. Water Research, **33**(2): 301-308.

Metcalf & Eddy, Inc. 2003. Wastewater Engineering Treatment and Reuse, 4th edition. McGraw-Hill, New York, NY.

Mulder, M. 1997. Basic Principles of Membrane Technology. Kluwer Academic Publishers, Dordrecht, Netherlands.

Ng, L.Y., Mohammad, A.W., Leo, C.P., and Hilal, N. 2013. Polymeric membranes incorporated with metal/metal oxide nanoparticles: A comprehensive review. Desalination, **308**: 15-33.

Peng, H., Volchek, K., MacKinnon, M., Wong, W.P., and Brown, C.E. 2004. Application of nanofiltration to water management options for oil sands operations. Desalination, **170**(2): 137-150.

Qui, S., Wu, L., Pan, X., Zhang, L., Chen, H., and Gao, C. 2009. Preparation and properties of functionalized carbon nanotube/PSF blend ultrafiltration membranes. Journal of Membrane Science, **342**: 165-172.

Shi, F., Ma, Y., Ma, J., Wang, P., and Sun, W. 2012. Preparation and characterization of PVDF/TiO_2 hybrid membranes with different dosage of nano-TiO_2. Journal of Membrane Science, **389**: 522-531.

Taylor, J.S., and Wiesner, M. 1999. Membranes. *In* Water Quality and Treatment: A Handbook of Community Water Supplies. *Edited by* R.D. Letterman. McGraw-Hill, New York, N.Y. pp. 11.1-11.71.

Wu, H., Tang, B., and Wu, P. 2013. Optimization, characterization, and nanofiltration properties test of MWNTs/polyester thin film nanocomposite membrane. Journal of Membrane Science, **428**: 425-433.

Yang, Y., Zhang, H., Wang, P., Zheng, Q., and Li, J. 2007. The influence of nano-sized TiO_2 fillers on the morphologies and properties of PSU UF membranes. Journal of Membrane Science, **288**(1-2): 231-238.

You, S.J., Semblante, G.U., Lu, S.C., Damodar, R.A., and Wei, T.C. 2012. Evaluation of the antifouling and photocatalytic properties of poly(vinylidene fluoride) plasma-grafted poly(acrylic acid) membrane with self-assembled TiO_2. Journal of Hazardous Materials, **237-238**: 10-19.

Zodrow, K., Brunet, L., Mahendra, S., Li, D., Zhang, A., Li, Q., and Alvarez, P.J.J. 2009. Polysulfone ultrafiltration membranes impregnated with silver nanoparticles show improved biofouling resistance and virus removal. Water Research, **43**(3): 715-723.

Zubot, W., MacKinnon, M.D., Chelme-Ayala, P., Smith, D.W., and Gamal El-Din, Mohamed. 2012. Petroleum coke adsorption as a water management option for oil sands process-affected water. Science of the Total Environment. 427-428: 364-372.

3. ADSORPTION LITERATURE REVIEW

3.1 Adsorption fundamentals

Sorption is defined as "the concentration or movement of contaminants from one phase to another" (Sawyer et al. 2003). Sorption processes include absorption and adsorption. Absorption refers to the movement of a substance of interest (i.e. contaminant) from one phase to a different phase. Often this is commonly from a fluid (gas or liquid) phase into a liquid or solid phase. The contaminant is taken in by the volume of the new phase. Adsorption, while sounding very similar, is not the same as absorption. Adsorption also refers to the movement of a substance of interest from one phase but only to the surface of another phase. The contaminant is not taken in by the volume of the new phase but rather condenses and becomes concentrated at the new phase surface/interface. In adsorption processes the substance that is being concentrated at the surface of the new phase is the adsorbate. The material that is providing the surface upon which the adsorbate is concentrating is referred to as the adsorbent. Although adsorption can occur at the air-liquid interface, a majority of adsorption phenomenon will occur at the liquid-solid interface (Metcalf and Eddy 2003).

3.1.1 Types of adsorption

The two types of adsorption include physical and chemical adsorption. Physical adsorption, also known as physisorption, occurs if the adsorbate is attracted to the adsorbent surface by intermolecular forces that are characterized as being weak with weak bonding energies. One example of such forces are van der Waals forces. Van der Waals forces are due to interactions between induced, permanent or transient electric dipoles and occur over very short distances. Physical adsorption is usually reversible and involves a low heat of adsorption in the range of 4-40 kJ/mol (Crittenden 2005). Physical adsorption does not include forces such as covalent

bonding and it does not include coulombic attraction of unlike charges. The adsorbate is not assumed to be attached to the adsorbent surface at any particular site, so physical adsorption is not considered as being site specific. In addition, this type of adsorption may lead to the formation of a multi-molecule layer of adsorbate material upon the adsorbent surface (Sawyer et al. 2003).

Chemical adsorption, also known as chemisorption, is characterized by the formation of covalent or ionic bonds that attach the adsorbate to the adsorbent surface. Chemical adsorption involves a higher heat of adsorption than physical adsorption and is greater than 200 kJ/mol (Crittenden 2005). In this instance, the forces that are attaching the adsorbate to the adsorbent are thought to be more site specific and form a layer that is one molecule thick only. While physical adsorption tends to be more reversible because of the weaker forces holding the adsorbate to the adsorbent, chemical adsorption is considered irreversible unless energy, heat for example, is applied to the adsorbent material (Crittenden 2005; Sawyer et al. 2003).

3.1.2 Factors that affect adsorption

From a very broad perspective the properties and surface chemistry of the adsorbate and adsorbent, and their interaction with the water containing the adsorbate material will all affect the adsorption. This is because simultaneous interactions may occur at the different interfaces involved in the adsorption process (Crittenden 2005). Some key factors that will affect adsorption are adsorbent and adsorbate surface chemistry, solution conditions (chemistry and temperature), physical adsorbent and adsorbate characteristics, and adsorbate-adsorbent interactions.

Adsorbate-adsorbent interactions that can occur include electrostatic interactions, van der Waals interactions, hydrogen bonding, hydrophobic interactions, π-π dispersion interactions, and

electron-donor acceptor complex interaction. Electrostatic interactions can be attractive or repulsive and depend on ionic strength of the solution in combination with charge densities of the adsorbent and adsorbent (Moreno-Castilla 2004). Van der Waals were mentioned in section 3.1.1. Hydrophobic bonding can occur between a hydrophobic adsorbent surface and hydrophobic adsorbates since there is a preference for each to be away from water, even if only partially. Hydrogen bonding is a dipole-dipole interaction that occurs between hydrogen which is bound to an electronegative atom and a nearby electronegative atom with a pair of electrons. Hydrogen bonding has a heat of adsorption of 42 kJ/mol (Crittenden 2005). Coughlin and Ezra (1968) proposed the hydrogen bonding interaction and the π-π dispersion interaction. Moreno-Castilla (2004) explains that the basis of the π-π dispersion interaction is that at the edge of adsorbent basal planes are acid surface oxygen groups that take electrons from the any π-electron system in the adsorbent, making electrically positive holes. This would have the effect of weakening the interactions between any π-electrons in the adosorbate and the π-electrons in the weakened basal planes of the adsorbent, reducing adsorbent uptake. A different take on the reduction in the adsorption of adsorbates with aromatic sectors is due to the electron-donor acceptor complex interaction that plays out between the electron donor carbonyl oxygen in the adsorbent and the adsorbate with aromatic ring that acts as the electron acceptor (Moreno-Castilla 2004). Upon oxidation of carbonyl groups to carboxyl groups the same electron-donor acceptor complex interaction does not occur.

The functional groups that are present on the surface of the adsorbent provide the sites needed for interactions with the adsorbate or surrounding solution to occur (Villacanas et al. 2006). Surface groups containing oxygen affect hydrophobicity which determines if a hydrophobic interaction will occur (Moreno-Castilla 2004). In addition to the surface chemistry

of the adsorbate, it is also important to consider the surface chemistry of the adsorbate which also provide sites needed for interactions. Surface chemistry has a large effect on the resulting hydrophobicity of the adsorbate. The more hydrophobic a compound is, the more likely it will partition out of water and make way towards a nearby surface (adsorbent). Overall, the chemistry of the water, or aqueous solution, will affect the ability of adsorbate to adsorb onto an adsorbent. The key factor in this case is solution pH which can affect dissociation of functional groups by changes in the concentration of hydronium and hydroxide ions. With respect to the solution, it is also important to mention temperature effects which determine how fast adsorption occurs (kinetics).

With respect to adsorbent and physical characteristics, surface area is one factor that affects adsorption. If an adsorbent provides a greater surface area there are more sites that are available for adsorption. Surface area is itself affected by the type of pore size distribution that the adsorbent material possesses. Pore size distribution is the range of pores that can be found in the adsorbent. The different sizes of pores in adsorbent are macropores, mesopores, micropores, and submicropores. Macropores are defined as being greater than 50 nm. Mesopores are pores are 2 to 50 nm. Micropores are less than 2 nm. Submicropores are even smaller than micropores. If the adsorbent material is only comprised of macropores, the material will have large void volumes and the overall surface area for a given unit volume will be quite small. If the adsorbent has a pore size distribution that shows the material is comprised of smaller sized pores (mesopores, micropores, and submicropores) then the void volume will decrease and the surface area will increase. This is mainly due to the presence of the micropores and submicropores as these pores contribute a majority of the surface area for a material.

While small pore size can greatly increase the surface area of the adsorbent, it can also affect the size of the adsorbate that can be adsorbed. The adsorbate size will determine which types of adsorbent pores it may enter. This will hinder larger sized adsorbate from accessing a large portion of the surface area if the adsorbate is too large to enter micropores and submicropores. Conversely, if the adsorbate is very small, then access to most surface area of an adsorbent will occur which will have the effect of increasing adsorption.

The surface chemistry of the adsorbate and adsorbent and the chemistry of the water, combined with the physical and textural properties of the materials all factor into determine of the different types of interactions that may occur between the adsorbent and the adsorbate.

3.1.3 Steps in adsorption

The adsorption process as discussed by Metcalf and Eddy (2003) involves four fundamental mass transfer steps that occur within the aquatic environment: 1) bulk solution transport, 2) film diffusion transport, 3) pore transport, and 4) adsorption.

In bulk solution mass transfer the adsorbate, usually organic material, will travel through the bulk of the liquid to the boundary layer of the fixed film that surrounds the adsorbent material. The transport phenomena involved in this first step are advection and dispersion. In film diffusion transport the adsorbate travels through the boundary layer of the fixed film surrounding the adsorbent to the entrance of the adsorbent pores. The main transport phenomenon involved in this step is diffusion. Usually this occurs slowly. In pore transport the adsorbate will travel further into the adsorbent via the pores. The transport phenomenon involved in the third step includes molecular diffusion through the liquid in the adsorbent pores and/or diffusion along the adsorbent surface. In adsorption the adsorbate material will attach to the

available sites on the adsorbent surface which includes the outer surface of the adsorbent and within the adsorbent pores (macropores, mesopores, micropores, and submicropores).

The slowest step to occur is deemed as the rate limiting step. Physical adsorption occurs very rapidly. For this type of adsorption process, the rate limiting step will tend to be a diffusion transport step. This can include either the second (film diffusion) or third (pore transport) adsorption steps. If chemical adsorption is the main adsorption process, then the rate limiting step is the adsorption of the adsorbate onto the adsorbent material.

3.1.4 Adsorption isotherms

The amount of adsorbate that is adsorbed by an adsorbent depends upon the concentration of the adsorbate in the bulk solution, the characteristics (i.e., porosity) of the adsorbate, and the temperature of the bulk solution (Metcalf and Eddy 2003). An adsorption isotherm quantitatively describes the equilibrium between the concentration of the adsorbate in the bulk solution (mass/volume) and concentration of adsorbate that becomes adsorbed to the adsorbent (mass adsorbate/mass adsorbent) at a constant temperature. Adsorption isotherms are determined in a laboratory setting by exposing a known amount of adsorbate in a fixed volume of liquid to various doses of adsorbent material for different amounts of time.

The amount of adsorbate removed by the adsorbent is called the adsorbent capacity. It is be represented by q_t. Adsorbent capacity, q_t, is given by equation 3.1.

$$q_t = \frac{(C_0 - C_t)V}{m} \qquad (3.1)$$

Where:

q_t is the amount of adsorbate removed by the adsorbent at time t (mg adsorbate/g adsorbent)

C_t is the concentration of adsorbate in the bulk solution at time t (mg adsorbate/L)

C_0 is the concentration of adsorbate at time 0, starting concentration (mg adsorbate/L)

V is the volume of aqueous phase containing the adsorbate (L)

m is the mass of adsorbent material (g).

When the rate of adsorption equals the rate of desorption then equilibrium is achieved. At this point the capacity of the adsorbent has been reached. At equilibrium, the concentration of adsorbate in the aqueous phase will show little to no change over time and is denoted by C_e, which replaces C_t in equation 3.1. The resulting adsorbent capacity at equilibrium is given by q_e, which will replace q_t in equation 3.1 (Crittenden 2005).

There are four adsorption isotherms that are commonly used to describe the adsorption step. They are Langmuir, Freundlich, linear and Brunauer, Emmett, and Teller (BET) isotherms. Each isotherm will be described in the sections to follow.

3.1.4.1 Langmuir isotherm

The Langmuir isotherm was developed using surface complexation theory and is described by equation 3.2. There are a few assumptions associated with Langmuir isotherm. First it assumes that a single adsorbate molecule binds to a single site on the adsorbent surface. Second it also assumes that all surface sites of the adsorbent have the same affinity for the adsorbate (Sawyer et al. 2003).

$$q = q_m \frac{K_{ads}C}{1+K_{ads}C} \qquad (3.2)$$

Where:

q is the mass of adsorbate per unit mass of adsorbent (mg adsorbate/g adsorbent)

q_m is the maximum amount of adsorbate that can cover the surface area of adsorbent in a monolayer coverage, monolayer capacity (mg adsorbate/g adsorbent)

K_{ads} is the measure of the affinity of adsorbate for adsorbent

C is the equilibrium concentration of adsorbate in the bulk solution after adsorption (mg adsorbate/L).

As C increases, it is assumed that adsorption sites become filled up. And mathematically, as C increases, then q approaches q_m. K_{ads} and q_m can be evaluated by using the linearized form of equation 3.2.

3.1.4.2 Freundlich and linear isotherms

The Freundlich isotherm can be derived from the Langmuir isotherm by assuming that surface sites on the adsorbent that have different affinities for different adsorbates, but also assuming that each site behaves according to the Langmuir isotherm. The Freundlich isotherm is given by equation 3.3.

$$q = KC^{1/n} \qquad (3.3)$$

Where:

q is the sorbed amount of adsorbate onto the adsorbent (mg adsorbate/g adsorbent)

K is the measure of the capacity of the adsorbent (mass adsorbate/mass adsorbent)

n is a measure of how affinity for the adsorbate is a function of changes in adsorption density.

K and *n* can be evaluated by using the linearized form of equation 3.3. When *n* is equal to 1, then the Freundlich isotherm becomes the linear isotherm given by equation 3.4.

$$q = KC \qquad (3.4)$$

When *n* is equal to 1 this means that all sites on the adsorbent surface have equal affinity for the adsorbate.

3.1.4.3 BET isotherm

Brunauer, Emmett, and Teller developed the BET isotherm. The BET isotherm is an extended form of Langmuir isotherm but it is modified to account for multilayer adsorption. This model assumes that layers of adsorbate accumulate at the adsorbent surface and that the Langmuir isotherm applies to each layer. The complex BET isotherm is given by equation 3.5.

$$\frac{q}{q_m} = \frac{bC}{(C_s - C)[1 + (b-1)C/C_s]} \qquad (3.5)$$

Where:

C_s is the saturation concentrations for the adsorbate in aqueous phase.

C_s and *b* are determined from equation 3.6, a rewritten version of equation 3.5.

$$\frac{C}{q(C_s - C)} = \frac{1}{bq_m} + \frac{b-1}{bq_m}\left(C/C_s\right) \qquad (3.6)$$

3.1.5 Diffusion and adsorption kinetics models

While adsorption isotherms give information regarding the sorbed concentration of adsorbate in relation to the concentration of adsorbate in the aqueous bulk solution, only the equilibrium isotherm includes the element of time. As it might be beneficial to determine how fast each step in the adsorption process takes one must then begin to observe and study the kinetics. With respect to adsorption, kinetics would be a study of how fast the adsorbate attaches in the adsorbent surface. As discussed in section 3.1.3, adsorption is not one step in of itself but four steps.

3.1.5.1 Diffusion model

Steps 1-3 of the four fundamental mass transfer steps involve the mass transport phenomenon known as diffusion. Diffusion is assumed to be the rate limiting step because it is often the step which takes the longest amount of time. The models which represent the mass transport phenomenon of diffusion can be further subdivided into two categories: the external mass transfer model and the internal diffusional models.

The external mass transfer model is representative of the bulk solution diffusion step. During this step the adsorbate in the bulk solution travels, by diffusion and advection, to the fixed film boundary layer surrounding the adsorbent material. Largitte and Pasquier (2016) indicated that this particular model could be neglected due to the fact that a larger portion of the mass transfer in this step would more than likely be due to the advection that would occur as a result of agitation felt by the batch reactor. Therefore this would basically eliminate the effect of diffusion, and thus eliminate the external mass transfer model.

As discussed by Largitte and Pasquier (2016), internal diffusional models represent the mass transfer of the adsorbate into the interior pores of the adsorbent material. Some internal

diffusional models include the Crank model, the Weber and Morris model, and the Bangham model. The Crank model is a partial differential equation describing the homogenous diffusion of an adsorbate within the adsorbent. It is assumed that there is a constant diffusivity at all points in the adsorbent and that the adsorbent particle is spherical. An exact solution for specific conditions does exist. As well, simplified Crank short time and long-time solutions exist. The Crank long time equation is called the Boyd equation. The Weber and Morris model was based upon batch adsorption studies of alkyl benzene sulfonates by activated carbon. This model was described by two linear plots and two different equations. There has been some controversy related to the use of one of the equations. Generalization of the Weber and Morris model led to the Bangham model. The intraparticle diffusion equation is given by equation 3.7 (Nethaji et al. 2013; Wang et al. 2010).

$$q_t = k_i t^{1/2} + c \qquad (3.7)$$

Where:

q_t is the amount of adsorbate adsorbed at any time, t (mg adsorbate/g adsorbent)

k_i is the intraparticle diffusion rate constant ($mg/g/hr^{1/2}$)

t is time ($hr^{½}$)

c is the intercept.

Determination of the value of q_t has been previously described in equation 3.1. As discussed by Nethaji et al. (2013), if the plot of q_t versus $t^{1/2}$ passes though the origin then this indicates that the intraparticle diffusion is the sole rate limiting step. However if the plot does not pass through the origin, but instead though an intercept, *c*, then the rate limiting step is a result of intraparticle diffusion and film diffusion. The intercept, c, is an indicator of the boundary layer

thickness. A larger intercept value indicates that the film diffusion though the boundary layer plays a more significant role in the rate limiting step (Wang et al. 2010).

According to Wang et al. (2010) some plots of q_t versus $t^{1/2}$ may have up to three distinct linear regions that are representative different stages of the adsorption process. The first region can be a sharply inclined linear pattern that represents the external mass transfer. The second region shows a linear pattern with a smaller slope that represents gradual adsorption where intraparticle diffusion is rate-limiting. In this region k_i and c are determined from slope and intercept. The third region shows a linear pattern with a very small slope. This area represents the gradual equilibrium that is obtained.

3.1.5.2 Kinetics of adsorption models

Step 4 of the mass transfer steps involves the actual adsorption of the adsorbate onto the adsorbent surface. Adsorption can be modelled by different kinetic models. Among them are the pseudo first-order (PFO) model and the pseudo second-order (PSO) model.

The pseudo first-order model first came about in 1898 by Lagergren who was using the model to describe the kinetics of the adsorption of oxalic and malonic acid onto the adsorbent, charcoal (Qui et al. 2009). The model was described by equation 3.8.

$$\frac{\mathrm{d}q_t}{\mathrm{d}t} = k_{PFO}(q_e - q_t) \qquad (3.8)$$

Where:

q_e and q_t are the adsorption capacities at time t and at equilibrium (mg/g)

k_{PFO} is the pseudo first order rate constant (hr^{-1})

t is time.

If equation 3.8 is integrated with the following boundary conditions t = 0 min and q_t = 0 mg/g and t = t min and $q_t = q_t$, then equation 3.9 is obtained.

$$\log(q_e - q_t) = log(q_e) - \frac{k_{PFO}}{2.303} t \qquad (3.9)$$

The PFO model is built upon several assumptions as described by Largitte and Pasquier (2016). The first is that sorption occurs on localized sites and the adsorbed ions do not interact with one another. The second assumption is that concentration of the adsorbate is constant. The third assumption is that surface coverage by the adsorbate does not affect the energy of adsorption. The fourth assumption is that a saturated monolayer of adsorbates on the adsorbent means that maximum adsorption had occurred. The last assumption is that the adsorbate uptake on the adsorbent material can be accurately represented by a first-order differential equation.

Blanchard et al. (1984) described the pseudo-second order (PSO) differential equation in an attempt to model the kinetics of ammonium ion adsorption by clinoptilolite, a zeolite. Ho and McKay (1998; 1999; 2000) used the PSO form of the differential equation in order to develop a kinetics model to describe the adsorption of divalent metal ions, Cu^{2+}, onto peat. A commonly used form of the differential equation is shown by equation 3.10.

$$\frac{\mathrm{d}q_t}{\mathrm{d}t} = k_{PSO}(q_e - q_t)^2 \qquad (3.10)$$

Where

k_{PSO} is the PSO rate constant of adsorption (g/mg/hr)

q_e is the amount of adsorbate removed at equilibrium (mg/g)

q_t is the amount of adsorbate removed at any time, t (mg/g).

Integrating using boundary conditions t=0 min and q_t = 0 mg/g and t = t min and $q_t = q_t$ leads to equation 3.11, which can be rearranged to the linear form shown by equation 3.12.

$$q_t = \frac{t}{\frac{1}{k_{PSO}q_e{}^2} + \frac{t}{q_e}} \tag{3.11}$$

$$\frac{t}{q_t} = \frac{1}{k_{PSO}q_e{}^2} + \frac{t}{q_e} \tag{3.12}$$

The pseudo-second order constant is determined by plotting t/q_t versus t (Ho et al 2006). The PSO model has been used to successfully model adsorption of metal ions, oils, herbicides, organic substances in aqueous solutions, and dyes (Ho 2006; Qiu et al. 2009). Ho (2006) has indicated that the PSO model is advantageous because the following parameters do not need to be known and can be determined from the PSO model: adsorption capacity, rate constant of PSO, and initial adsorption rate.

3.2 Literature Review: Adsorption and OSPW

Activated carbon (AC) is a very common adsorbent material used for removal of organics from different types of process waters. In an effort to remove NAs from OSPW, AC has been used as an adsorbent. In addition to AC, other types of adsorbents such as petroleum coke and biochar have been utilized and studied for removal of NAs from OSPW.

3.2.1 Activated carbon

Activated carbon (AC) is a common adsorbent that has been used extensively for water treatment (Sawyer et al. 2003). AC can be separated into two different groups based upon size and adsorption capacity: powdered activated carbon (PAC) and granular activated carbon (GAC) (Metcalf and Eddy 2003). While PAC has a smaller diameter (0.074 mm) than GAC (diameter >

0.1 mm), both materials have a fairly high surface area, 700-1300 m^2/g for GAC and 800-1800 m^2/g for PAC. AC is prepared by making char from organic material (walnut hulls, almonds, bones, wood, etc.) using a method known as carbonization (Metcalf and Eddy 2003). Carbonization involves exposing a material to enough heat in an inert environment (no O_2) in order to convert organic material to a solid porous carbon. Activation of the char is accomplished by two methods: physical and chemical. Physical activation involves exposure to gases (CO_2 and steam) at high temperatures (800-900°C). Chemical activation involves treating the char with a chemical agent (potassium hydroxide, zinc chloride, or phosphoric acid) (Iranmanesh et al. 2014). During activation the AC develops its internal pore structure, which has a great impact on the adsorbent surface area (Metcalf and Eddy 2003). While AC is an ideal adsorbent material, its widespread use is restricted by preparation cost (Frankel et al. 2016).

Pourrezaei et al. (2014a) conducted a study that accessed the performance of petroleum coke (PC) in comparison to powdered activated carbon (PAC) and granular activated carbon (GAC) as an adsorbent material used for the treatment of OSPW. The surface areas of the PAC and GAC used were 800 m^2/g and 912 m^2/g. These were both higher than the surface area for the raw PC. SEM imaging showed that the PAC and GAC were highly porous structures. It was determined that PAC and GAC had pores in the range of 0.5-36 nm with the highest number of pores in the size range of 0.6-1.4 nm. The use of GAC and PAC as adsorbents for treatment of OSPW led to at least a 93% removal of COD and AEF regardless of contact time or adsorbent dose. AEF adsorption using GAC had the highest correlation coefficients for Freundlich and Langmuir isotherm. For PAC adsorbent, the highest correlation coefficient occurred with the Freundlich isotherm. Maximum adsorption capacity for GAC was 51 mg/g and was 71 mg/g for

PAC. The adsorption of AEF onto PAC and GAC was found to occur mainly due to the adsorbent porosity as opposed to the surface functionality.

Iranmanesh et al. (2014) prepared AC by activating biochar made from sawdust. The study focused largely on the activation conditions and how they affected the resulting properties for AC. The produced AC had a surface area that ranged from 367-750 m^2/g for physical activation and was 895 m^2/g for chemical activation. With respect to physical activation, it was found that the surface area increased with increasing activation temperature up to a certain value. After this point the surface area decreased with any increase of activation temperature due to extensive carbon-CO_2 reaction and increase of ash. Physical activation led to AC that had more micropores, while chemical activation led to the presence of more mesopores. Carbon content in the produced AC was approximately 54% for chemical activation, 64% for commercially available AC, and as high as 85.33% for physical activation. Commercial AC was found to have the lowest uptake of NAs, followed by physically activated AC. Chemically activated AC had the highest uptake of NAs. This was thought to be a result of the surface area and not to the carbon content of the adsorbent material.

Islam et al. (2014a, 2014b, 2015, 2016) published four articles involving research that pertained to the use of a GAC fluidized bed biofilm reactor and the combined effects of adsorption and biodegradation of the NAs. The first paper introduced the idea of constructing a fluidized bed biofilm reactor (FBBR) by using GAC as support media (Islam et al. 2014a). In this way simultaneous organic adsorption and biodegradation occurred and optimal operating conditions resulted in the removal of 51% of COD, 56% of AEF, and 96% of classical NAs. The GAC media was able sustain formation of diverse microbial populations within the biofilms originally formed by endogenous microbial populations within OSPW.

The promising results led to further of studies involving use of GAC FBBR for treatment of OSPW that had been pretreated with ozone (Islam et al. 2014b). Ozonation of OSPW prior to treatment by GAC FBBR resulted in increased GAC adsorption capacity. It also reduced the NAs cyclicity in the OSPW. This increased the biodegradability of the OSPW. Ozonation followed by adsorption and biodegradation under optimal operating conditions resulted in the removal of 62% of COD, 88% of AEF, and 99.9% of classical NAs.

Islam et al. (2015) then investigated the synergistic mechanisms of the GAC FBBR system that combined adsorption and biodegradation of OSPW. In order to do this the sole effect of each of the following were investigated: 1) GAC adsorption of NAs in OSPW. 2) biodegradation of NAs in OSPW, and 3) the effect of the combined GAC FBBR system on NAs in OSPW. In addition the effect of ozonation was also included as a factor of interest. FBBR with 0.4 g GAC/L was used to remediate raw and ozonated OSPW in a 28 day batch treatment. Classical and oxidized NAs in raw OSPW decreased by 93. % and 73.7%. Oxidation of OSPW led to an increase of classical and oxidized NAs removal (96.2% and 77.1%) in the pre-treated OSPW. A majority of the NAs removal was found to be attributed to GAC adsorption alone, as biodegradation alone was found contribute at most 10% removal of classical NAs for raw and ozonated OSPW. GAC adsorption only and the combined adsorption/biodegradation treatments of raw and ozonated OSPW resulted in NAs removal of >90%. Synergistic effects for the combined adsorption/biodegradation combination were observed for removal of COD, total Ox-NAs, and AEF.

Islam et al. (2016) went on to perform further studies involving the use of GAC FBBR for treatment of synthesized OSPW. The main goal in these studies was to gain further understanding of how GAC adsorption and biodegradation contributed to removal in the GAC

FBBR system and how this knowledge could help to optimize the bioreactor biodegradation. This study focused on obtaining more information surrounding the microbial communities within the biofilms by characterizing them more precisely using next generation high throughput pyrosequencing. Despite briefly highlighting the impact of biodegradation and adsorption on removal of NAs, this paper does not focus too much on adsorption. As seen previously (Islam et al. 2014b, 2015) ozonation of OSPW led to increased NAs removal by biodegradation and adsorption (18% and 73%) when compared to their removals in raw OSPW (14% and 63%). 454-pyrosequencing results indicated that within 28 days divergent microbial communities formed for the raw and oxidized OSPW despite starting with the same biofilm composition. Further studies investigating how different factors can result in changes within the biofilm community may be useful in order to understand the full potential that microorganisms may have in the environmental sector, specifically for remediation of wastewater.

3.2.2 Petroleum coke

Petroleum coke (PC) is a dry waste produced as a result of the delayed or fluid thermal coking processes used to upgrade bitumen to a synthetic crude oil (Small et al. 2012). About 15% of bitumen is converted to PC (Zubot et al. 2012). For each barrel of synthetic crude oil produced by Syncrude Canada Ltd. there is approximately 20 kg of PC waste material (Zubot et al. 2012). Consequently there is a large amount of PC available and stored on site. This makes PC a material that was worth researching since it has high carbon content. Unlike AC, PC has a much small surface area. Zubot et al. (2012) determined that the surface area of PC was 5.7 m^2/g. PC activation has been shown to increase the surface area up to 250-374 m^2/g for different experimental conditions (Zubot et al. 2012). Small et al. (2012) achieved a higher PC surface area (578 m^2/g) by physical activation of delayed coke with increased activation time (6 hr) at

900°C and an increased steam rate. In an alternate study, PC activation by microwave was used to increase PC surface area to 440 m^2/g for fluid coke, and to a high value of 1131 m^2/g for delayed coke (Chen and Hashisho 2012).

Zubot et al. (2012) found that chemically, PC is mostly carbon (>80%) with high amounts of sulphur (4-6 wt.%) that make it unsuitable for use as a fuel. Vanadium comprises a larger portion of the fraction of trace elements (4.4 wt.%) found within PC. Within OSPW, a majority of the vanadium leached from PC was vanadium (V), as opposed to vanadium (IV). Elevated levels of vanadium were found to be a possible contributor to the toxicity of OSPW as determined by the *Ceriodaphnia dubia* bioassay. Pourrezaei et al. (2014) observed that the vanadium concentration increases for increasing PC dose (50 mg/L to 400 g/L) in OSPW during a 12 hour timeframe and does not reach solid-liquid equilibrium. This result is in agreement with the short term adsorption study conducted by Zubot et al. (2012). The increase in vanadium concentration in the aqueous phase was thought to increase with increasing pH due to increasing vanadium mobility at higher pH and a high carbonate concentration in OSPW (Pourrezaei et al. 2014). Zubot et al. (2012) found that for long time periods, the vanadium concentration decreases 50-60% during the first 3 to 4 months, and decreases by as much as 80% after a period of one year. This decrease in vanadium was attributed to possible sorption of vanadium by metal oxides in the PC, or by the PC itself.

Gamal El-Din et al. (2011) used PC adsorption as one pre-treatment option for fresh OSPW prior to ozonation. The PC used was untreated. Using a dose of 22% by wt., PC adsorption was responsible for reducing the total acid-extractable organics (TAO) in the OSPW from 75 mg/L to 5.7 mg/L. PC adsorption in combination with ozonation of OSPW led to the further reduction of TAO to 1.4 mg/L. The treated OSPW was found to be no longer toxic to *V.*

fischeri. The combined treatment decreased the amount of non-biodegradable organic pollutants in OSPW. In-depth adsorption studies regarding the use of PC as an adsorbent were not detailed in this study.

Zubot et al. (2012) shared detailed results of utilizing PC as an adsorbent for the treatment of OSPW in order to remove NAs and total acid-extractable organics (TAO). Syncrude Canada Ltd. supplied the OSPW and PC for use in the adsorption and kinetics experiments. Increasing doses of PC (9.9-39.1 wt.%) led to high removal of NAs (64-96%) as determined by the total ion intensity by peak. A PC dose of 19.9 wt.% led to a reduction of NAs by 82%. These results are in agreement with Gamal El-Din et al. (2011) who found that a PC dose of 22 wt.% decreased TAO by 91% and NAs by 84%. However Zubot et al. (2012) further found that PC more effectively adsorbed NAs with higher molecular weight and more ring structures because these NAs were more hydrophobic and therefore less soluble within OSPW. Removal trends of TAO were found to be similar to NAs removal however NAs removal occurred more rapidly. The utilization of PC adsorption for OSPW treatment was found to reduce the biologically resistant organic fraction. Adsorption of TAO was found to exhibit a two stage uptake as indicated by kinetics modeling using the intraparticle diffusion model, with an initial higher rate of adsorption followed by a slower second stage of adsorption attributed to the existence of sites of lower reactivity and/or diffusion into micropores. The adsorption of TAO from OSPW by PC fit the Langmuir, Freundlich, and Langmuir-Freundlich models, with resulting adsorption capacities ranging from 0.1 to 0.46 mg/g, and averaging 0.26 mg TAO/g PC.

Pourrezaei et al. (2014) conducted a study that accessed the performance of PC in comparison to activated carbon (AC) and granular activated carbon (GAC) as an adsorbent material used for the treatment of OSPW. The general trend found that was in agreement with

results by Zubot et al. (2012) was that higher acid extractable fraction (AEF) removal occurred for higher doses of PC. This was attributed to the higher surface area available with higher doses of PC. While Zubot et al. (2012) studied the effect of contact time on resulting OSPW, the time frame was on the order of hundreds of days. In contrast, Pourrezaei et al. (2014) looked at the effect of time on the adsorption of AEF and COD for contact time up to 12 hours. For this time frame, it was found that Langmuir and Freundlich isotherms resulted in high correlation coefficients for GAC and PC. PAC had a high correlation coefficient for only the Freundlich isotherm. The adsorption capacity for PC adsorption of AEF in OSPW was calculated to be 1.0 mg/g. This value was much lower than the adsorption capacity of GAC (51 mg/g) and PAC (71 mg/g).

3.2.3 Biochar

As mentioned previously, although AC is a common adsorbent material its use has been limited by the costs associated with its production for wide scale and large scale utilization (Frankel et al. 2016). An alternate adsorbent material that has started to see use is biochar. Biochar is the porous carbon residual that is left when biomass is subjected to thermal energy under limited O_2 or anaerobic conditions (Inyang and Dickenson 2015).

Inyang and Dickenson (2015) discuss three processes used to produce either non-activated biochar or activated biochar. These are gasification, slow pyrolysis, and fast pyrolysis. Slow pyrolysis occurs at temperatures between 350-800°C and results in a higher yield of biochar when compared to gasification and fast pyrolysis. Higher temperatures often result in the formation of biochar with a higher surface area due to the fact that increased temperatures lead to increased burn off of carbonaceous material. Gasification and pyrolysis processes result in solid

biochar. Pyrolysis retention times are short in comparison to slow pyrolysis and the process itself occurs at a lower temperature range (425-550°C). This leads to a biochar that will not have as much carbonaceous material burnoff, and will therefore exhibit lower specific surface area and porosity when compared with biochar produced by slow pyrolysis. Gasification occurs at high temperatures (≥ 800°C) but for shorter retention times on the order of seconds to hours. This results in a biochar that has a higher specific area and porosity than both slow and fast pyrolysis.

Biochar that has not been activated by physical or chemical means can have a low surface area in comparison to AC, however the costs associated with production of the material can be substantially lower than AC. The lower costs are due in part reduced energy requirements needed for production of the biomass. In addition, non-activated biomass will not need the added activation steps. The cost of producing biomass was estimated to be about 1/6 of the cost to produce AC (Ahmad et al. 2012).

Bhuiyan et al. (2017) prepared biochar from wheat straw, pulp mill sludge, switchgrass, mountain pine, and aspen wood and hemp shives and used the resulting material to perform adsorption experiments with OSPW. The biochar that resulted in the highest AEF reduction and AEF adsorption capacity from highest to lowest were as follows: wheat straw (21% and 0.59 mg/g), pull mill sludge, switchgrass, mountain pine, hemp shives and lastly aspen wood (0.04 mg/g and 1.4%). Reduction of metal content in the wheat straw by acid washing resulted in a reduction of AEF adsorption capacity. Addition of metal content in aspen wood by hydrolysis of $Fe(NO_3)_3 \cdot 9H_2O$ resulted in an increase of AEF adsorption capacity. A biomass with high metal content provided the highest removal of AEF from OSPW. This is explained by the addition of Fe and Al metals within the biomass likely exist as hydroxides or oxides, providing Lewis acids

sites within the biomass. These sites attract and bind with naphthenates in NAs, which are carboxylate functional groups. The surface areas of the produced biomass ranged from 14-420 m^2/g. The higher surface area of the aspen wood did not have an effect on the resulting AEF adsorption capacity.

3.2.4 OSPW Adsorption Summary

Pourrezaei et al. (2014) conducted an excellent study that compared adsorption of OSPW by two of the main groups of adsorbent material discussed, AC and PC. PC reduced AEF in OSPW by 60% after 12 hours and at a dose of 200 g/L. In comparison, both GAC and PAC reduced AEF in OSPW by more than 93% for a dose as low as 50 g/L regardless of contact time. The adsorption capacity of PC was found to be 1.0 mg/g, while the adsorption capacities of GAC and PAC were found to be 51 mg/g and 71 mg/g. In this study PC had a relatively low surface area of 7.4 m^2/g when compared with PAC surface area (800 m^2/g) and GAC surface area (912 m^2/g).

In contrast to Pourrezaei et al. (2014), Gamal El-Din et al. (2011) used a dose of 22% by wt. (220 g/L) PC to reduce TAO by 92.4%. Although the dose used is a bit higher than that used by Pourrezaei et al. (2014), the resulting reduction of the organic fraction was about 30% higher for Gamal El-Din et al. (2011). The high result obtained by Gamal El-Din et al. (2011) is in some agreement with that given by Zubot et al. (2012), a PC dose of 19.9 wt.% (199g/L) led to the reduction of the organic fraction by 82%.

Gamal El-Din et al. (2011) did not go on to analyze the adsorption capacity of the PC used, however Zubot et al. (2012) did further analysis. The PC adsorption capacities ranged from 0.1 to 0.46 mg/g, with an average value of 0.26 mg/g. This value for the PC adsorption is slightly

lower than that given by Pourrezaei et al. (2014), but in general they are in agreement. In addition, Zubot et al. (2012) determined that the surface area for the PC was 5.7 m^2/g, which is in agreement with the value obtained by Pourrezaei et al. (2014).

For AC and PC, surface area is a key factor that affects the adsorption capacity of the adsorbents. In general it appears that higher surface area leads to an increased adsorption capacity and increased removal of NAs. This is not the case for biochar adsorbent material as was demonstrated by the experiments performed by Bhuiyan et al. (2017). The biochar material with one of the higher surface areas was aspen wood (420 m^2/g). Aspen wood biochar was found to have the lowest adsorption capacity of 0.04 mg/g. In addition it had the lowest AEF reduction for all of the biochar materials produced. Conversely, the biochar material with the highest adsorption capacity and AEF removal was biochar made using wheat straw, which only had a surface area of 20 m^2/g.

One of the key differences between AC and the biochar material is the activation step. The biochar materials highlighted in the study by Bhuiyan et al. (2017) did not go through physical or chemical activation. It is noted by others that physical activation of the biochar will increase the surface area (Inyang and Dickenson 2015). However, the PC used in the above mentioned studies were all instances of PC that was non-activated, but it did not follow a similar pattern as some of the biochar materials. While both the PC and biochar adsorbent material were not activated, it is not easy to compare PC and biochar. PC is more than just the carbonaceous residual left after heating biomass. As mentioned previously, it is comprised of many different types of trace elements.

3.3 References

Ahmad, M., Lee, S.S., Dou, X., Mohan, D., Sung, J., Yang, J.E., and Ok, Y.K. 2012. Effects of pyrolysis temperature on soybean stover- and peanut shell-derived biochar properties and TCE adsorption in water. Bioresource Technology, **118**: 536-544.

Bhuiyan, T.I., Tak, J.K., Sessarego, S., Harfield, D., and Hill, J.M. 2017. Adsorption of acid-extractable organics from oil sands process-affected water onto biomass-based biochar: Metal content matters. Chemosphere, **168**; 1337-1344.

Blanchard, G., Maunaye, M., and Martin, G. 1984. Removal of heavy metals from waters by means of natural zeolites. Water Research, **18**(12): 1501-1507.

Chen, H. and Hashisho, Z. 2012. Fast preparation of activated carbon from oil sands coke using microwave –assisted activation. Fuel, **95**: 178-182.

Coughlin, R.W., and Ezra, F.S. 1968. Role of surface acidity in the adsorption of organic pollutants on the surface of carbon. Environmental Science and Technology, **2**: 291-297.

Crittenden, J.C. 2005. MWH's water treatment: principles and design, 2nd edition. John Wiley & Sons, Hoboken, N.J.

Frankel, M., Bhuiyan, T.I., Veksha, A., Demeter, M.A., Layzell, D.B., Helleur, R.J., Hill, J.M., and Turner, R.J. 2016. Removal and biodegradation of naphthenic acids by biochar and attached environmental biofilms in the presence of co-contaminating metals. Biosource Technology, **216**: 352-361.

Gamal El-Din, M., Fu, H., Wang, N., Chelme-Ayala, P., Perez-Estrada, L., Drzewicz, P., Martin, J.W., Zubot, W. and Smith, D.W. 2011. Napthenic acids speciation and removal during petroleum-coke adsorption and ozonation of oil sands process-affected water. Science of the Total Environment, **409**: 5119-5125.

Ho, Y-S. 2006. Review of second-order models for adsorption systems. Journal of Hazardous Materials, **B136**: 681-689.

Ho, Y-S., and McKay, G. 1998. Sorption of dye from aqueous solution by peat. Chemical Engineering Journal, **70**: 115-124.

Ho, Y-S., and McKay, G. 1999. Pseudo-second order model for sorption processes. Process Biochemistry, **34**: 451-465.

Ho, Y-S., and McKay, G. 2000. The kinetics of sorption of divalent metal ions onto sphagnum moss peat. Water Research, **34**: 735-742.

Inyang, M. and Dickenson, E. 2015. The potential role of biochar in the removal of organic and microbial contaminants from potable and reuse water: A review. Chemosphere, **134**: 232-240.

Iranmanesh, S., Harding, T., Abedi, J., Seyedeyn-azad, F., and Layzell, D.B. 2014. Adsorption of naphthenic acids on high surface area activated carbons. Journal of Environmental Science and Health, Part A, **49**: 913-922.

Islam, M.S., Dong, T., Sheng, Z., Zhang, Y., Liu, Yang, and Gamal El-Din, M. 2014a. Microbial community structure and operational performance of a fluidized bed biofilm reactor treating oil sands process-affected water. International Biodeterioration and Biodegradation, **91**: 111-118.

Islam, M.S., Dong, T., McPhedran, K ,Sheng, Z., Zhang, Y, Liu, Yang, and Gamal El-Din, M. 2014b. Impact of ozonation pre-treatment of oil sands process-affected water on the operational performance of a GAC-fluidized bed biofilm reactor. . Biodegradation, **25**: 811-823.

Islam, M.S., Zhang, Y., McPhedran, K , Liu, Yang, and Gamal El-Din, M. 2015. Granular activated carbon for simultaneous adsorption and biodegradation of toxic oil sands process-affected water organic compounds. Journal of Environmental Management, **152**: 49-57.

Islam, M.S., Zhang, Y., McPhedran, K , Liu, Yang, and Gamal El-Din, M. 2016. Mechanistic investigation of industrial wastewater naphthenic acids removal using granular activated carbon (GAC) biofilm based processes. Science of the Total Environment, **541**: 238-246.

Largitte, L. and Pasquier, R. 2016. A review of the kinetics adsorption models and their application to the adsorption of lead by an activated carbon. Chemical Engineering Research and Design, **109**: 495-504.

Metcalf & Eddy, Inc. 2003. Wastewater Engineering Treatment and Reuse, 4th Edition. McGraw-Hill, New York, N.Y.

Moreno-Castilla, C. 2004. Adsorption of organic molecules from aqueous solutions on carbon materials. Carbon, **42**: 83-94.

Nethaji, S., Sivasamy, A., and Mandal, A.B. 2013. Adsorption isotherms, kinetics and mechanism for the adsorption of cationic and anionic dyes onto carbonaceous particles prepared from *Junglans regia* shell biomass. International Journal of Environmental Science and Technology, **10**: 231-242.

Plazinski, W., Dziuba, J., and Rudzinski, W. 2013. Modeling of sorption kinetics: the pseudo-second order equation and the sorbate intraparticle diffusivity. Adsorption, **19**: 1055-1064.

Pourrezaei, P., Alpatova, A., Chelme-Ayala, P., Perez-Estrada, L., Jensen-Fontaine, M., Le, X.C., and Gamal El-Din, M. 2014a. Impact of petroleum coke characteristics on the adsorption of the organic fractions from oil sands process-affected water. International Journal of Environmental Science and Technology, **11**: 2037-2050.

Pourrezaei, P., Alpatova, A., Chelme-Ayala, Khosravi, K., Drzewicz, P., Chen, Y., Chelme-Ayala, P., and Gamal El-Din, M. 2014b. Removal of organic compounds and trace metals from oil sands process-affected water using zero valent iron enhanced by petroleum coke. Journal of Environmental Management, **139**: 50-58.

Qui, H., LV, L., Pan, B., Zhang, Q-j, Zhang, W-m, and Zhang, Q-x. 2009. Critical review in adsorption kinetic models. Journal of Zheijiang University SCIENCE A, **10**(5): 716-724.

Sawyer, C.N., McCarty, P.L., and Parkin, G.F. 2003. Chemistry for Environmental Engineering and Science, 5th Edition. McGraw-Hill, New York, N.Y.

Small, C., Hashisho, Z., and Ulrich, A.C. 2012. Preparation and characterization of activated carbon from oil sands coke. Fuel, **92**: 69-76.

Villacanas, F., Pereira, M.F.R., Orfao, J.J.M., and Figueiredo, J.L. 2006. Adsorption of simple aromatic compounds on activated carbons. Journal of Colloid and Interface Science, **293**: 128-136.

Wang, L., Zhang, J., Zhao, R., Li, C., Li, Y., and Zhang, C. 2010. Adsorption of basic dyes on activated carbon prepared from *Polygonum orientale* Linn: Equilibrium, kinetic and thermodynamic studies. Desalination, **254**: 68-74.

Zubot, W., MacKinnon, M.D., Chelme-Ayala, P., Smith, D.W., and Gamal El-Din, M. 2012. Petroleum coke adsorption as a water management option for oil sands process-affected water. Science of the Total Environment, **427-428**: 364-372.

4. THE EFFECT OF CARBOXYL MULTIWALLED CARBON NANOTUBES CONTENT ON THE STRUCTURE AND PERFORMANCE OF POLYSULFONE MEMBRANES[1]

4.1 Introduction

The Athabasca oil sands in northern Alberta, Canada are the third largest deposit of oil in the world, however they require large amounts of water to refine due to the extraction of bitumen from oil sands via a hot water extraction process that involves approximately 3 m^3 of water for every m^3 of oil sands processed (Holowenko et al. 2002; Klamerth et al. 2015). Water that has come into contact with the oil sands, referred to as oil sands process water (OSPW), is retained in tailing ponds due to a zero discharge policy but may be recycled for bitumen extraction processes (Zubot et al. 2012). While the recycling of OSPW has decreased the need for freshwater withdrawal from the Athabasca River basin, it has also led to the continual decrease in water quality of OSPW, thus resulting in a complex mixture containing water, organic and inorganic compounds, salts, minerals, suspended solids, dissolved solids, and trace metals (Allen 2008). Prior to release from the tailing ponds into the natural environment, OSPW must be treated (Zubot et al. 2012). Different treatment methods to remediate OPSW have been studied and include: coagulation/flocculation (Kim et al. 2011; Pourrezaei et al. 2011; Pourrezaei et al. 2012), advanced oxidation processes (Afzal et al. 2015; Anderson et al. 2012; Klamerth et al. 2015; Shu et al. 2014; Wang et al. 2016), and adsorption (Gamal El-Din et al. 2011; Pourrezaei

[1] A version of this chapter has been published as: Benally, C., Li, M., and Gamal El-Din, M. 2018. The effect of carboxyl multiwalled carbon nanotubes content on the structure and performance of polysulfone membranes for oil sands process-affected water treatment. Separation and Purification Technology, **199**: 170-181.

et al. 2014; Small et al. 2012; Zubot et al. 2012) and membrane filtration (Alpatova et al. 2014; Dong et al. 2014; Kim et al. 2011; Kim et al. 2012a; Kim et al. 2013; Loganathan et al. 2015; Peng et al. 2004).

Treatment of OSPW with traditional membrane filtrations systems has been applied at different levels. High pressure membrane filtration systems, including nanofiltration (NF) and reverse osmosis (RO), have been used to treat OSPW (Kim et al. 2011; Kim et al. 2012a; Kim et al. 2013; Loganathan et al. 2015; Peng et al. 2004). Of the mentioned studies using high pressure membrane filtration, only Peng et al. (2004) performed high pressure membrane filtration of OSPW with no pre-treatment; however the water treated had low concentrations of suspended solids. Other high pressure membrane filtration studies involved pre-treatment of OSPW by coagulation-flocculation (CF) (Kim et al. 2011), coagulation-flocculation-sedimentation (CFS) (Kim et al. 2012a), and coagulant addition followed by ceramic ultrafiltration (CUF) (Loganathan et al. 2015). The water entering the high pressure membrane filtration systems had to be of elevated quality compared to that of raw OSPW in order to reduce the occurrence of membrane fouling. Low pressure membrane filtration systems, including microfiltration (MF) and ultrafiltration (UF), have also been used to treat OSPW (Alpatova et al. 2014; Dong et al. 2014). MF and UF membrane treatment have the advantage of producing high quality permeate at lower costs with little or no pre-treatment involved (Dong et al. 2014; Zaidi et al. 1992). Dong et al. (2014) and Alpatova et al. (2014) investigated the use of ceramic MF and UF membranes for OSPW treatment. Kim et al. (2013) fabricated polysulfone (PSU) UF membranes as pre-treatment for high pressure membrane filtration.

Polysulfone (PSU) is a polymer commonly used to form membranes for wastewater treatment due to its chemical and structural stability combined with mechanical robustness

(Richards et al. 2012). The main drawback of using PSU is its hydrophobic nature, which can lead to an increase in membrane fouling (Blanco et al. 2006). Inclusion of relatively hydrophilic nanoparticles within the polymer matrix can result in decreased surface hydrophobicity, increased permeate flux, and decreased membrane fouling (Kim et al. 2013). Carbon nanotubes are the most widely used nanoparticle in membrane applications because they possess excellent mechanical, electrical, thermal, and antibacterial properties, as well as the ability to adsorb organic compounds (Kim et al. 2013). A previously mentioned study by Kim et al. (2013) focused on the use PSU/multi-walled carbon nanotube (MWNT) membranes to pre-treat OSPW prior to high pressure membrane filtration. In addition, the study investigated the combined effect of low pressure membrane filtration with PSU membrane containing 0 or 10 wt. % MWNT followed by high pressure membrane filtration. The effect of varying the casting components was not major a factor in the study. Other literature suggests that an optimum loading of MWNT in PSU should lie below 4 wt. % (Choi et al. 2006; Qui et al. 2009).

In the present study, the effect of adding mMWNT to low pressure UF PSU membranes is studied in more detail, especially as it pertains to the membrane morphology formation and basic filtration performance. The sole effect of varying mMWNT content is investigated by omitting pore forming agent polyvinylpyrrolidone (PVP). Acid modification of MWNT is by-passed by procuring COOH modified MWNT (mMWNT) for incorporation into PSU membranes. The objectives of the present study were to: (1) fabricate polymeric nanocomposite membranes using polysulfone (PSU) and varying amounts of -COOH modified multi-walled carbon nanotubes (mMWNT), (2) evaluate the effect of casting mixture composition on resulting membrane morphology and pore size, and (3) evaluate the effect of casting mixture composition on membrane pure water flux and rejection.

4.2 Experimental methods and materials

4.2.1 OSPW and chemicals

Raw OSPW was collected from an oil sands tailing pond in Fort McMurray, Alberta, Canada and stored in a cold room at 4°C. Polysulfone (PSU), polyethylene glycol (PEG), and ACS grade N,N-dimethylformamide (DMF) were all purchased from Sigma-Aldrich (St. Louis, MO, USA). MWNT (average inner diameter: 5-10 nm, length: 10-30 μm) modified with carboxylic acid groups (-COOH) were purchased from Sun Innovations Incorporated (Freemond, CA, USA). Barium chloride ($BaCl_2$), iodine (I_2), hydrochloric acid (HCl), sulfuric acid (H_2SO_4) and potassium iodide (KI) were purchased from Fisher Scientific (Ottawa, ON, Canada). Milli-Q water was produced using a Milli-Q Ultrapure Water System (Millipore Corporation, Bedford, MA, USA).

4.2.2 Membrane preparation

PSU pellets were dried at approximately 150°C for 4 hours and dissolved in enough DMF to produce a solution with a 15/85 weight percent composition of PSU/DMF. The solution was stirred for 24 hours at 50°C and kept in a dark environment (covered with foil) to reduce bubble formation (Kim et al. 2012b). The nanoparticle, mMWNT, was added to the PSU/DMF solution in the following weight percent ratios of PSU to mMWNT: 100/0, 99.8/0.2, 99.5/0.5, 99/1, 98/2, 95/5. Each membrane mixture was sonicated for approximately 15 minutes to break up mMWNT aggregates and then gently stirred with no heat for approximately 24 hours. PSU nanocomposite membranes were fabricated by immersion precipitation phase inversion casting method (Ballinas et al. 2004). In general, the immersion precipitation phase inversion method involves the casting of a thin film of polymer/solvent solution onto a support, which is then placed into a non-solvent

bath where simultaneous diffusion of solvent into the non-solvent bath, and diffusion of non-solvent into the polymer/solvent film will lead to thermodynamic instability and instant liquid-liquid demixing whereby the membrane is formed (Mulder 2000).

For each membrane mixture, approximately 10 g of solution was poured onto a level, dry glass plate. A stainless steel Doctor-Blade casting knife was used to cast the membrane solution onto the glass substrate in a film with a thickness of approximately 100-150 μm. After 30 seconds of exposure to room temperature air, the glass plate was submerged in a room temperature Milli-Q water bath until the membrane detached from the glass surface and there was no further water movement due to the diffusion of DMF from the casted film and diffusion of water into the film. Fabricated membranes were rinsed, placed in a container with fresh Milli-Q water, and stored at 4°C. The membranes fabricated for this study were assigned a sample name in the given format: mMWNT-x, where x is the wt. % content of mMWNT in the corresponding fabricated membrane (see Table 4.1).

Table 4.1 Composition of casting mixtures and fabricated membranes.

	Composition of casting mixture (wt. %)			Solid membrane composition (wt. %)	
Sample name	PSU	DMF	mMWNT	PSU	mMWNT
mMWNT-0	15	85	0	100	0
mMWNT-0.2	15	84.97	0.03	99.8	0.2
mMWNT-0.5	14.99	84.94	0.07	99.5	0.5
mMWNT-1	14.98	84.87	0.15	99	1
mMWNT-2	14.95	84.75	0.30	98	2
mMWNT-5	14.89	84.37	0.74	95	5

4.2.3 Membrane characterization

Fabricated membranes were characterized by two main methods: contact angle and scanning electron microscopy (SEM) in conjunction with imaging software. Using the imaging software in conjunction with SEM images, membrane pore size was estimated.

To characterize membrane surface wettability (hydrophilicity), contact angle measurements were determined by the sessile drop method (membrane roughness was ignored). The contact angle is the angle that is formed by the liquid-solid interface line and the line that is tangent to the liquid-vapor interface when a drop of water is placed upon the surface of interest (Yuan et al. 2013). A smaller contact angle indicates that the surface was hydrophilic enough for the water drop to spread out, whereas a larger contact angle will indicate that the surface was not as hydrophilic and that water contained within the droplet minimized its contact with the surface by spreading out upon the surface to a lesser degree. Fabricated membranes were dried and the support side (dull side) of the membrane was attached to a glass slide with the membrane side of interest (selective or support) facing up. For each membrane sample 6-7 drops of Milli-Q water were applied along the membrane surface (sessile drop method) and the resulting contact angles were measured using a contact angle goniometer (FTA-200, First Ten Angstroms). The average of the resulting contact angle measurements was calculated along with the standard deviation. Each contact angle was reported to the nearest integer with an error of +/- 2°.

The membrane support surface and cross section morphologies were imaged using a low resolution scanning electron microscope (SEM) (Vega-3, Tescan) operating in high vacuum mode using a voltage setting of 10-20 kV. Secondary electron images were acquired. Preparation of the cross section samples involved the cutting of the membrane sample, three different methods were used: simple cutting with scissors, a quick cut method with a razor blade, and

finally samples were placed into liquid nitrogen until stiff and then snapped in half to produce a clean edge. The support membrane surface and cross section samples were mounted to pin stubs and coated with gold using a sputter coater (Sputter Coater S150B, Edwards) for approximately 1 minute to make the samples electrically conductive. Selective membrane surface samples were analyzed by the University of Alberta Department of Earth and Atmospheric Sciences Scanning Electron Microscope Laboratory using a field-emission SEM (Sigma 300 VP, Zeiss) with finer resolution at higher magnification for visualization of the smaller pores. Secondary electron images were acquired using an in-lens detector. The selective membrane samples were coated with carbon for approximately 1 minute to make the samples electrically conductive and analyzed at 100 kx magnification.

The pore size of fabricated membranes was estimated using the SEM micrographs in combination with imaging software (ImageJ and Image-Pro Plus). The support layer of the fabricated membranes was analyzed using ImageJ software and the selective layer was analyzed using Image-Pro Plus software. For the support layer, three different images of each membrane type were used for the analysis. For the analysis performed the SEM images used had been magnified 5 kx and had an area of 1559 μm^2. With each image, first the scale was set using the length of the scale bar and entering in the known distance and the unit of length. Next, the image was changed to an 8-bit image (under Type option) and the threshold was adjusted manually. It is important to note that the threshold is adjusted so that it is a good binary representation of membrane. Ideally only the pores would be showing. However, this is not always possible. So the threshold is adjusted so that it returns a binary representation of the membrane in which a majority of the sections that are colored, or absent of color, are the pores themselves. Finally the pores were analyzed using the Analyze Particles option under Analyze in the toolbar. This

returned information such as area, mean, min, max, and length for each pore. For each area, the average pore size was determined. For each membrane, the average of the average pore size for each area analyzed was reported with the standard deviation showing the error between the average pore size values.

The selective surfaces of the membranes were analyzed by the use of Image-Pro Plus. A very similar method to that used for the support side analysis was used for the selective side. The SEM micrographs of the selective membrane surfaces were magnified at least 100k x. Under high magnification the surface unevenness was amplified which greatly affected adjustment of the image threshold. This was solved by flattening the image with the software and by analysis of smaller membrane surface areas (11000 nm^2 – 80000 nm^2). As with the support side, the threshold was adjusted so that it returned a binary representation of the membrane area in which a majority of the sections that are colored, or absent of color, were the pores themselves. Finally the pores were analyzed using the "Count and measure objects" option in the toolbar.

4.2.4 Membrane permeability

The pure water permeate flux of fabricated membranes was determined with Milli-Q feed water and the use of a dead-end low pressure membrane filtration system shown in Figure 4.1. The membrane filtration systems consists of a custom made stainless steel cell, one gear pump (Model GJ-N21.PF2S.A, Micropump Inc.), one gear pump drive (Model 75211-10, Cole-Parmer Instrument Company), one electronic balance (Adventurer Pro model AV8101, Ohaus), and a data acquisition system. Milli-Q water from a feed tank was pumped into the dead end filtration membrane cell and through the membrane coupon. Permeate was collected and measured with an electronic balance attached to a data acquisition system. The balance was set to record the mass of permeate every 15 seconds.

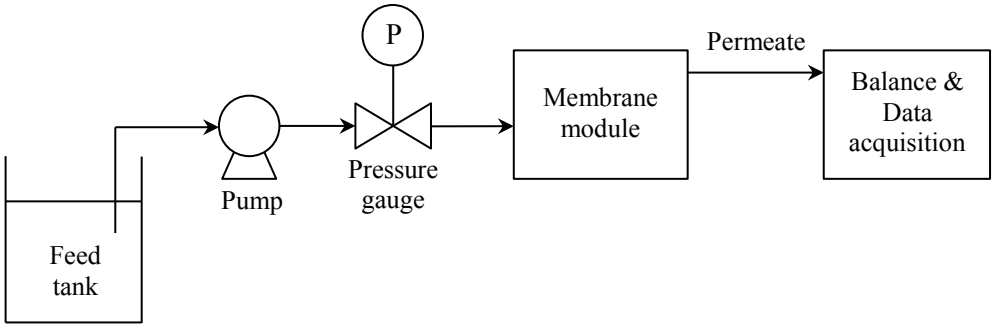

Figure 4.1 Schematic of dead-end low pressure membrane filtration system used to conduct membrane permeability tests.

Fabricated membranes were cut into circular coupons with an approximate diameter of 67 mm (effective membrane diameter was 45 mm) and placed into the membrane cell with the selective surface facing the flow of water. Membranes were compacted at 400 kPa with Milli-Q water for at least 90 minutes, or until a steady state flux was obtained. To gain a quick understanding of how the pure water flux varied with respect to operating pressure, for each membrane the transmembrane pressure (TMP) was varied from 200-600 kPa, in 100 kPa increments. The membrane was allowed to flow for a short period of time (~15 minutes) while the weight of permeate was recorded for each TMP. The permeate flux of Milli-Q water, J_0 ($L \cdot m^{-2} \cdot h^{-1}$), was calculated using equation 4.1.

$$J_O = \frac{V}{At} \qquad (4.1)$$

V (L) is the volume of permeate passing through the membrane; A (m^2) is the effective membrane area; and t (min) is the filtration time. For this study, the effective membrane area used was 15.9 cm^2. To gain a better understanding how pure water flux at TMP of 400 kPa could vary as a function of mMWNT added, longer pure water flux filtration studies were performed whereby the water was allowed to flow at least 60 minutes. This included a period of time that a

membrane may take to reach steady flow once began. Equation 4.1 was used to calculate permeate flux for the longer filtration pure water flux studies.

4.2.5 Membrane rejection

The selectivity of the fabricated membranes was evaluated by performing rejection tests using 1 g/L PEG (3 to 100 kDa) solutions. The selectivity tests were conducted using the dead-end low pressure membrane filtration system (described in section 2.4) operating at a TMP of 400 kPa. The membranes used for the rejection testing were the fabricated membranes that had already been compacted with Milli-Q water at a TMP of 400 kPa. The concentration in the feed was known (1 g/L) and the concentration in resulting permeate was determined by a colorimetric method (Sabde et al. 1997) in combination with UV/visible spectrophotometry. First 4 ml of sample solution was added to 1 ml of 5% w/v $BaCl_2$ in 1M HCl. Then 1 ml of 5 mM I_2 in 0.2% w/v KI was added. After a reaction time of 5 minutes, the mixture was read at 535 nm against a reagent blank using a spectrophotometer (Genesys 10S UV-Vis, Thermo Scientific). The rejection (R%) was calculated using equation 4.2.

$$R(\%) = \left(1 - \frac{C_p}{C_f}\right) \times 100 \qquad (4.2)$$

Where:

C_f (g/L) is the concentration of PEG in the feed solution

C_p (g/L) is the determined concentration of PEG in the permeate stream.

4.3 Results and discussion

The characterization results for the fabricated membranes are given in the following sections: contact angle, membrane morphology and pore size, membrane permeability and membrane rejection.

4.3.1 Contact angle

The hydrophilicity of the fabricated PSU membranes containing varying amounts of mMWNT was evaluated by the determination of surface contact angle. The results for the support and selective membrane surfaces for each fabricated membrane are shown in Figure 4.2. In general, a lower contact angle is indicative of a more hydrophilic surface with higher water permeability possibly due to increased water uptake and water diffusivity (Kim et al. 2012b). In addition, hydrophilic surfaces are found to be less prone to fouling caused by the attachment of bacteria, natural organic matter (NOM) or proteins to the surface of the membrane (Zhu et al. 2013). Therefore, membrane selective surfaces that are more hydrophilic, and thus have smaller contact angles, are preferred and may result in higher permeate flux and less membrane fouling. Sample mMWNT-0, PSU with no added mMWNT, had the highest selective surface contact angle (96° ± 4°) and support surface contact angle (73° ± 3°) and was the most hydrophilic of all membranes fabricated for this study.

Addition of mMWNT (0.2 wt.% through 5 wt.%) resulted in a decreased average contact angle of the selective surface of the fabricated membranes ranging from 78° ± 2° to 73° ± 2°. Membrane sample mMWNT-5 had the lowest average contact angle (73° ± 2°) resulting in the selective membrane surface that was the most hydrophilic of all fabricated membranes. The trend of increased surface hydrophilicity with increasing mMWNT content has been noted in similar

membrane modification studies using modified MWNT. An increase in hydrophilicity with increase of acid modified MWNT content was reported by Kim et al. (2012b). In a different study, Kim et al. (2013) noted that an increase of acid modified MWNT content (0 to 10 wt. %) in PSU membrane with polyvinylpyrrrolidone (PVP) resulted in a large decrease in contact angle from approximately 74° to 55°. Qui et al. (2009) observed a decrease in contact angle with increasing amounts of functionalized MWNT up to 0.19 wt.%, and then an increase in contact angle for further additions of functionalized MWNT (up to 0.5 wt.%) in PSU with a fabric support. Choi et al. (2006) reported a decrease of contact angle for increasing amount of acid modified MWNT (up to 4 wt.%) incorporated within a PSU membrane. For the mentioned studies it is hypothesized that the decreasing contact angle of the inspected membrane surface is a direct result of the functional groups (carboxyl and hydroxyl functional groups) contained within the MWNT that result from acid modification (Kim et al. 2012b; Kim et al. 2013). In the study by Choi et al. (2006), a contact angle decrease of approximately 7° occurred between PSU membranes containing 0.5 and 1 wt. % of acid modified MWNT. This same trend is not seen in Figure 4.2. When error bars are taken into account, membrane samples mMWNT-0.2, mMWNT-0.5, mMWNT-1, and mMWNT-2 had roughly the same increase in hydrophilicity of the selective surface of the membranes when compared with mMWNT-0.

A key difference between the membranes fabricated in the current study and the studies by Choi et al. (2006) and Kim et al. (2012b; 2013) was the in the modification of the added MWNT. For this particular study, MWNT used were obtained pre-modified with only carboxyl functional groups, while the MWNT in the studies by Choi et al. (2006) and Kim et al. (2012b; 2013) were acid modified and contained both hydroxyl and carboxyl functional groups. The results suggest

that the hydroxyl functional groups present on the acid modified MWNT played a large role in increasing the hydrophilicity of the selective surface of the PSU membranes.

The resulting range of contact angles obtained for the support side of fabricated membranes was not as large as that observed for the corresponding selective membrane surfaces, 72 ° ± 3° to 64° ± 3°. However the trend of decreasing contact angle with increasing mMWNT content is observed. Overall the contact angles for the support side of the membranes are lower than the selective membrane surfaces. The support sides of the membranes are more hydrophilic, however they are also more porous. Initially one might assume that the support side might have more mMWNT that have migrated to the surface to affect the resulting contact angle. However, taking in to account the large pore size of the support layer it may be possible that the water droplet has a greater surface area to interact with due the large surface pores and the water may even enter into the pores of the support side of the membranes, thereby decreasing the contact angle of the water droplet.

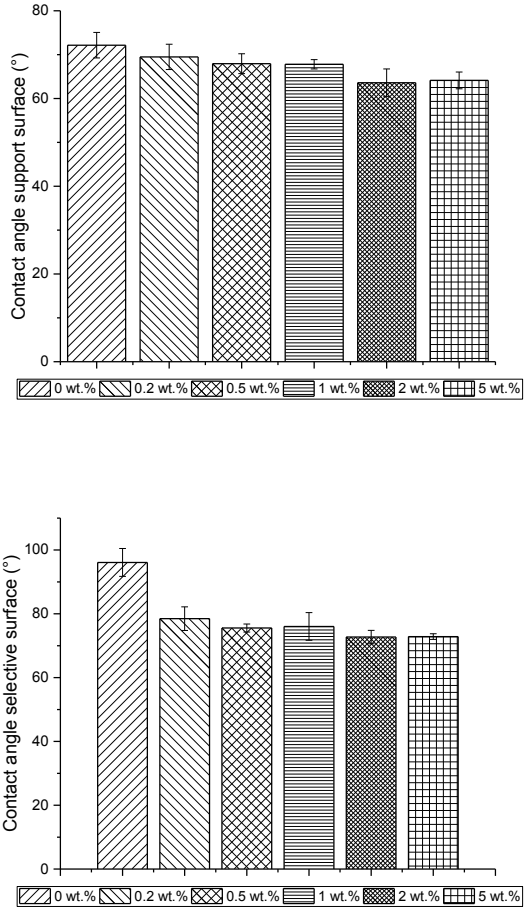

Figure 4.2 Contact angle for the support and selective surface of PSU with varying amounts of mMWNT.

4.3.2 Membrane morphology

SEM images of the fabricated membrane selective surfaces and cross sections were obtained in order to analyze the effect of mMWNT content on the morphology of the PSU membrane. Figure 4.3 shows the resulting cross sectional images obtained for the three different methods of sample preparation. Figure 4.4 shows SEM images of the selective layer with an inset showing the SEM cross section using the direct freeze fracture preparation method. Figure 4.5 shows SEM images of the support layer. Table 2 adds quantitative data to Figures 4.4 and

4.5 by displaying the average pore diameter for the selective and support surfaces of the fabricated membranes.

Cross sectional images can allow one to view the structures formed inside a membrane. While this sounds simple, it was found that preparation techniques play a large role in obtaining ideal samples needed. Much of the literature reviewed had little to no mention for preparation techniques used for cross sectional SEM imaging. The methods used for this research included scissor sectioning, razor sectioning, and finally direct freeze fracture using liquid nitrogen (Ferlita et al. 2008). Figure 4.3 shows the results of three different methods of cross sectional sample preparation methods. Using scissors, the membrane samples were effectively pinched together (Figure 4.3a). The quick cut method using a sharp razor blade resulted in a cross section that had more detail but still showed deformation of the polymer (Figure 4.3b). Finally, the direct freeze fracture method led to samples with crisper edges and minimal deformation of the polymer. Scissor and razor sectioning cross sectional sample preparation methods were not used for further analysis of the membrane morphologies. The cross sectional images presented in Figure 4.4 use the direct freeze fracture preparation method.

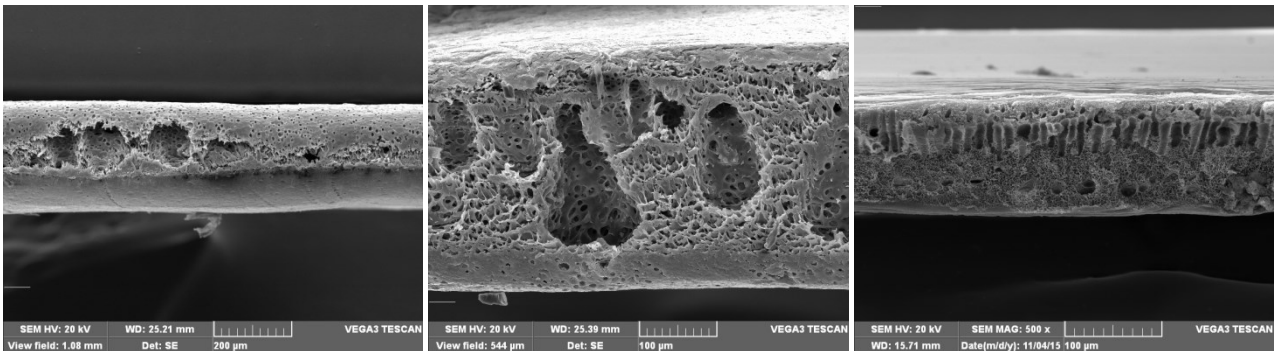

a **b** **c**

Figure 4.3 Cross sectional SEM images of membrane samples (a) mMWNT-0.5 membrane prepared by scissor sectioning, (b) mMWNT-0.5 membrane prepared by razor sectioning, and (c) mMWNT-1 membrane prepared by direct freeze fracture.

PSU membrane samples mMWNT-0, mMWNT-0.2, and mMWNT-0.5 (Figure 4.4 a-c) have finger pores that traverse at least half of the length of the cross section from top to bottom. For the plain PSU membrane (sample mMWNT-0) finger pores are fairly uniform in length, straight in shape, and travel along a path that is approximately 90° to the horizontal (Figure 4.4 a-xs). Addition of mMWNT in small amounts (0.2 and 0.5 wt. %) resulted in finger pores that were slightly curved in shape and were slanted in comparison to membrane sample mMWNT-0. Additionally, for membrane sample mMWNT-0.5, noticeable voids in the support area of the membrane are visible (Figure 4.4 c-xs). When a higher loading of mMWNT (1-5 wt. %) is incorporated into the membranes, a noticeable pore structure change is shown in Figure 4.4 d-f (xs). Membrane samples mMWNT-1 and mMWNT-2 (Figure 4.4 d-xs & e-xs) have finger pores that are larger in width, shorter in length and less uniform when compared with mMWNT-0. Membrane sample mMWNT-5 ceases to have uniform finger pores but does display an array of macro voids (Figure 4.4 f-xs).

The formation of finger pores, or macro voids (MSs) can be explained by the two step mechanism model for the formation of membranes (Young et al. 1995). Initially, the top layer of

solvent in the casted film will diffuse almost instantaneously into the non-solvent bath thereby forming a dense skin on the top layer. The dense skin layer will then have an effect on the formation of the sublayers in the membrane. If the skin layer restrains diffusion of solvent out of the casted film but allows non-solvent into the membrane then a sublayer with many pores or MVs will form. If the skin layer does not restrict diffusion of the solvent but does restrict non-solvent, then a dense sublayer with few pores will form. Additionally, formation MVs can be due to the liquid-liquid de-mixing process of the solvent/non-solvent during phase inversion (Ballinas et al. 2004).

Usually MVs are formed when the solvent and non-solvent exchange at a lower rate (Young et al. 1995). Addition of surfactant molecules in the polymer solution can reduce interfacial tension gradient between MV and the casting solution, thus resulting in less MV formation and a lower MV size (Ballinas et al. 2004). While the mMWNT are not surfactants themselves, they may act to decrease the surface tension between the solvent and non-solvent during phase inversion. The trend of diminishing finger pores voids is notable in the cross sectional SEM images as higher amounts of mMWNT is added to the PSU matrix. Also, adding more mMWNT results in a denser sponge-like layer in the fabricated membranes. This can be explained by the increase of viscosity of the PSU/mMWNT casting solution due to addition of increasing amounts of mMWNT. This results in delayed phase separation during phase inversion (Celik et al. 2011).

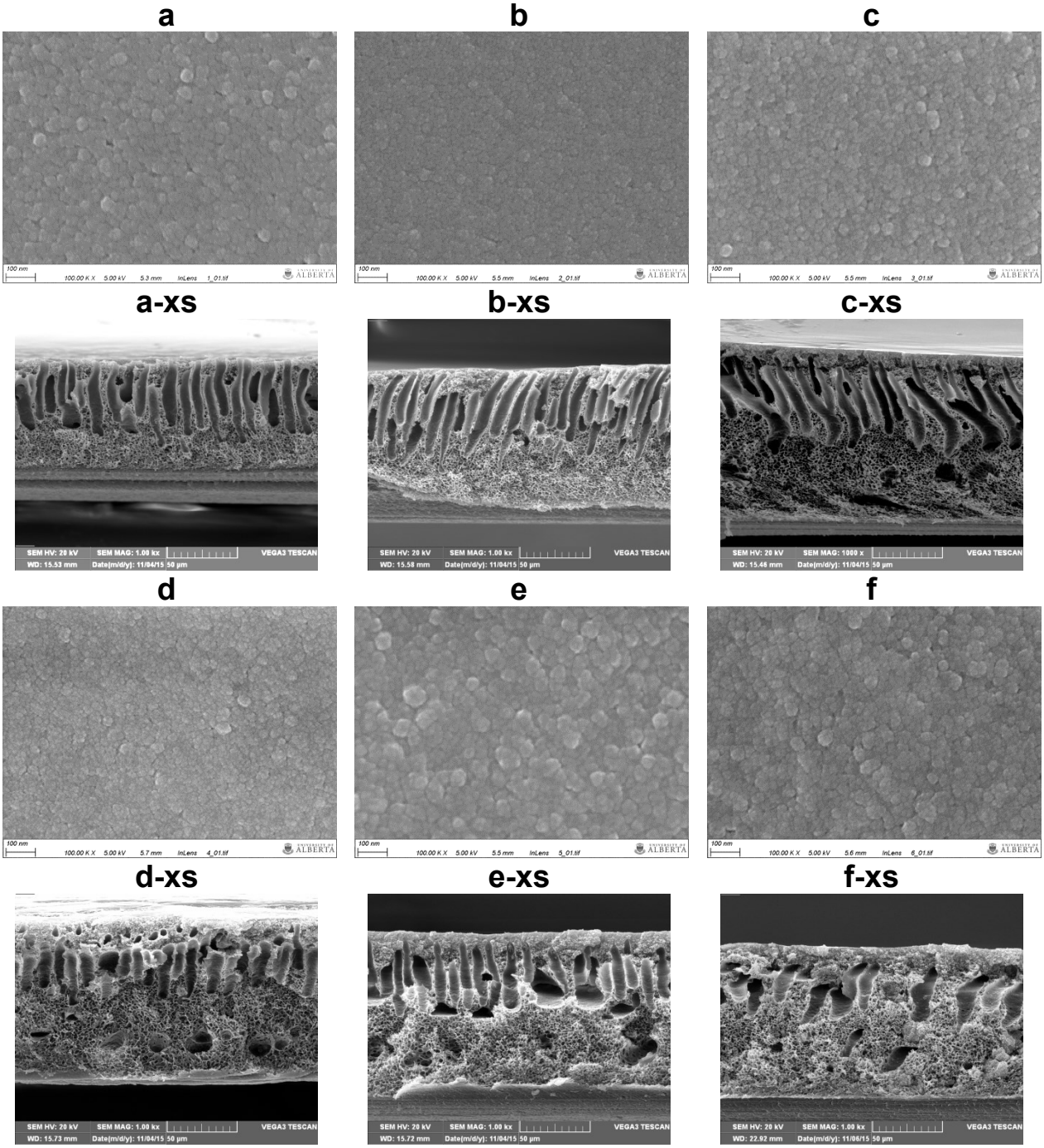

Figure 4.4 SEM images shown at 100k x magnification of selective layer of PSU membrane with the following wt.% of added mMWNT: (a) 0, (b) 0.2, (c) 0.5, (d) 1, (e) 2, and (f) 5. SEM images with the ending "-xs" are cross sectional images taken at 1k x magnification. The support layer is shown on the bottom of the membrane cross section and the skin layer is located at the top of the membrane cross section.

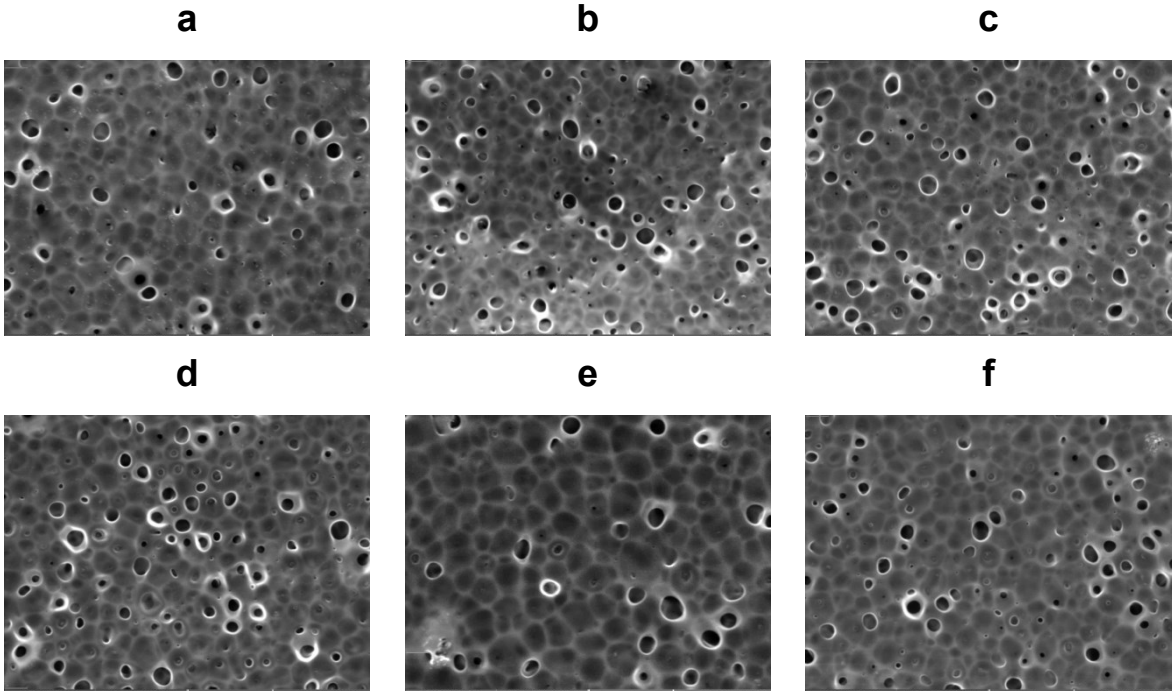

Figure 4.5 SEM images at approximately 5 kx magnification of support layer of PSU membrane with the following wt. % of COOH modified MWNT added: (a) 0, (b) 0.2, (c) 0.5, (d) 1, (e) 2, and (f) 5.

SEM images of the selective layer of the fabricated membranes at 100kx magnification are shown in Figure 4.4. Addition of 0.2, 0.5 and 1 wt.% mMWNT to PSU led to selective surfaces (Figure 4.4 b-d) with pores that are visually finer when compared with those seen on plain PSU (Figure 4.4 a). This is supported by the decrease in selective surface average pore diameter for addition of 0.2, 0.5, and 1 wt. % mMWNT as compared with plain PSU, found in Table 4.2. Further addition of mMWNT (2 and 5 wt. %) result in a selective surface that is visually rougher than that of plain PSU. This is supported by the increase in selective surface average pore diameter for addition of 2 and 5 wt. % mMWNT when compared with plain PSU (Table 4.2).

From Figure 4.5 it can be seen that the support surface of the fabricated membranes have pores that are much larger in size than those found on the selective membrane surface (Figure 4.4). Pores formed on the support surface of fabricated membranes are about 125 times greater

in size than the pores formed on the selective surface (Table 4.2). In comparison to membrane mMWNT-0, the average support surface pore size decreases with addition of mMWNT, the exception is membrane mMWNT-2. As mentioned in section 4.3.1, the existence of the larger pores on the support side of the fabricated membranes may have had a big effect on resulting lower contact angles obtained for the support surfaces as compared with the selective surfaces.

Table 4.2 Support and selective surface average pore size for fabricated membranes determined using SEM images and imaging software (ImageJ and Image-Pro Plus).

Sample	Support side pore diameter			Selective side pore diameter		
	average (μm)	min (μm)	max (μm)	average (nm)	min (nm)	max (nm)
mMWNT-0	0.73 ± 0.03	0.11	2.48	5.7 ± 0.2	4.8	6.5
mMWNT-0.2	0.63 ± 0.06	0.06	1.73	5.1 ± 0.1	4.6	5.7
mMWNT-0.5	0.64 ± 0.06	0.06	2.16	5.2 ± 0.1	4.6	5.8
mMWNT-1	0.64 ± 0.07	0.06	2.38	5.5 ± 0.1	4.6	6.3
mMWNT-2	0.93 ± 0.08	0.06	2.72	5.9 ± 0.1	4.9	7.0
mMWNT-5	0.64 ± 0.02	0.05	2.42	5.9 ± 0.1	4.9	6.9

4.3.3 Membrane permeability

Figure 4.6 shows (a) the pure water flux for PSU membranes with varying amounts of mMWNT as a function of operating pressure and (b) the effect of mMWNT content within the PSU casting solution on the pure water flux of the fabricated membranes for one operating pressure of 400kPa. Figure 4.6 a shows a trend that is common for many pure water permeation studies through membranes, for all fabricated membranes an increase in operating pressure results in a higher pure water flux (Choi et al. 2006). The higher TMP adds more force to push more water through the membrane. Figure 4.6 b shows that the pure water flux at 400 kPa initially decreases with additions of 0.2 wt. % and 0.5 wt. % mMWNT. Further addition of mMWNT (1, 2, and 5 wt. %) within the PSU membrane results in an increase in water permeation for TMP of 400 kPa.

Similar studies suggest that further addition of mMWNT loading within the membrane may result in an eventual decrease in resulting water permeation. Qui et al. (2009) found that a maximum pure water flux occurred for the PSU membranes with 0.19 wt. % MWNT added. Choi et al. (2006) found that the pure water flux was a maximum for the PSU membranes containing 1.5 wt. % MWNT, and decreased with further additions of MWNT (up to 4 wt. %). The trend commonly seen is increasing water flux with increasing addition of MWNT up to a certain point, and then a decreasing pure water flux with further addition of mMWNT. No previous studies involving PSU membranes and MWNT have shown a trend showing an initial decrease in water permeation with addition of mMWNT, followed by an increase in water permeation with further addition of mMWNT as shown in Figure 4.6 b. The trend observed in Figure 4.6 b is similar to that observed in Table 4.2, specifically for the reported selective side average pore diameter values. The lowest flux values occur for mMWNT-0.2 and mMWNT-0.5,

while the lowest average pore diameter values occur for the same two membranes. If error bars on Figure 4.6 b are taken into account, highest pure water flux occurs for additions of 2 and 5 wt. % mMWNT. This is in agreement with the average pore size values reported in Table 2. This suggests that pore size diameter on the selective surface of the membrane has a large influence on the pure water flux. Ohya et al. (1998) reported results which showed that increase in pore size led to a higher pure water flux for glass membranes.

While water flux can be affected by pore size, the change in membrane morphology due to addition of MWNTs can also affect pore size. Laninovic (2005) demonstrated that addition of nonsolvent additives in polymer solutions can lead to a decrease in water flux largely due to changes in membrane morphology. As seen in Figure 4.4 a-xs, the finger pores formed in plain PSU traverse over half the membrane thickness and are unidirectional and perpendicular to the membrane skin layer, all of which lead to a membrane that will give less hydrodynamic resistance, and thus a higher water flux (Laninovic 2005). Examination of the cross sections of membranes mMWNT-0.2 (Figure 4.4 b-xs) and mMWNT-0.5 (Figure 4.4 c-xs) show that the while the finger pores are present, they are less unidirectional or not perpendicular to the membrane skin layer. These changes in membrane morphology, in combination with the decrease in membrane pore size, may be the main factors which result in the decreased pure water flux for mMWNT-0.2 and mMWNT-0.5.

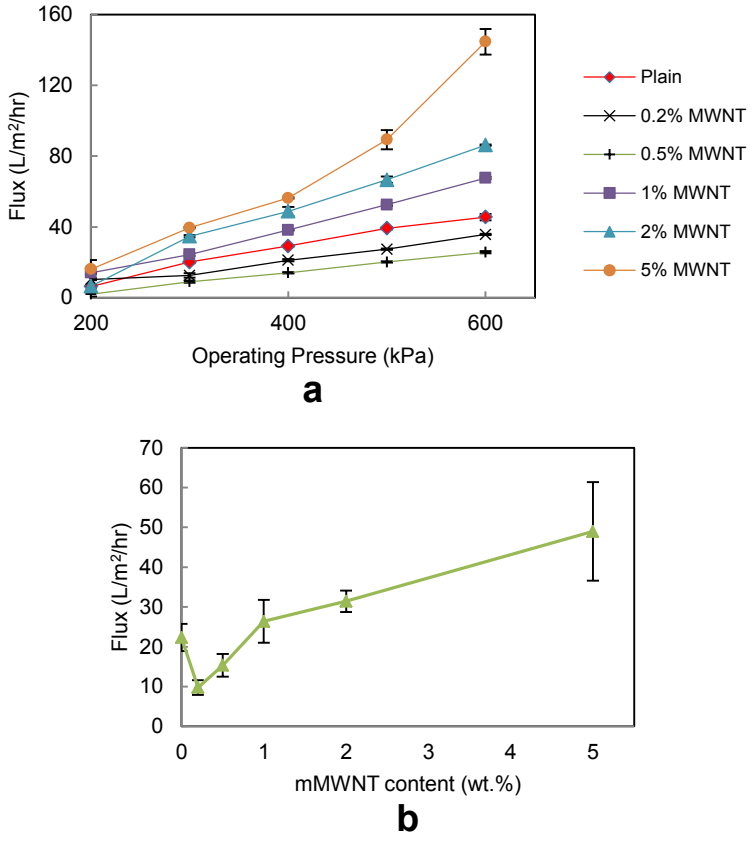

Figure 4.6 Pure water flux as a function of: (a) operating pressure for different mMWNT content (wt. %), short filtration time and (b) mMWNT content (wt. %) for operating pressure of 400 kPa, long filtration time.

4.3.4 Membrane rejection

Figure 4.7 shows the permeate flux and the rejection ratio of 1 g/L solution of PEG (100 kDa) through the fabricated PSU membranes with varying amounts of mMWNT at transmembrane pressure of 400 kPa. All fabricated membranes containing mMWNT had a higher rejection when compared with plain PSU membrane. The highest rejection, 92.3%, occurred with mMWNT-0.2. Membrane samples mMWNT-0.5 and mMWNT-2 had the second and third highest rejection, 84.3% and 83.1%. The decrease in pore size for mMWNT-0.2 and mMWNT-0.5 (Table 2) are likely a major factor in the higher rejection values for these membranes. Decreased selective surface average pore sizes and changes in membrane

morphology resulted in a decrease in pure water flux, so a decrease in the amount of PEG 100 kDa going through these particular membranes can be explained partially by the variance of selective side average pore size.

The initial flux of PEG through the membranes was followed a pattern similar to that for the pure water flux in Figure 4.6 b, with the exception of membrane mMWNT-1. The pure water flux for membrane mMWNT-1 was higher than that for membranes mMWNT-0.2 and 0.5. In the case of the PEG flux, mMWNT-1 has the lowest initial flux at 11.6 $L/m^2/h$. This may be due to variation from membrane to membrane.

While membrane mMWNT-0.2 has the highest rejection, it also took one of the longest time periods for the PEG filtration to occur when compared with all other membrane samples because it had the second lowest flux. The next highest rejection occurs with membrane mMWNT-0.5, however this membrane had the third lowest PEG flux for all six membranes. Sample mMWNT-2 resulted in a rejection only 1.225% less than that given for mMWNT-0.5 but with a PEG flux over twice that which resulted for mMWNT-0.5.

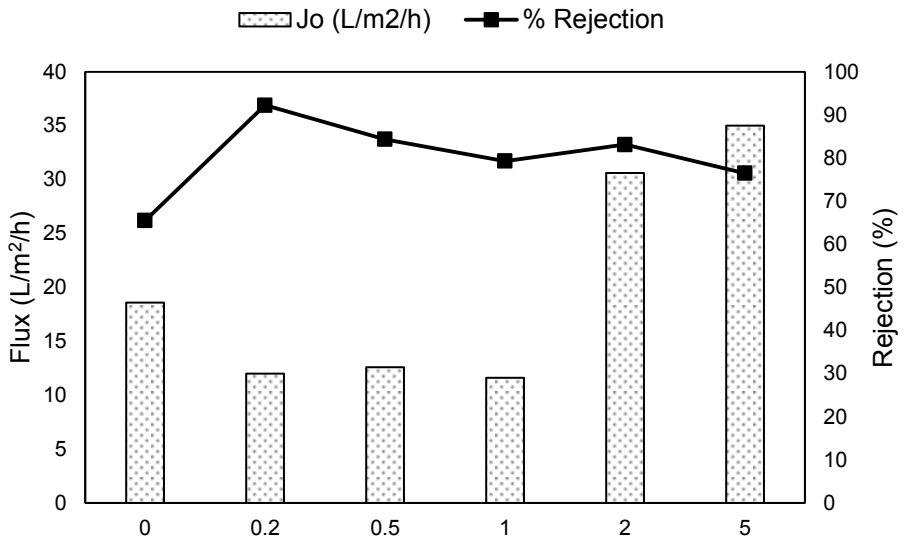

Figure 4.7 Initial flux (J_0) and rejection (%) of PEG (average molecular weight 100 kDa) by PSU membranes with the indicated wt.% mMWNT content at a constant TMP of 400 kPa.

4.4 Conclusions and future experiments

This study investigated the effect of incorporating -COOH modified MWNT within low pressure PSU membrane and how this affects membrane structure formation and performance. Nanocomposite PSU membranes containing 0, 0.2, 0.5, 1, 2 and 5 wt. % -COOH modified MWNT were fabricated by the phase inversion casting method. Addition of mMWNT to PSU resulted in increased hydrophilicity of selective membrane surface due to the presence of the carboxyl groups on the MWNT. Small addition of mMWNT (up to 1 wt. % mMWNT) resulted in decreased average pore size on the selective membrane surface, after which further addition of mMWNT resulted in an increased selective surface average pore size. Pure water flux followed the same general trend, decreasing with small additions of mMWNT (up to 0.5 wt. %), followed by an increasing pure water flux with higher addition of mMWNT (1 wt. % to 5 wt. %). PEG flux had a similar but varied pattern, it decreased with small addition of mMWNT (up to 1 wt. %), followed by increase in PEG flux with higher addition of mMWNT (2 and 5 wt. %). All

nanocomposite membranes had a higher rejection of 100 kDa PEG than plain PSU membrane. The highest rejection, 92.3%, occurred with mMWNT-0.2, however a fairly high rejection combined with high PEG flux resulted for mMWNT-2.

When taking both rejection and water permeability into account, it would be interesting to further investigate the performance of samples mMWNT-0.2 and mMWNT 2 with respect to OSPW filtration. Membranes mMWNT-0.2 and mMWNT-2 give fairly high PEG rejections, with membrane mMWNT-2 giving a pure water flux and PEG flux which are both double that for membrane mMWNT-0.2. Additionally, membrane mMWNT-0 should be included in the OSPW filtration experiments as a control sample. The study could also include the analysis of the filtration of OSPW to determine plausible fouling mechanisms involved. Finally the raw OSPW and resulting permeate should be analyzed to show how the effect of the mMWNT on the resulting permeate water quality.

4.5 References

Afzal, A., Chelme-Ayala, P., Drzewicz, P., Martin, J.W., and Gamal El-Din, M. 2015. Effects of Ozone and Ozone/Hydrogen Peroxide on the Degradation of Model and Real Oil-Sands-Process-Affected-Water Naphthenic Acids. Ozone: Science and Engineering, 37: 45-54.

Allen, E.W. 2008. Process water treatment in Canada's oil sands industry: I. Target pollutants and treatment objectives. Journal of Environmental Engineering and Science, **7**: 123-138.

Alpatova, A., Kim, E-S, Dong, S., Sun, N., and Chelme-Ayala, P. 2014. Treatment of oil sands process-affected water with ceramic ultrafiltration membrane: Effects of operating conditions on membrane performance. Separation and Purification Technology, **122**: 170-182.

Anderson, J., Wiseman, S., Wang, N., Moustafa, A., Perez-Estrada, L., Gamal El-Din, M., Martin, J., Liber, K., and Giesy, J. 2012. Effectiveness of ozonation treatment in eliminating toxicity of oil sands process-affected water to Chironomus-dilutus. Environmental Science and Technology, **46**: 486-493.

Ballinas, L., Torras, C., Fierro, V., and Garcia-Valls, R. 2004. Factors influencing activated carbon polymeric composite membrane structure and performance. Journal of Physics and Chemistry of Solids, **65**: 633-637.

Blanco, J-F., Sublet, J., Nguyen, Q.T., and Schaetzel, P. 2006. Formation and morphology studies of different polysulfones-based membranes made by wet phase inversion process. Journal of Membrane Science, **283**: 27-37.

Celik, E., Park, H., Choi, H., and Choi, H. 2011. Carbon nanotube blended polyethersulfone membranes for fouling control in water treatment. Water Research, **45**: 274-282.

Choi, J-H., Jegal, J., and Kim, W-N. 2006. Fabrication and characterization of multi-walled carbon nanotubes/polymer blend membranes. Journal of Membrane Science, **284**: 406-415.

Dong, S., Kim, E-S, Alpatova, A., Noguchi, H. Liu, Y., and Gamal El-Din, M. 2014. Treatment of oil sands process-affected water by submerged ceramic membrane microfiltration system. Separation and Purification Technology, **138**: 198-209.

Ferlita, R., Phipps, D., Safarik, J., and Yeh, D. Cryo-Snap: 2008. A simple modified freeze-fracture method for SEM imaging of membrane cross-sections. Environmental Progress, **27**: 204-209.

Gamal El-Din, M., Fu, H., Wan, N., Chelme-Ayala, P., Perez-Estrada, L., Drzewicz, P., Martin, J.W., Zubot, W., and Smith, D.W. 2011. Naphthenic acids speciation and removal during petroleum-coke adsorption and ozonation of oil sands process-affected water. Science of the Total Environment, **409**: 5119-5125.

Holowenko, F.M., MacKinnon, M.D., and Fedorak, P.M. 2002. Characterization of naphthenic acids in oil sands wastewaters by gas chromatrography-mass spectrometry. Water Research, **36**: 2843-2855.

Kim, E-S, Liu, Y., and Gamal El-Din, M. 2011. The effects of pretreament on nanofiltration and reverse osmosis membrane filtration for desalination of oil sands process-affected water. Separation and Purification Technology, **81**: 418-428.

Kim, E-S, Liu, Y., and Gamal El-Din, M. 2012a. Evaluation of Membrane Fouling for In-Line Filtration of Oil Sands Process-Affected Water: The Effects of Pretreatment Conditions. Environmental Science and Technology, **46**: 2877-2884.

Kim, E-S., Hwang, G., Gamal El-Din, M., and Liu, Y. 2012b. Development of nanosilver and multi-walled carbon nanotubes thin-film nanocomposite membrane for enhanced surface water treatement. Journal of Membrane Science, **394-395**: 37-48.

Kim, E-S, Liu, Y., and Gamal El-Din, M. 2013. An in-situ integrated system of carbon nanotubes nanocomposite membrane for oil sands process-affected water treatment. Journal of Membrane Science, **29**: 418-427.

Klamerth, N., Moreira, J., Li, C., Singh, A., McPhedran, K.N., Chelme-Ayala, P., Belosevic, M., and Gamal El-Din, M. 2015. Effect of ozonation on the naphthenic acids' speciation and toxicity of pH-dependent organic extracts of oil sands process-affected water. Science of the Total Environment, **506-507**: 66-75.

Laninovic, V. 2005. Relationship between type of nonsolvent additive and properties of polyethersulfone membranes. Desalination, **186**: 39-46.

Loganathan, K., Chelme-Ayala, P., and Gamal El-Din, M. 2015. Pilot-scale study on the reverse osmosis treatment of oil sands tailings pond water: Impact of pretreatment on process performance. Desalination, **360**: 52-60.

Mulder, M. 2000. Phase Inversion Membranes. *In* Reference Module in Chemistry, Molecular Sciences and Chemical Engineering, pp. 3331-3346.

Ohya, H., Kim, J., Chinen, A., Aihara, M., Semenova, S., Negishi, Y., Mori, O., and Yasuda, M. Effects of pore size on separation mechanisms of microfiltration of oily water using porous glass tubular membrane. Journal of Membrane Science, **145**: 1-14.

Peng, H., Volchek, K., MacKinnon, M., Wong, W., and Brown, C. 2004, Application of nanofiltration to water management options for oil sands operations. Desalination, **120**: 137-150.

Pourrezaei, P., Alpatova, A., Chelme-Ayala, P., Perez-Estrada, L.A., Jensen-Fontaine, M., Le, X.C., and Gamal El-Din, M. 2014. Imact of petroleum coke characteristics on the adsorption of the organic fractions from oil sands process-affected water. International Journal of Environmental Science and Technology, **11**: 2037-2050.

Pourrezaei, P., Drzewicz, P., Yingnan, W., Gamal El-Din, M., Perez-Estrada, L., Martin, J., Anderson, J., Wiseman, S., Liber, K., and Geisy, J. 2011. The Impact of Metallic Coagulant on the Removal of Organic Compounds from Oil Sands Process-Affected Water. Environmental Science and Technology, **45**: 8452-8459.

Pourrezaei, P. Wang, Y.; Perez-Estrada, L.; Martin, J.; and Gamal El-Din, M. 2012. Coagulation/flocculation/sedimentation treatment of oil sands process-affected water. *In* Annual Conference of the Canadian Socieity for Civil Engineering 2012: Leadership in Sustainable Infrastructure, Edmonton, Alberta 2012. CSCE 2012.

Qui, S., Wu, L., Pan, X., Zhang, L., Chen, H., and Gao, C. 2009. Preparation and properties of functionalized carbon nanotube/PSF blend ultrafiltration membranes. Journal of Membrane Science, **342**: 165-172.

Richards, H.L., Baker, P., and Iwuoha, E. 2012, Metal nanoparticle modifie polysulfone membranes for use in wastewater treatment: a critical review. Journal of Surface Engineered Materials and Advanced Technology, **2**: 183-193.

Sabde, A., Trivedi, M., Ramachandhran, V., Hanra, M., and Misra, B. 1997. Casting and characterization of cellulose acetate butyrate based UF membranes. Desalination, **1997**: 223-232.

Shu, Z., Li, C., Belosevic, M., Bolton, J.R., and Gamal El-Din, M. 2014. Application of a solar UV/cholorine advanced oxidation process to oil sands process-affected water remediation. Environmental Science and Technology, **48**: 9692-9701.

Small, C.C., Ulrich, A.C., and Hashisho, Z. 2012. Adsorption of Acid Extractable Oil Sands Tailings. Journal of Environmental Engineering, **138**: 833-840.

Wang, C., Klamerth, N., Huang, R., Elnakar, H., and Gamal El-Din, M. 2016. Oxidation of oil sands process-affected water by potassium ferrate (VI). Environmental Science and Technology, **50** (8): 4238-4247.

Young, T.H., and Chen W. 1995. Pore formation mechanisms of membranes from phase inversion process. Desalination, **103**: 233-247.

Yuan, Y., and Lee, T.R. 2013. Contact angle and wetting properties. *In* Springer Series in Surface Science Techniques. *Edited by* G. Bracco and B. Holst. Heidelberg, Springer, pp. 3-34.

Zaidi, A., Simms, K., and Kok, S. 1992. The use of micro/ultrafiltration for the removal of oil and suspended solids from oilfield brines. Water Science & Technology, **25**(10): 163-176.

Zhu, X., Loo, H.E., and Bai, R. 2013. A novel membrane showing both hydrophylic and oleophobic surface properties and its non-fouling performances for potential water treatment applications. Journal of Membrane Science, **436**: 47-56.

Zubot, W., MacKinnon, M.D., Chelme-Ayala, P., Smith, D.W., and Gamal El-Din, M. 2012. Petroleum coke adsorption as a water management option for oil sands process-affected water. Science of the Total Environment, **427-428**: 364-372.

5. THE EFFECT OF CARBOXYL MULTIWALLED CARBON NANOTUBES CONTENT ON THE PERFORMANCE OF POLYSULFONE MEMBRANES FOR OIL SANDS PROCESS WATER TREATMENT[2]

5.1 Introduction

The Athabasca oil sands in northern Alberta, Canada are one of the largest deposits of oil in the world (Allen 2008). The oil sands are composed of approximately 10% bitumen mixed with 5 % water and 85% mineral solids (sand, clay and silt) (Zubot et al. 2012). Before bitumen can be upgraded to produce synthetic crude oil it must first be extracted from the oil sands by a hot water extraction process that uses large amounts of water, roughly 3 m^3 of water is needed for every m^3 of oil sands processed (Klamerth et al. 2015). The water that has contacted the oil sands is called oil sands process water (OSPW) and is not released into the environment due to a zero discharge approach mainly due to its acute toxicity to aquatic lifeforms that include fish, bacteria, benthos, and also non-aquatic mammals (mice) (Islam et al. 2014). OSPW can be recycled for bitumen extraction processes but this has led to further decrease of OSPW quality (Allen et al. 2008).

OSPW is a saline mixture of suspended and dissolved solids, inorganics (metals), and organic compounds (e.g., naphthenic acids) which are acutely and chronically toxic to various aquatic organisms (Kim et al. 2011). OSPW is considered brackish water due to high salinity and

[2] A version of this chapter has been published as: Benally, C., Li, M., and Gamal El-Din, M. 2018. The effect of carboxyl multiwalled carbon nanotubes content on the structure and performance of polysulfone membranes for oil sands process-affected water treatment. Separation and Purification Technology, **199**: 170-181.

total dissolved solids (TDS) (Kim et al. 2011). OSPW is similar in some aspects to flowback water and produced water from hydraulic fracturing, but hydraulic fracturing water can be much more complex and diverse. Both flowback and produced hydraulic fracturing waters are highly saline, and contain salts, organics (aliphatic compounds, aromatic compounds, resin and asphaltine compounds), metals, metalloids and other inorganics found in the shale layers (e.g., Se, V, Sr, B, Mn, N, Cd, Cu, Zn, Ba, Pb, Ra, Hg, and Cr) (Shrestha et al. 2017). In addition, flowback and produced hydraulic fracturing waters contain known carcinogens such as benzene, toluene, xylene, toxins, and biocides.

Before OSPW can be released in a lawful manner into the natural environment, OSPW must be treated (Zubot et al. 2012). Some treatment methods to remediate OPSW have included: coagulation/flocculation (Pourrezaei et al. 2011; Pourrezaei et al. 2012), advanced oxidation processes (Afzal et al. 2015; Anderson et al. 2012; Klamerth et al. 2015), adsorption (Gamal El-Din et al. 2011; Small et al. 2012; Zubot et al. 2012), and membrane filtration (Alpatova et al. 2014; Dong et al. 2014; Kim et al. 2011; Kim et al. 2012; Kim et al. 2013; Loganathan et al. 2015; Peng et al. 2004). Treatment of OSPW with traditional membrane filtrations systems has been applied at different filtration levels. Nanofiltration (NF) and reverse osmosis (RO) have been used to treat OSPW (Kim et al. 2011; Kim et al. 2012; Kim et al. 2013; Loganathan et al. 2015; Peng et al. 2004) with a majority of these studies requiring pre-treatment of the feed water. Membrane treatment with little or no pre-treatment can be accomplished by microfiltration (MF) and ultrafiltration (UF) (Dong et al. 2014; Zaidi et al. 1992). Two studies involving ceramic MF and UF for treatment of OSPW have been conducted (Alpatova et al. 2014; Dong et al. 2014). One study by Kim et al. (2013) involved the fabrication of polysulfone (PSU) UF membranes as pre-treatment for high pressure membrane filtration of OSPW. This led to the more detailed look

at the formation of nanocomposite polysulfone (PSU) membranes for eventual treatment of OSPW, and is described in Chapter 4.

As discussed in Chapter 4, PSU is a polymer with chemical and structural stability that is often used to fabricate membranes for wastewater treatment (Richards et al. 2012). Although the hydrophobic nature of PSU can increase membrane fouling, it has been found that inclusion of hydrophilic nanoparticles within the polymer can decrease surface hydrophobicity, increase permeate flux, and decrease membrane fouling (Blanco et al. 2006; Kim et al. 2013). Carbon nanotubes are a commonly used nanoparticle in membrane applications due to excellent mechanical, electrical, thermal, and antibacterial properties, in addition to adsorptive properties (Kim et al. 2013). In the previous chapter (Chapter 4) the effect of adding carboxyl modified multi-walled carbon nanotubes, mMWNT, to low pressure UF PSU membranes was studied with emphasis on membrane morphology, pore size formation and basic filtration performance. When taking both rejection and water permeability into account, membranes mMWNT-0.2 and mMWNT-2 gave fairly high PEG rejection while membrane mMWNT-2 had a pure water and PEG flux which were both more than double that for membrane mMWNT-0.2.

In this chapter the use of the fabricated membranes for treatment of OSPW will be evaluated. The objectives of the present study were to: (1) evaluate how variation of mMWNT content in fabricated membranes affects OPSW filtration performance and resulting permeate water quality, (2) evaluate how mMWNT content in fabricated membranes affects membrane fouling resistance during OSPW filtration, and (3) determine the dominant fouling mechanism(s) during filtration of OSPW.

5.2 Experimental methods and materials

5.2.1 OSPW and chemicals

Raw OSPW was collected from an oil sands tailing pond in Fort McMurray, Alberta, Canada and stored in a cold room at 4°C. Dichloromethane (DCM) - HPLC grade and Optima® grade, hydrochloric acid (HCl), and sulfuric acid (H_2SO_4) were purchased from Fisher Scientific (Ottawa, ON, Canada). Milli-Q water was produced using a Milli-Q Ultrapure Water System (Millipore Corporation, Bedford, MA, USA).

5.2.2 Polysulfone membranes

The membranes used for this study were polysulfone (PSU) membranes containing varying amounts of MWNT (average inner diameter: 5-10 nm, length: 10-30 μm) modified with carboxylic acid groups (-COOH), or mMWNT. Details regarding the fabrication of the membranes can be seen in section 4.2.2. As noted in Chapter 4, membranes used for this study were assigned a sample name in the given format: mMWNT-x, where x is the wt. % content of mMWNT in the corresponding fabricated membrane. Membranes used for the following OSPW filtration experiments were mMWNT-0, mMWNT-0.2, mMWNT-0.5, mMWNT-1, mMWNT-2, and mMWNT-5.

5.2.3 OSPW filtration

OSPW filtration experiments through previously fabricated membranes were conducted by using raw OSPW feed water and a dead-end low pressure membrane filtration system shown in Figure 4.1. The low pressure membrane filtration system consists of a custom made stainless steel cell, one gear pump (Model GJ-N21.PF2S.A, Micropump Inc.), one gear pump drive (Model 75211-10, Cole-Parmer Instrument Company), one electronic balance (Adventurer Pro

model AV8101, Ohaus), and a data acquisition system. Feed water from the feed tank was pumped into the dead end filtration membrane cell and through the membrane. The transmembrane pressure (TMP), or operating pressure, was read using the pressure gauge. Permeate was collected in a container and the mass was weighed with an electronic balance attached to a data acquisition system. The balance was set to record the mass of permeate every 15 seconds. More specific details are discussed in section 4.2.4.

As discussed in section 4.2.4, the permeate flux of pure water, J_0 ($L \cdot m^{-2} \cdot h^{-1}$), and OSPW, J_{0S} ($L \cdot m^{-2} \cdot h^{-1}$), was calculated using general equation 4.1.

5.2.4 OSPW fouling analysis and determination of fouling mechanisms

Short term filtration of raw OSPW was conducted to investigate membrane fouling resistance and to determine possible fouling mechanisms involved during filtration of OSPW. All membranes used for this study were fabricated previously and include membranes mMWNT-0, mMWNT-0.2, mMWNT-0.5, mMWNT-1, mMWNT-2, and mMWNT-5.

The membrane of interest was first compacted at 400 kPa using Milli-Q water for 120 minutes. This was followed by filtration of raw OSPW at 400 kPa for 240 minutes. After OSPW filtration, each membrane was subjected to a series of steps to clean the membrane. First, each membrane was rinsed with Milli-Q water to remove the visible fouling layer. Next, the membrane was subjected to reverse filtration with Milli-Q water for 30 minutes at a slightly higher pressure (450-500 kPa) than that used for OSPW filtration. Lastly, the membranes were soaked in Milli-Q water for at least 2 hours. Milli-Q water was then filtered through the cleaned membranes for 120 minutes at TMP of 400 kPa in order to determine the permeate flux recovery after cleaning.

OSPW fouling resistance ratios were determined using equations 5.1 to 5.3 described by Vantanpour et al. (2011).

$$R_t = (1 - \frac{J_{OS}}{J_O}) \times 100 \qquad (5.1)$$

$$R_r = (\frac{J_C - J_{OS}}{J_O}) \times 100 \qquad (5.2)$$

$$R_{ir} = (\frac{J_O - J_C}{J_O}) \times 100 \qquad (5.3)$$

R_t (%) is the total fouling ratio, and represents the total flux decline due to fouling (Kim et al. 2013). R_t can be broken into two categories: reversible fouling, R_r (%), and irreversible fouling, R_{ir} (%). In the above equations J_0 ($L \cdot m^{-2} \cdot h^{-1}$) is the Milli-Q water flux for a fresh membrane, J_{0S} ($L \cdot m^{-2} \cdot h^{-1}$) is the OSPW permeate flux and J_C ($L \cdot m^{-2} \cdot h^{-1}$) is the Milli-Q water flux after cleaning. Each type of flux was determined using permeate mass data collected for every membrane and equation 4.1.

Fouling of the fabricated membranes due to OSPW filtration was further investigated by determination of plausible fouling mechanism(s) involved. OSPW permeate flux data was fit to four different membrane fouling mechanism models: complete pore blocking, standard pore blocking, intermediate pore blocking, and cake filtration. These models have been described in detail by Wei et al. (2012) and more recently by Alpatova et al. (2014). Complete pore blocking is described by equation 5.4:

$$\frac{dV}{dt} = J_0 - k_b V \qquad (5.4)$$

where V (L) is the volume of permeate passing through the membrane; t (min) is the filtration time, J_0 ($L \cdot m^{-2} \cdot h^{-1}$) is the permeate flux of Milli-Q water, and k_b is the coefficient of complete

pore blocking. Data in the form of (dV/dt) versus V was plotted. Standard pore blocking is described by equation 5.5:

$$\frac{t}{V} = \frac{1}{J_0} + \frac{k_S}{2} t \qquad (5.5)$$

where k_s is the coefficient of standard pore blocking. The data in the form of (t/V) versus t was plotted. Intermediate pore blocking is described by equation 5.6:

$$\frac{dt}{dV} = \frac{1}{J_0} + k_i t \qquad (5.6)$$

where k_i is the coefficient of intermediate pore blocking. Data in the form of (dt/dV) versus t was plotted. Cake filtration is described by equation 5.7:

$$\frac{t}{V} = \frac{1}{J_0} + \frac{k_c}{2} V \qquad (5.7)$$

where k_c is the coefficient of cake filtration. Data in the form of (t/V) versus V was plotted. The resulting plots were analyzed and that resulting plots with the highest coefficient of determination (R^2) gave an indication of the type of fouling mechanism(s) governing membrane filtration of raw OSPW.

5.2.5 OSPW and permeate quality analysis

Long term filtration of raw OSPW was conducted using three selected membrane samples: mMWNT-0, mMWNT-0.2, and mMWNT-2. These membranes were chosen based upon results from pure water flux data and the rejection testing that is discussed in Chapter 4. Raw OSPW was filtered through compacted membranes at a TMP of 400 kPa for at least 48 hours to obtain a minimum of 2000 mL permeate for permeate water quality analysis.

Water analyses were conducted for raw OSPW and permeate resulting from filtration through the three fabricated membranes. Turbidity was determined using a digital, direct-reading turbidimeter (model 965-10A, Orbeco-Hellige) and the method described in section 2130 of Standard Methods for the Examination of Water and Wastewater (Eaton et al. 2016). Total solids (TS) and total suspended solids (TSS) were determined using the gravimetric methods described in section 2540 of Standard Methods for Examination of Water and Wastewater (Eaton et al. 2016). Silt density index (SDI_{15}) was determined by use of a portable SDI kit and a pump assembly kit (SDI-2000 & SDI-PU, Applied Membranes Inc.) in conjunction with the ASTM Standard Test Method for Silt Density Index (SDI) – section D4189-07 (ASTM 2014). Acid-extractable fraction (AEF) of raw OSPW and resulting permeates were extracted twice with DCM and determined by Fourier transform infrared (FT-IR) spectroscopy (Nicolet 8700, Thermo Scientific). The resulting FT-IR spectrums were analyzed by obtaining peak values at 1743 cm^{-1} and 1706 cm^{-1}.

5.2.6 Fouled membrane surface analysis

Fouled membranes from the long term filtration experiments detailed in section 5.2.5 were analyzed by X-ray photoelectron spectroscopy (XPS) (AXIS 165, Kratos Analytical). Also analyzed were clean membrane samples for comparison. XPS analysis was conducted at the University of Alberta nanoFAB with specific details as follows. Room-temperature XPS experiments were performed using Kratos Axis spectrometer with monochromatized Al K_{α} ($h\upsilon$ = 1486.71 eV). The spectrometer was calibrated by the binding energy (84.0 eV) of Au $4f_{7/2}$ with reference to Fermi level. The pressure of analysis chamber during experiments is better than 5×10^{-10} Torr. A hemispherical electron-energy analyzer working at the pass energy of 20 eV was used to collect core-level spectra while survey spectrum within a range of binding energies from

0 to 1100 eV was collected at analyzer pass energy of 160 eV. Compositions were calculated from the survey spectra using the major elemental peaks and sensitivity factors provided by the database. CASA XPS was used for component analysis.

Fouled membranes were also analyzed by scanning electron microscopy (SEM) (Sigma 300 VP-FESEM, Zeiss) and energy dispersive X-ray spectroscopy (EDS) (Bruker). The Sigma 300 VP-FESEM was run in variable pressure mode. Backscatter electron SEM images and secondary electron SEM images were acquired. Membrane samples were cut to size and attached to an aluminum stub. No gold or carbon coating was needed since the system was run in variable pressure mode. SEM analysis was conducted at University of Alberta Department of Earth and Atmospheric Sciences Scanning Electron Microscope Laboratory.

5.3 Results and discussion

5.3.1 OSPW filtration performance

The first four hours of OSPW filtration through fabricated membranes and membrane flux recoveries after cleaning are shown in Figure 5.1 a. Figure 5.1 b shows the normalized OSPW flux for the four hour filtration time. Three distinct phases of filtration are apparent in Figure 5.1 a: 1) Milli-Q water filtration for the first 120 minutes, 2) raw OPSW filtration from 120 to 360 minutes, 3) recovery Milli-Q filtration after simple cleaning and backwash for the last 120 minutes. For all membranes, the initial Milli-Q filtration flux was higher than the flux obtained during OPSW filtration and recovery Milli-Q flux after cleaning. In general, OSPW flux showed a decreasing trend. This was to be expected as the membranes experienced fouling due to OSPW filtration. The recovery Milli-Q flux after cleaning resulted in a flux higher than OSPW flux but not as high as initial Milli-Q water flux. This is the result of the effects of fouling that remain

after cleaning and backwash. A similar trend was observed for the three stages of the permeate flux recovery tests using raw OSPW and low pressure PSU membranes with 0 and 10 wt.% mMWNT (Kim et al. 2013).

Membrane mMWNT-0 had an average pure water flux of 26.7 $L/m^2/h$, which dropped by nearly half to an average OPSW flux of 13.3 $L/m^2/h$. Permeate flux recovery for mMWNT-0 was 66.7%. Addition of mMWNT increased the flux of Milli-Q water and OSPW through membranes mMWNT-1, -2, -5, with the highest amount of mMWNT resulting in highest permeate flux. This is the same trend that has been noted for the pure water flux through fabricated membranes (Chapter 4). Membranes mMWNT-0.2 and mMWNT-0.5 both resulted in a lower pure water flux than mMWNT-0, but only mMWNT-0.2 had a lower OSPW flux than that of mMWNT-0. As discussed in Chapter 4, this result may occur due to the decreased average pore size of the selective surface of the membranes. As shown in Table 5.1, the permeate flux recovery for composite membranes was higher than that for MWNT-0. The highest permeate flux recovery of 99.1% resulted with membrane mMWNT-2. Addition of 5 wt.% mMWNT lead to a permeate flux recovery of 80.2%, still higher than mMWNT-0, but showing a decreasing trend in comparison to PSU membranes containing smaller additions of mMWNT. The higher permeate flux recovery for PSU membranes with mMWNT may be the combined result of increased hydrophilicity and membrane surface negativity due to addition of mMWNT (Kim et al. 2013). Fouling due to the filtration of OSPW would also play a large role in the resulting flux recovery ratios obtained.

Figure 5.1 b shows the normalized OSPW flux through fabricated membranes for the first four hours of filtration. Membrane mMWNT-0 has the sharpest initial decrease in normalized flux within the first 10 minutes of filtration, but then experiences a gradual increase in

normalized flux over the rest of the four hour filtration time. This is the only membrane with this trend. It would be expected that one would continue to see a gradual decrease in the normalized OSPW flux. All other membranes show a gradual decrease in normalized flux. Composite membranes with the highest normalized flux to smallest during hours 1 and 2 are as follows: mMWNT-0.2 > mMWNT-2 > mMWNT-0.5 > mMWNT-1 > mMWNT-5. The order slightly changes for hours 3 and 4, the normalized flux for mMWNT-0.5 is becomes slightly higher than mMWNT-2. Addition of 5 wt. % mMWNT resulted in the composite membrane with the largest decrease in normalized OSPW flux during the four hour filtration time. This was the same membrane with the lowest permeate flux recovery after OSPW filtration and cleaning, as shown in Table 5.1.

Figure 5.2 shows the normalized flux results for longer term OSPW filtration through membranes mMWNT-0, mMWNT-0.2, and mMWNT-2 as a function of permeate volume. From Figure 5.2, it can be seen that the flux for mMWNT-0 decreases at a very fast rate once filtration of OSPW begins. This may be due to the increased tendency of fouling noted for membrane mMWNT-0. Membranes mMWNT-0.2 and mMWNT-2 have comparable normalized flux values that begin to diverge after 700 mL of accumulated permeate volume. At this point, mMWNT-2 experiences a larger decrease in normalized flux. After 800 mL of permeate accumulation, mMWNT-0 and mMWNT-0.2 show approximately the same rate of flux decrease, as indicated by the approximately equal slope for these curves. After 800 mL of accumulated permeate, mMWNT-2 had a higher rate of flux decrease, as indicated by the steeper slope for this membrane data set. For longer filtration times, the composite membranes had a lower tendency for fouling to occur initially. Overall, the plain membrane (mMWNT-0) experienced the greatest membrane fouling.

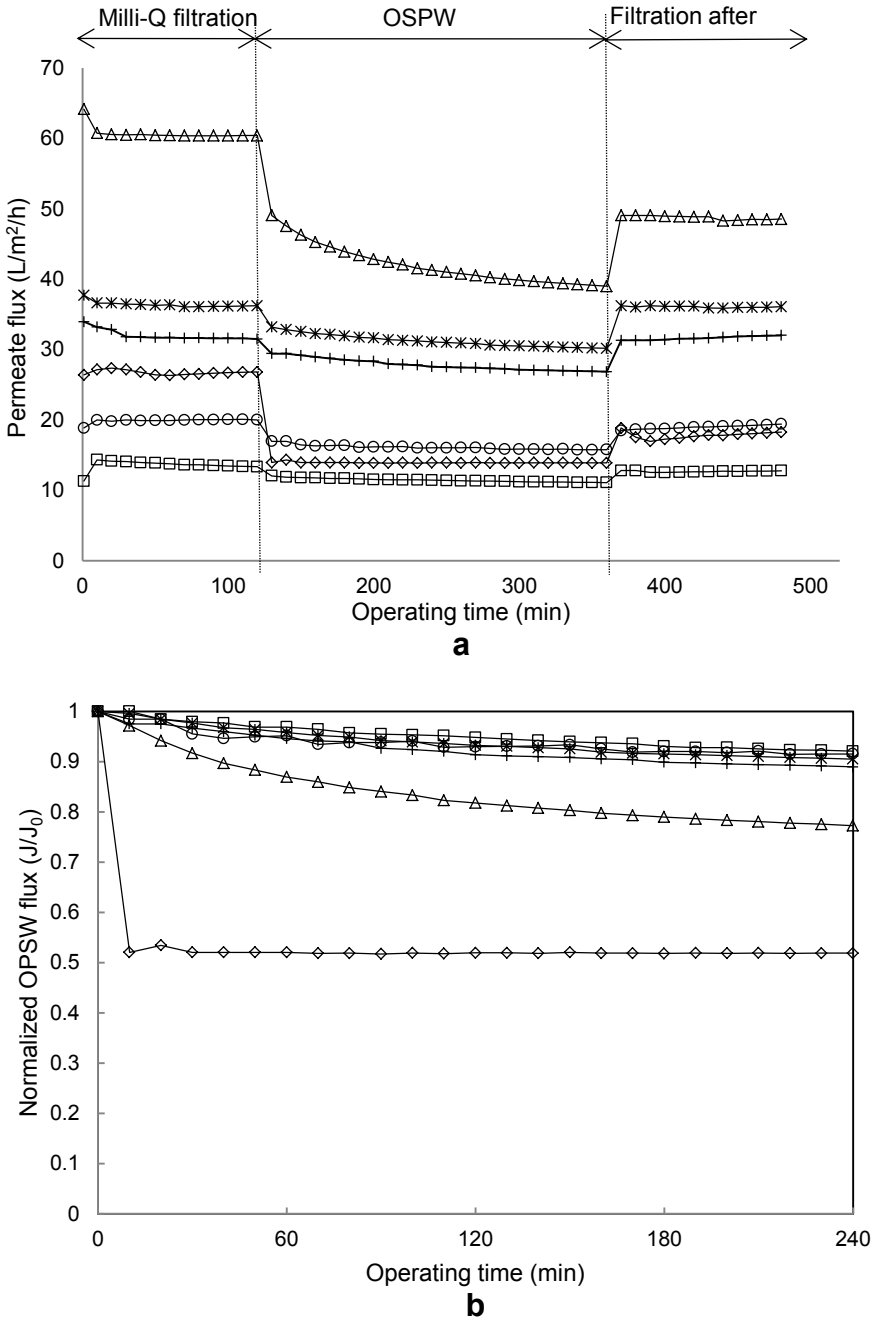

Figure 5.1 (a) Flux recovery test after OPSW filtration using PSU membranes with varying amounts of mMWNT; (b) normalized flux of OPSW through PSU membranes. All filtration occurred at TMP of 400 kPa. Milli-Q filtration lasted 120 minutes, raw OSPW filtration lasted 240 minutes, and Milli-Q filtration after backwash lasted 120 minutes. ◇ – 0 wt.% mMWNT; □ – 0.2 wt.% mMWNT; ○ – 0.5 wt.% mMWNT; + – 1 wt.% mMWNT; ✳ – 2 wt.% mMWNT; Δ – 5 wt.% mMWNT.

Table 5.1 Permeate flux recovery for each fabricated membrane after OPSW filtration and backwash/cleaning

Sample name	Flux recovery (%)
mMWNT-0	66.7
mMWNT-0.2	93.5
mMWNT-0.5	95.4
mMWNT-1	98.7
mMWNT-2	99.1
mMWNT-5	80.2

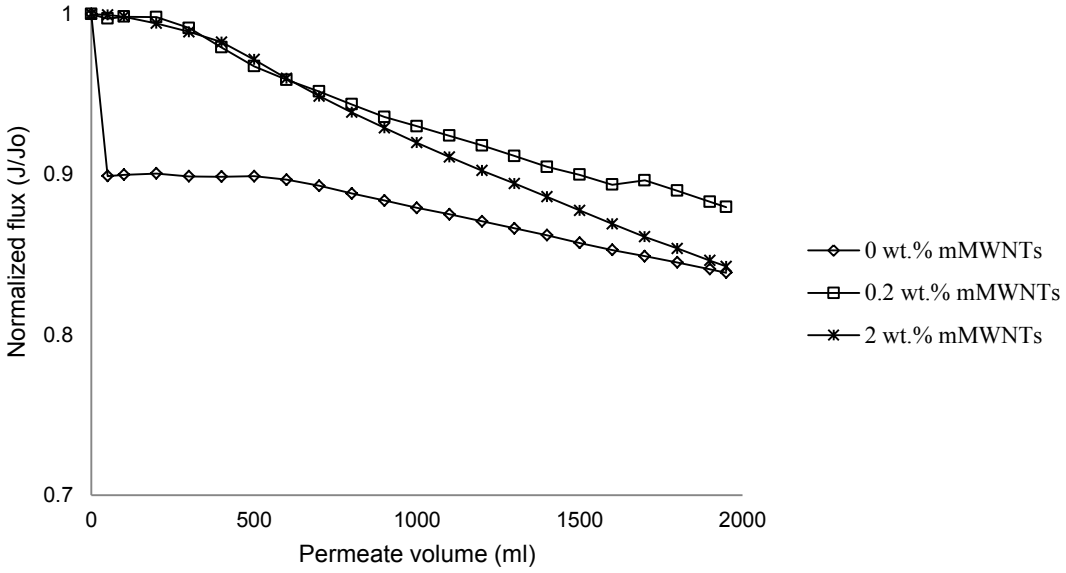

Figure 5.2 Normalized flux of raw OSPW though PSU membranes with 0, 0.2 and 2.0 wt. % mMWNT at a constant TMP of 400 kPa as a function of permeate volume (mL) for long filtration time.

5.3.2 OSPW fouling analysis and mechanism

Table 5.2 shows the fouling ratios for each membrane which were determined using flux data from the four hour OSPW filtration experiment. The fouling ratios were calculated using the Milli-Q water flux, the raw OSPW permeate flux, and recovery Milli-Q water flux after

backwash for each tested membrane. Flux was determined using equation 4.1 and the fouling ratios were determined using equations 5.1, 5.2, and 5.3.

R_t is the total fouling ratio and is the highest for mMWNT-0 at 50.4%. The addition of mMWNT led to a reduced R_t. R_t was in the range of 13.1%-18.9% for membranes mMWNT-0.2.-0.5,-1,-2. Membrane mMWNT-5 had a higher fouling ratio of 30.8%, which was still less than the fouling ratio for mMWNT-0. Addition of mMWNT did not lead to a gradually decreasing R_t which indicates that it was not linearly dependent on addition of mMWNT alone, as was seen for contact angle. R_r is the portion of the total fouling ratio that is reversible and R_{ir} is the portion of the total fouling ratio that is irreversible. For all membranes tested, R_r and R_{ir} were highest for mMWNT-0 at 17.1% and 33.3%. The higher irreversible fouling ratio for mMWNT-0 was likely due to the hydrophobic surface in combination with a lower surface charge (Kim et al. 2013). Membranes with the lowest ratio of irreversible fouling were mMWNT-1 and mMWNT-2. This data was supported by the results of Table 5.1, where membranes mMWNT-1 and mMWNT-2 experienced the highest flux recovery after OSPW filtration and backwash.

Overall results show that addition of mMWNT to PSU membranes reduced the total fouling ratio, reversible fouling ratio and irreversible fouling ratios for all amounts of mMWNT added. The fouling ratios did not follow a simple trend that is easy to discern. Membrane mMWNT-0 was the most hydrophobic of all the membranes tested. While hydrophobicity may have been a primary factor for the high value of R_t for mMWNT-0, it does not explain the second highest R_t value observed for mMWNT-5. In addition to hydrophobicity, the selective side pore diameter size and the flux of permeate going through each membrane may factor into the resulting total fouling ratio results.

The fouling mechanism of OSPW filtration through the fabricated PSU membranes was determined using four fouling models (complete blocking, standard blocking, intermediate blocking, and cake filtration). Short term OSPW filtration data were fit to the four classic fouling models and the resulting correlation values (R^2) are shown in Figure 5.3. For all membranes, the fouling models with the highest correlation value for each data set were the standard blocking and the cake filtration models. More specifically, the standard blocking model resulted in the highest correlation value for membrane mMWNT-0, while the cake filtration model gave the highest correlation values for all the composite membranes. These results are consistent with OSPW fouling mechanism determination performed by Alpatova et al. (2014) for 1 kDa ceramic UF membrane. Other fouling mechanism studies conducted for ultrafiltration PSU membranes using dead-end configuration and a wastewater that had high levels of suspended particles, fats, grease and proteins, revealed that the main fouling mechanisms during early filtration were cake layer formation and intermediate blocking (Zhou et al. 2015).

For the standard blocking model it is assumed that particle sizes in solution are less than the size of the membrane pore and are able to enter and become adsorbed onto the inner surface of the pore walls leading to a reduction of pore volume and permeate volume over time, eventually even leading to pore blocking (Masoudnia et al. 2013). In terms of reversible and irreversible fouling, intuitively one would most closely associate standard blocking with irreversible fouling, and thus with R_{ir}, because the adsorbed particles inside the pores more than likely would not be as readily removed during membrane cleaning or backwashing. For the cake filtration model, it is assumed that the membrane pore sizes are smaller than the size of the particles in the feed water, so no particles enter the membrane pores (Masoudnia et al. 2013). Instead the particles accumulate on the membrane surface forming a cake layer that grows over

time and may lead to flux decline by blocking any particles from coming into contact with the membrane surface. In terms of reversible and irreversible fouling, cake filtration would most closely be associated with reversible fouling, and thus with R_r, because the cake layer could be washed away easily during membrane cleaning or backwash. The results for the fouling mechanism due to OSPW filtration through PSU membrane with and without mMWNT are consistent with results given for the fouling ratio values, R_r and R_{ir} (Table 5.2). For example, standard blocking being the highest contributor to fouling for mMWNT-0 is consistent with resulting R_{ir} value being greater than R_r for this membrane. Additionally, cake filtration being the highest contributor to fouling for the composite membranes is consistent with resulting R_r values being greater than R_{ir} values for the specified membranes, the exception being mMWNT-5. However, for all membranes studied, the fouling of fabricated membranes due to the filtration of OSPW could be described almost equally by both the standard blocking and cake filtration mechanisms.

Table 5.2 Fouling resistances of fabricated PSU membranes with mMWNT calculated based upon the short term OSPW flux results found in Figure 5.1 a. R_t is total fouling ratio. R_r is the reversible fouling ratio. R_{ir} is the irreversible fouling ratio.

Sample name	Fouling ratios (%)		
	R_t	R_r	R_{ir}
mMWNT-0	50.4	17.1	33.3
mMWNT-0.2	15.6	9.1	6.5
mMWNT-0.5	18.9	14.3	4.6
mMWNT-1	13.1	11.8	1.3
mMWNT-2	14.2	13.2	0.9
mMWNT-5	30.8	11.1	19.7

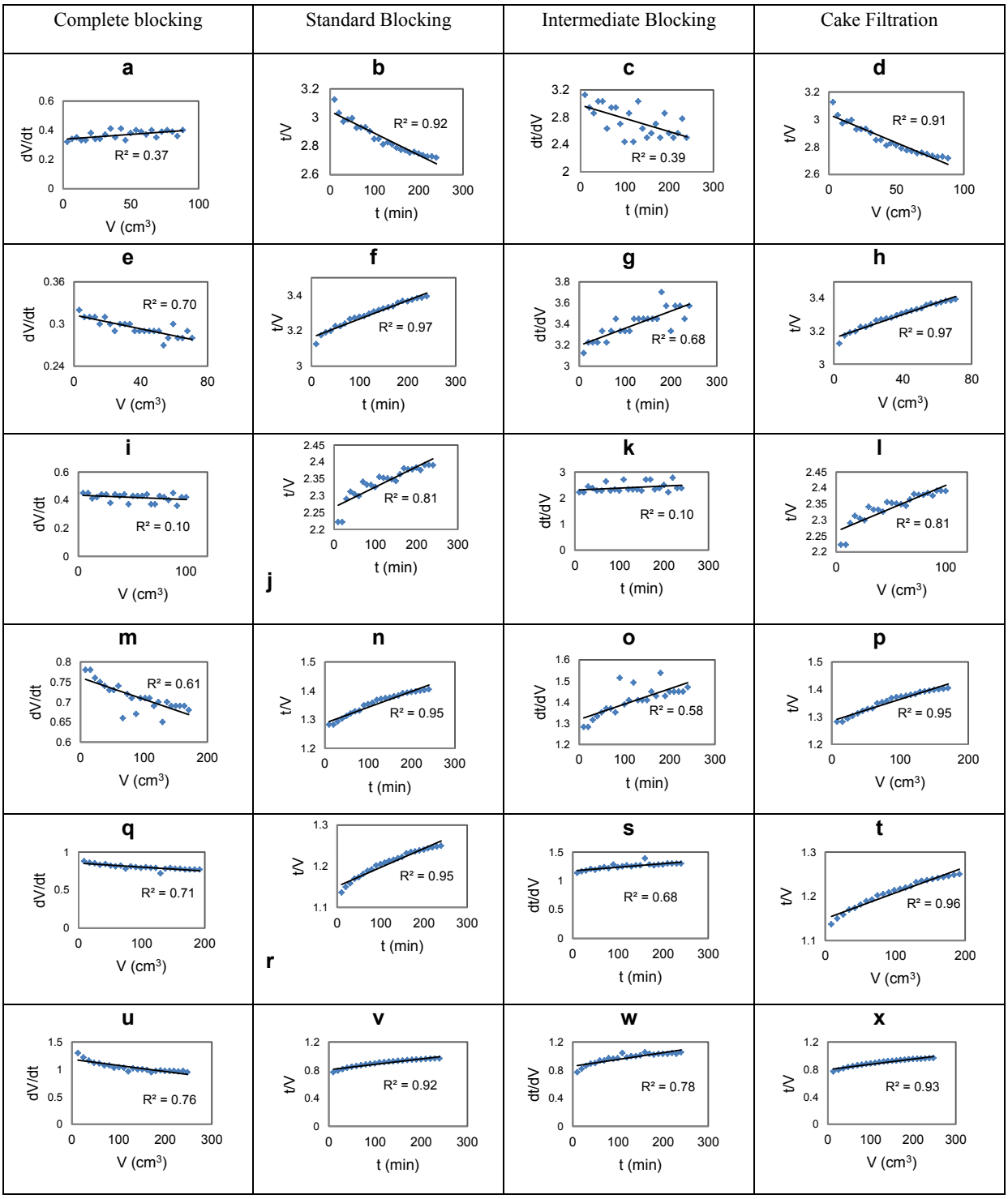

Figure 5.3 Short term OSPW filtration data (240 minutes) fit to classic fouling models (complete, standard, intermediate, and cake). PSU membrane with 0 wt.% mMWNT: fig. a-d; 0.2 wt.% mMWNT: fig. e-h; 0.5 wt.% mMWNT: fig. i-l; 1 wt.% mMWNT: fig. m-p; 2 wt.% mMWNT: fig. q-t; 5 wt.% mMWNT: fig u-x.

OSPW fouled membranes were analyzed by scanning electron microscopy (SEM) (Sigma 300 VP-FESEM, Zeiss) and energy dispersive X-ray spectroscopy (EDS) (Bruker). Figure 5.4 b and c shows a caked fouling layer formed on membrane mMWNT-0 after OSPW filtration. This is contrasted against a high magnification SEM image (Figure 5.4 a) of a pristine sample of membrane mMWNT-0. The pores on the selective surface of membrane mMWNT-0 are uniformly covered by the fouled cake layer. At low magnification the cake layer appears smooth but at higher magnification (10k x) the texture of the cake layer is apparent. The pristine membrane has no such surface topography that is visible. In addition to membrane mMWNT-0, SEM images of fouled membrane samples mMWNT-0.2 and mMWNT-2 can be seen in Figure 5.5. As with membrane mMWNT-0, the textured foul layer is visible for both mMWNT-0.2 and mMWNT-2.

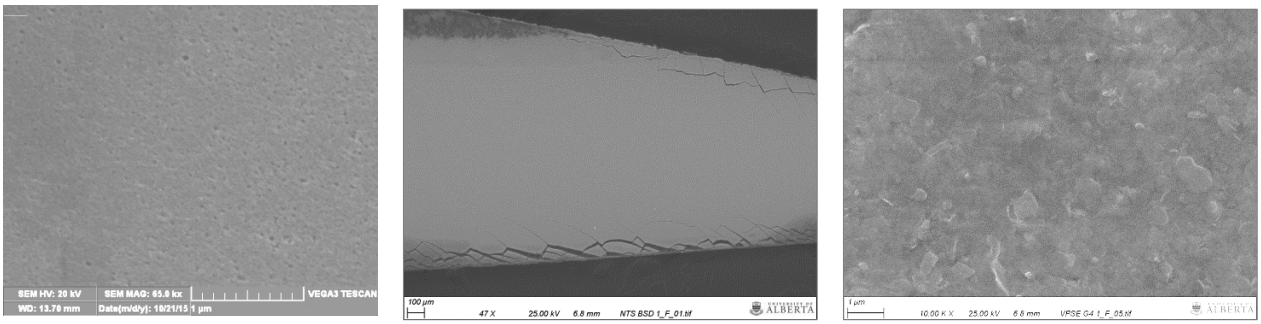

Figure 5.4 SEM images of membrane mMWNT-0: (a) pristine sample magnified 65k x taken with Tescan VEGA3 SEM using secondary electron imaging in high vacuum mode, (b) OSPW fouled sample magnified 47x taken with Zeiss Sigma 300 VP-FSEM using backscatter electron imaging in variable pressure mode, and (c) OSPW fouled sample magnified 10k x taken with a Zeiss Sigma 300 VP-FSEM using secondary electron imaging in variable pressure mode.

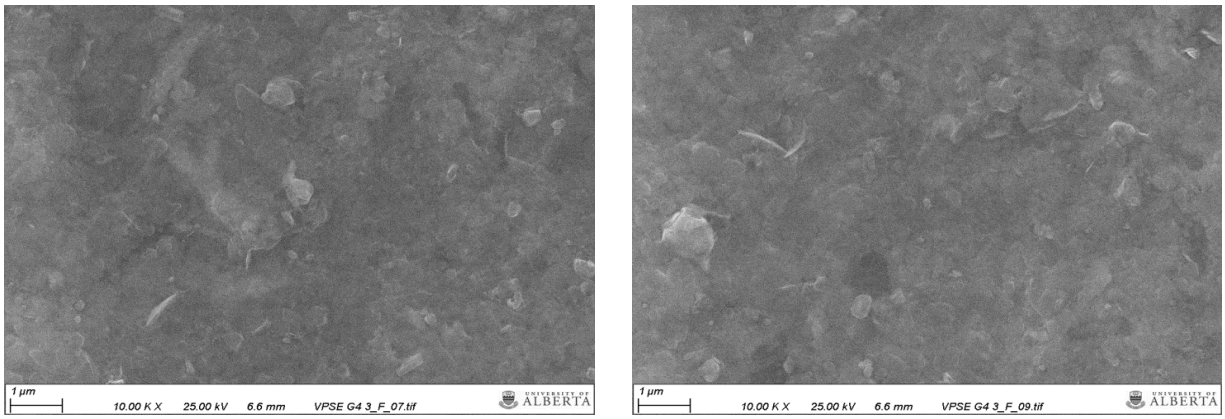

a b

Figure 5.5 SEM images of OSPW fouled membranes magnified 10kx taken with a Zeiss Sigma 300 VP-FSEM using secondary electron imaging in variable pressure mode: (a) mMWNT-0.2 and (b) mMWNT-2.

To further investigate the fouling of the PSU membranes with and without mMWNT the membrane samples were analyzed by Energy Dispersive X-ray Spectroscopy (EDS). Figures 5.6 and 5.7 show EDS results for pristine and OSPW fouled membrane sample mMWNT-0. Figures 5.8 and 5.9 show EDS results for pristine and OSPW fouled PSU composite membrane sample mMWNT-0.2. Figures 5.10 and 5.11 show EDS results for pristine and OSPW fouled PSU composite membrane sample mMWNT-2. EDS analysis for pristine membranes mMWNT-0 (Figure 5.6), mMWNT-0.2 (Figure 5.8) and mMWNT-2 (Figure 5.10) results in a similar surface composition for all membranes with strong peaks of carbon, oxygen and sulfur. Carbon was found to be in the range of 75.24 – 75.81%. Oxygen was in the range of 16.28 – 17.08%. Sulfur was in the range of 7.49 – 7.69 %. These results are to be expected as the membranes are fabricated with PSU and may or may not have added mMWNT. PSU is composed of C, O, H and S. Added mMWNTs detected at the membrane surface will only be comprised of C, O and H.

EDS analysis of the fouled membranes mMWNT-0 (Figure 5.7), mMWNT-0.2 (Figure 5.9), and mMWNT-2 (Figure 5.11) showed that the foulants were composed not only of C, O, S, but also the added components Na, Mg, Al, Si, Cl (for mMWNT-0.2 only), K, Ca, Ti, and Fe. The largest contributors to the foulant layers were found to be O, C, Si and Al. Membrane sample mMWNT-0.2 had some areas of salt (NaCl) that influenced the resulting values for Na and Cl, making these two elements the next largest contributors for this membrane.

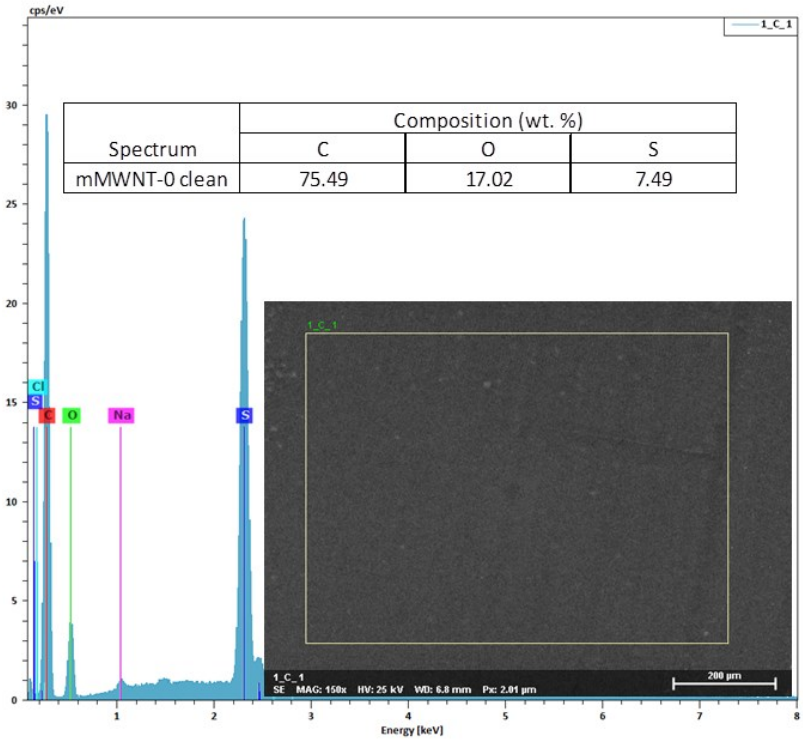

Figure 5.6 EDS analysis of pristine PSU membrane mMWNT-0.

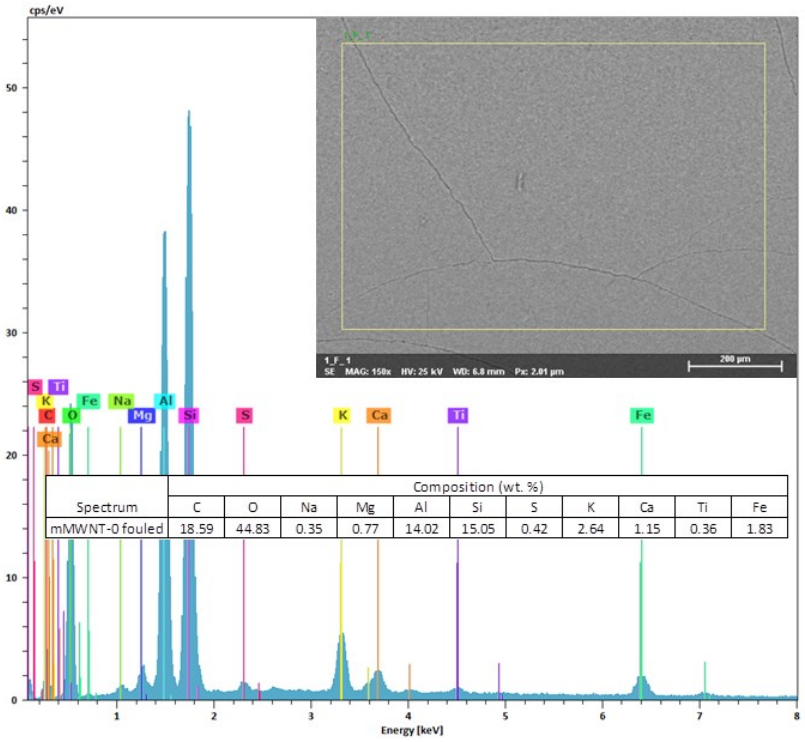

Figure 5.7 EDS analysis of OSPW fouled PSU membrane mMWNT-0.

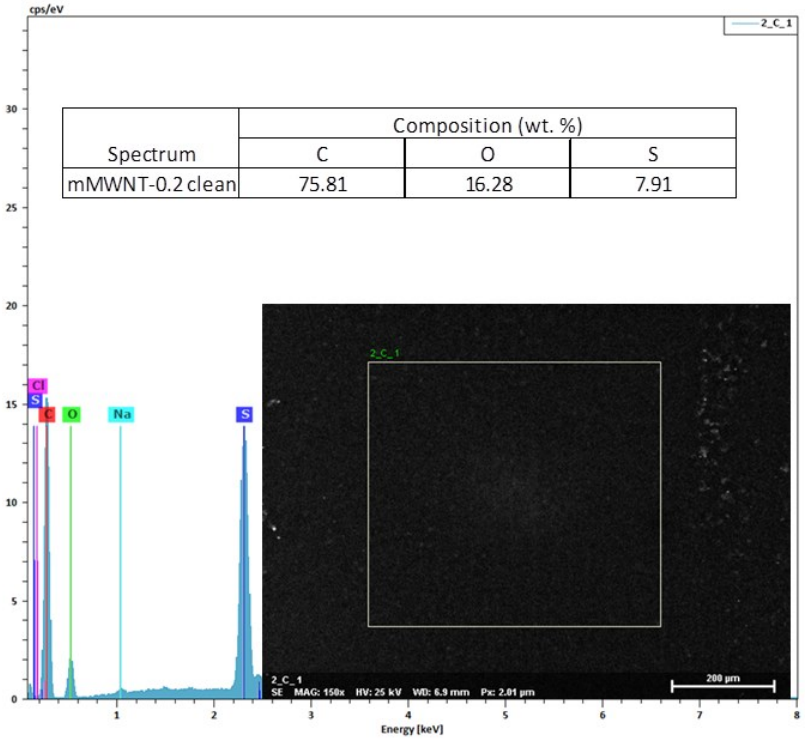

Figure 5.8 EDS analysis of pristine PSU composite membrane mMWNT-0.2.

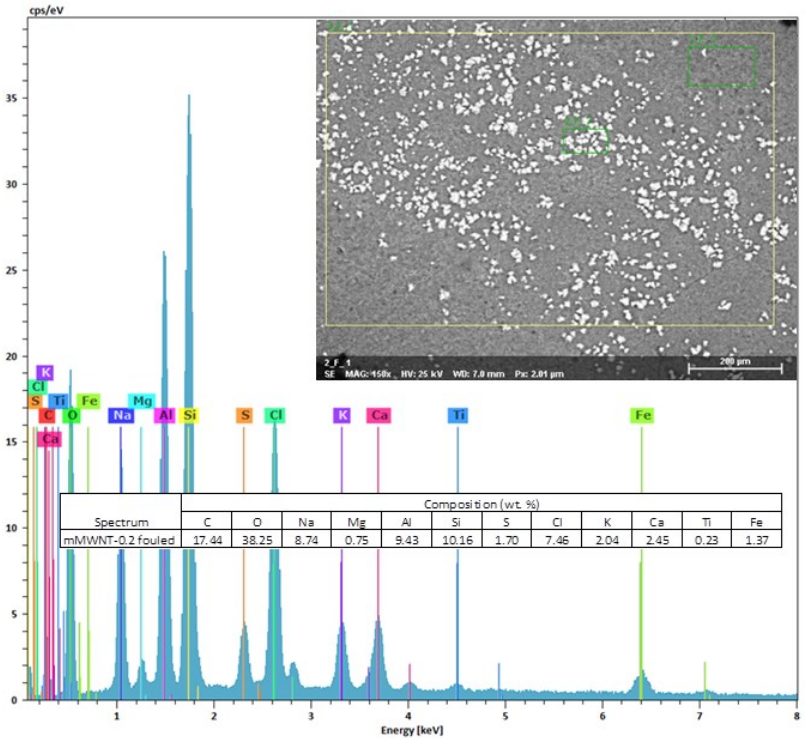

Figure 5.9 EDS analysis of OSPW fouled PSU composite membrane mMWNT-0.2.

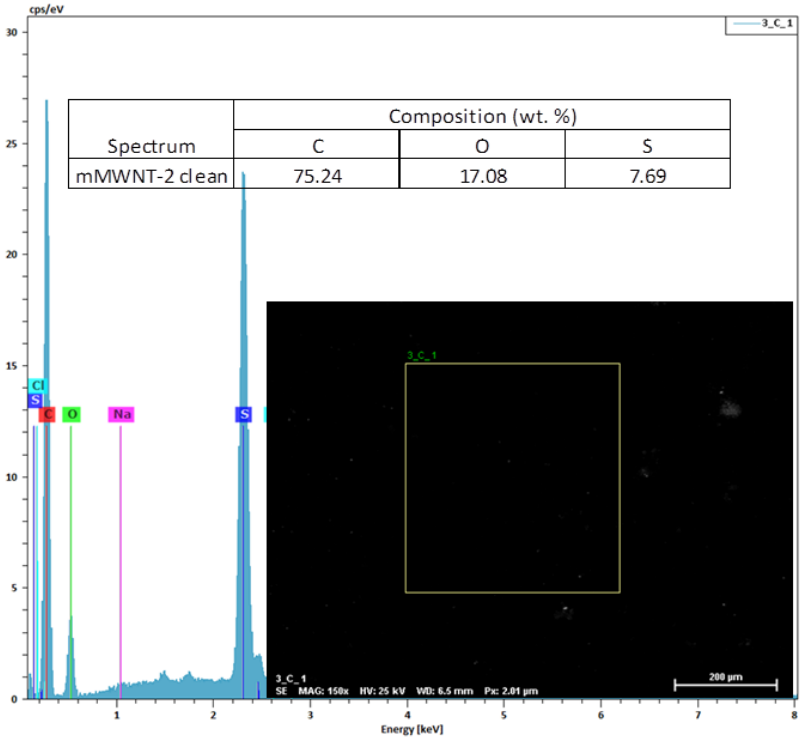

Figure 5.10 EDS analysis of pristine PSU composite membrane mMWNT-2.

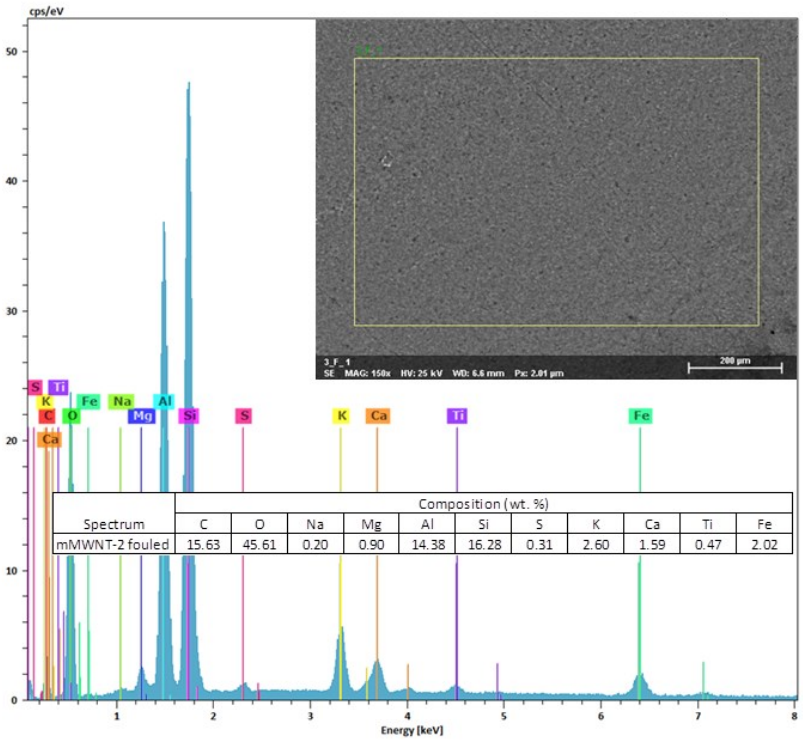

Figure 5.11 EDS analysis of OSPW fouled PSU composite membrane mMWNT-2.

XPS spectra from survey scans of pristine and fouled membranes mMWNT-0, mMWNT-0.2 and mMWNT-2 are shown in Figure 5.12, Figure 5.13, and Figure 5.14 respectively. The XPS spectra support the composition data found by EDS analysis. XPS spectra of pristine membranes are comprised of peaks for C, O, S and N (except for mMWNT-0) in that order from largest contributor to smallest. XPS spectra for fouled membranes are comprised of peaks for O, Si, C, Al, K, Fe, N, Mg, Na, and Ca. For all fouled membranes the four largest components of the fouling layer are (from largest to smallest): O, Si, C, and Al. This data is supported by the EDS analysis of the fouled membrane surfaces.

The composition of the foulant layers on membranes were analyzed by both EDS and XPS. The results give similar fouling layer compositions. They both give data that suggest the fouling

layers found on the analyzed membranes are largely composed of clay or silt material with some salts, minerals, and some heavy metals. This is to be expected as the oil sands themselves are composed of clay, sand, silt, water, bitumen (Zubot et al. 2012).

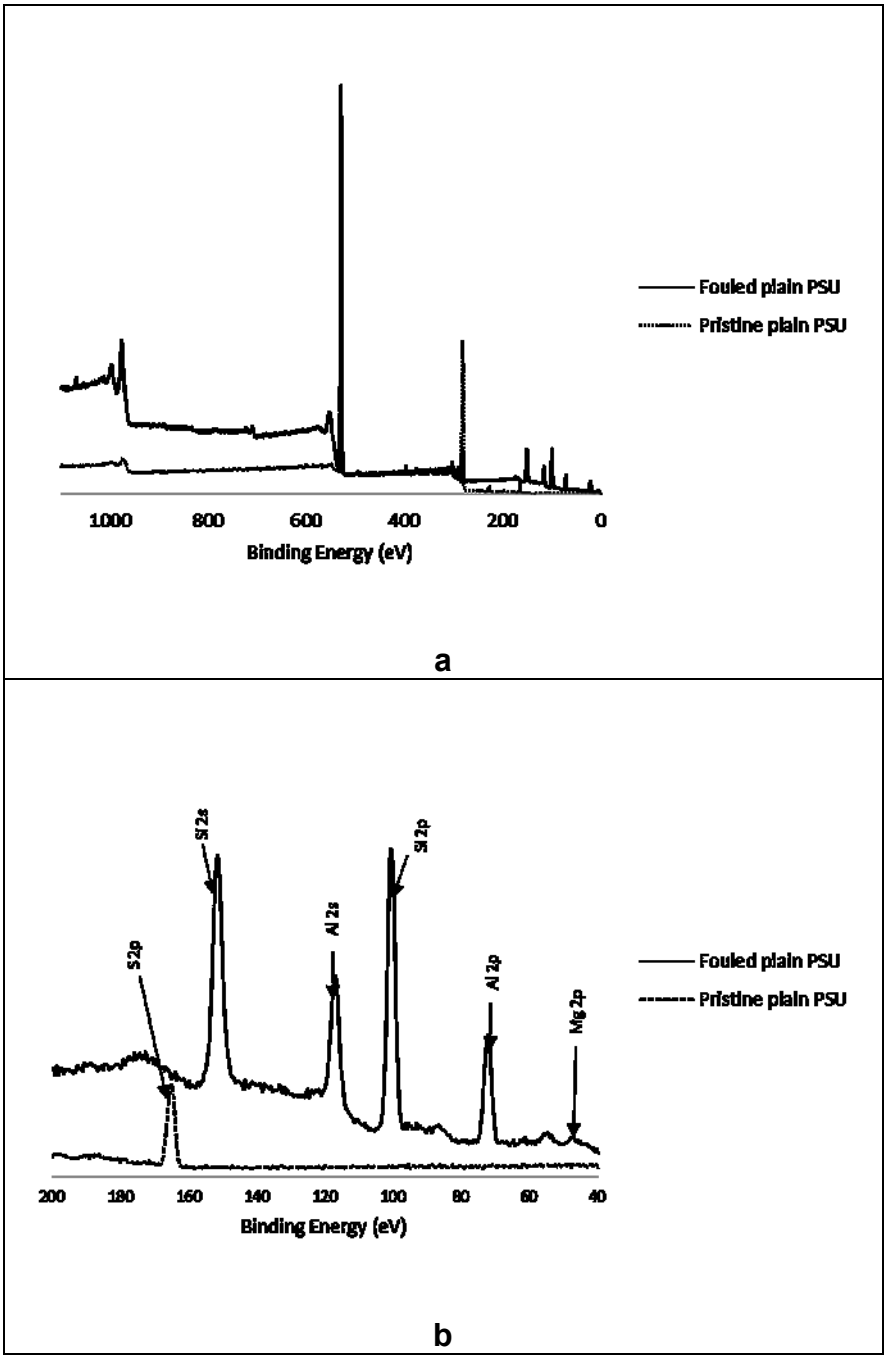

Figure 5.12 XPS spectra from survey scans of the selective surface of pristine and OSPW fouled PSU membrane (mMWNT-0): (a) full-scale and (b) partial scale.

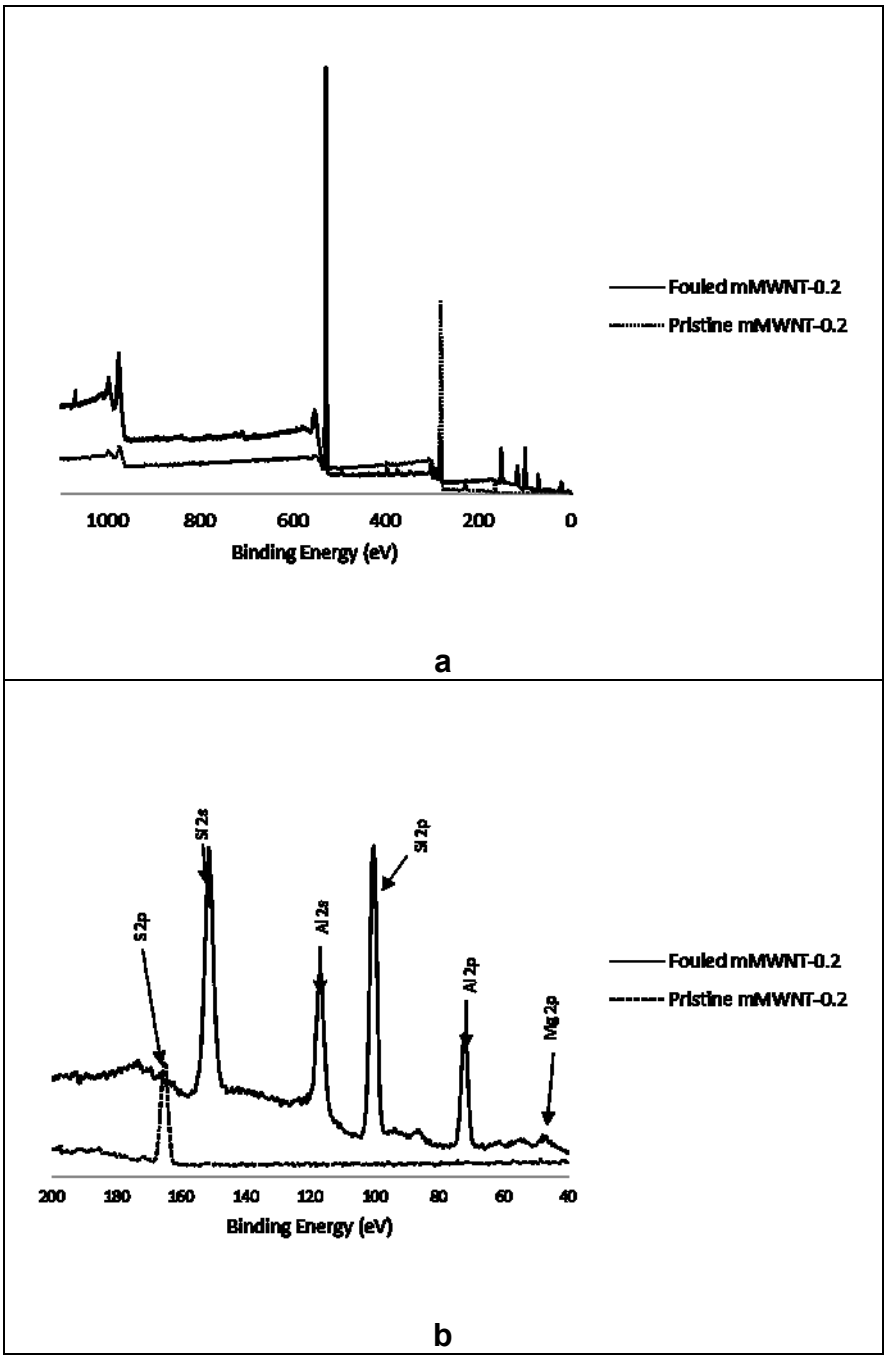

Figure 5.13 XPS spectra from survey scans of the selective surface of pristine and OSPW fouled PSU composite membrane (mMWNT-0.2): (a) full-scale and (b) partial scale.

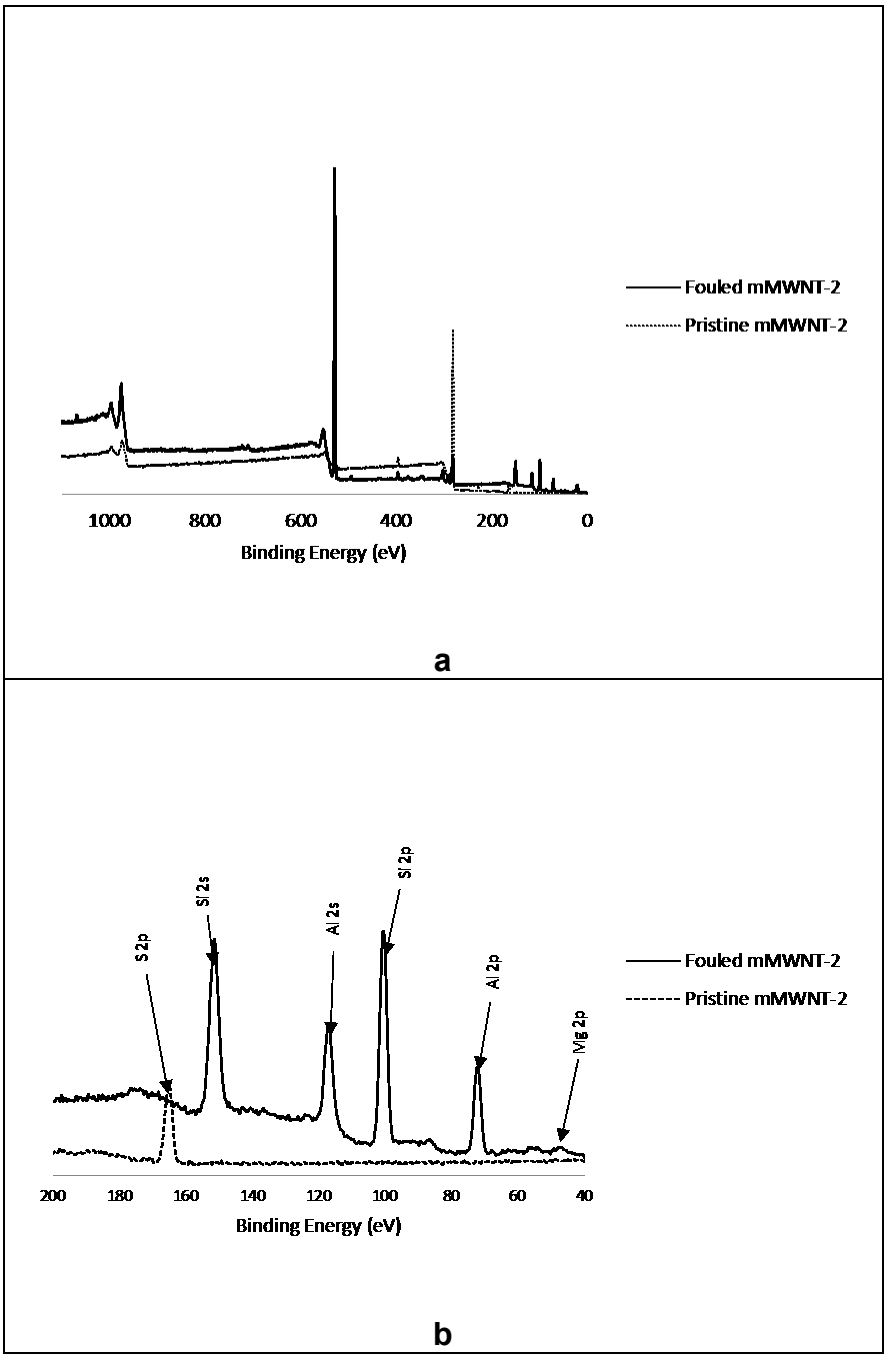

Figure 5.14 XPS spectra from survey scans of the selective surface of pristine and OSPW fouled PSU composite membrane (mMWNT-2): (a) full-scale and (b) partial scale.

5.3.3 OSPW permeate and water quality

Table 5.3 displays the results of water quality analysis for the four hour OSPW filtration and the longer term OSPW filtration. In general, the turbidity of resulting permeates decreases from 28.30 ± 2.28 NTU for raw OSPW to approximately 1 NTU or less. Turbidity data for the longer OSPW filtration did not show any significant differences to the resulting turbidity for the short term OSPW filtration.

There was a significant difference between total solids (TS) values for permeate obtained within 4 hours filtration and permeate obtained after days of OSPW filtration. For mMWNT-0, TS was 8.5% lower for the short term filtration than for long term OPSW filtration. For the composite membranes, TS from mMWNT-0.2 was 19.1% lower for the short term filtration versus long term filtration, and TS from mMWNT-2 was 11.6% lower for short term filtration. This indicates that over time, the resulting permeate experiences a decrease in water quality, especially with respect to total solids, as is seen in Table 5.3 for TS data for mMWNT-0, mMWNT-0.2, and mMWNT-2. However, in the long-term filtration, the total suspended solid (TSS) decreased when compared to the result from short-term filtration. It might be due to the fact that the accumulated fouling layer on the membrane surface could behave as a barrier to the particles as well.

Silt density index (SDI) is a widely accepted method to quantify a water sample's potential for fouling and is often used to ascertain whether a particular water is clean enough for NF or RO filtration (Farahani et al. 2016; Nahrstedt and Carmago-Schmale 2008). The SDI of feedwater for RO membranes should be less than 3 (Farahani et al. 2016). For the longer filtration, silt density index (SDI_{15}) was determined for raw OSPW and the permeate resulting from the membranes mMWNT-0, mMWNT-0.2, and mMWNT-2. Table 5.3 shows that raw OSPW had

an SDI_{15} of 4.18. Membrane mMWNT-0 produced permeate with an SDI_{15} of 1.04. The addition of mMWNT to PSU resulted in permeates with SDI_{15} of 0.70 for mMWNT-0.2 and 0.97 for mMWNT-2. Permeate resulting from filtration of OSPW through PSU with and without mMWNT had SDI_{15} values which fell between those obtained by Alpatova et al. (2014) and Dong et al. (2014). This is to be expected as Alpatova et al. (2014) used CFS in combination with UF for treatment of OSPW which resulted in lower SDI_{15}, while results obtained by Dong et al. (2014) were the result of CF followed by MF which resulted in SDI_{I5} values slightly above 1. With no membrane filtration at all, gravity settling or CFS could only get resulting SDI for OSPW down in the range of 1-2.

Short term OSPW filtration results indicate that TSS may or may not be decreased by filtration of OSPW through the fabricated membranes. Membranes mMWNT-0.2, mMWNT-0.5, and mMWNT-2 showed a notable decrease of TSS in the resulting permeate when compared with TSS of raw OSPW. Membranes mMWNT-0, mMWNT-1, and mMWNT-5 showed no decrease, or even an increase in TSS in the permeate resulting from OSPW filtration when compared with TSS for raw OSPW. These results indicate that membranes mMWNT-0, mMWNT-1 and mMWNT-5 may have less impact in the remediation of OSPW. These results are also consistent with the rejection results discussed in section 4.3.4. Membranes mMWNT-0, mMWNT-1, and mMWNT-5 had the lowest rejection values for the 6 membranes that were tested. Based upon the rejection results, mMWNT-0.2 and mMWNT-2 were chosen for the long term OSPW filtration experiment discussed in section 5.2.5 with results shown in Figure 5.2.

It is not known if subjection to longer term OSPW filtration would have resulted in an increase or decrease for permeate TSS for membranes mMWNT-1 and mMWNT-5 since longer OSPW filtration studies were not conducted for these membranes. Longer term OSPW filtration

resulted in lower TSS values (12.5 ± 2.5 mg/L) for permeate from membrane mMWNT-0 than the TSS for short term OSPW filtration permeate for the same membrane (18 ± 2 mg/L). The same phenomenon is seen for membrane mMWNT-2 to a lesser degree. However, long term OSPW filtration does not lead to significantly different TSS values than those found for short term OSPW filtration through membrane mMWNT-0.2. The formation of a cake layer may help to impede particles in the raw OSPW from traveling through the membrane, thus reducing TSS. For membrane mMWNT-0.2, smaller pores led to a reduced permeate flux. A reduced flux would mean that a cake layer would form but at a slower rate. For a longer time span, it might be possible that mMWNT-0.2 would see decreased levels TSS in the permeate.

The removal of AEF was measured for the permeate resulting from the longer OSPW filtration experiments and results are shown in Table 5.3. For the particular sample used, the AEF concentration in the raw OSPW was 47.8 ± 0.3 ppm. AEF removal for the plain PSU membrane, mMWNT-0, is 0.6 ± 0.6%. Addition of mMWNT results in a notable increase in AEF removal, 12.5 ± 1.1% for mMWNT-0.2 and 14.5 ± 0.9% for mMWNT-2. AEF removal by UF membrane is not efficient, as was noted by Alpatova et al. (2014). Results obtained for the long term filtration of raw OSPW using PSU with and without mMWNT show a similar trend as noted by Alpatova et al. (2014) and Kim et al. (2013). The higher removal of AEF for the composite membranes may be due to the increased membrane hydrophilicity with addition of mMWNT. Composite membranes with mMWNT have been shown to have a more hydrophilic surface. This could lead to less hydrophobic-hydrophobic interactions occurring between the membrane and AEF, and more hydrophobic-hydrophilic interactions, which could result in increased adsorption of AEF onto the membrane surface or within the pores (Moustafa et al. 2014).

Table 5.3 Permeate and raw OSPW water characterization data. Turbidity, total solids (TS), total suspended solids (TSS), and silt density index (SDI15) are given for raw OSPW. Turbidity, TS and TSS are given for permeates from short term OSPW filtration through PSU membranes with 0, 0.2, 0.5, 1, 2 and 5 wt.% mMWNT. Turbidity, TS, TSS, SDI_{15}, and acid extractable fraction (AEF) removal are given for permeates from long term OSPW filtration through PSU with 0, 0.2, and 2 wt. % mMWNT content.

	Short term OSPW filtration (4 hours)			Longer term OSPW filtration (>48 hours)				
Sample name	Turbidity (NTU)	TS (mg/L)	TSS (mg/L)	Turbidity (NTU)	TS (mg/L)	TSS (mg/L)	SDI15	AEF removal (%)
Raw OSPW	28.30 ± 2.28	2002 ± 6	17.5 ± 0	28.30 ± 2.28	2002 ± 6	17.5 ± 0	4.18	-
mMWNT-0	1.10 ± 0.08	1810 ± 10	18 ± 2	0.93 ± 0.05	1978 ± 2	12.5 ± 2.5	1.04	0.6 ± 0.6
mMWNT-0.2	0.81 ± 0. 02	1560 ± 10	2 ± 2	0.78 ± 0.03	1928 ± 2	0*	0.70	12.5 ± 1.1
mMWNT-0.5	0.92 ± 0.03	1610 ± 20	8 ± 8	-	-	-	-	-
mMWNT-1	0.95 ± 0.04	1775 ± 5	20 ± 4	-	-	-	-	-
mMWNT-2	0.89 ± 0.03	1700 ± 20	4 ± 0	0.92 ± 0.06	1924 ± 12	0*	0.97	14.5 ± 0.9
mMWNT-5	1.19 ± 0.6	1825 ± 5	14 ± 6	-	-	-	-	-

* These values were consistently calculated as low negative values, therefore a value of 0 was assigned for TSS

5.4 Conclusions

This study investigated the effect of incorporating -COOH modified MWNT within low pressure PSU membrane and how this affected membrane performance, especially with respect to treatment of OSPW. Nanocomposite PSU membranes containing 0, 0.2, 0.5, 1, 2, and 5 wt. % -COOH modified MWNT were previously fabricated by the phase inversion casting method. This chapter focused on treatment of OSPW using the nanocomposite membranes. Addition of mMWNT resulted in a reduced tendency for membrane fouling to occur, as shown by the decreased fouling ratios and increased flux recovery ratios for the nanocomposite membranes as compared with plain PSU membrane. The dominant fouling mechanisms during filtration of OSPW were found to be standard blocking and cake filtration. The standard blocking model resulted in the highest correlation value for membrane mMWNT-0, while the cake filtration model gave the highest correlation values for all nanocomposite membranes. SEM with EDS and XPS analysis resulted in data that shows that the fouling layer is composed mainly of clay or silt material mixed with salts, minerals, and some heavy metals. With respect to water quality, all fabricated membranes effectively reduced turbidity to values below 2 NTU. TS was found to be affected by filtration time, lower filtration led to a higher reduction of TS in the analyzed permeates, while longer filtration time led to higher TS in the resulting permeates. Addition of 0.2 and 2 wt. % mMWNT within the PSU membrane matrix led to OSPW filtration permeates which had SDI_{15} values which were 32.7% and 6.7% less than the SDI_{15} for plain PSU. All three membranes mMWNT-0, mMWNT-0.2 and mMWNT-2 resulted in permeates that were suitable for continued treatment with NF or RO membranes. Addition of 0.2 and 2 wt. % mMWNT within the PSU membrane matrix led to increased AEF removal that were 11.9% and 13.9% higher than AEF removal by plain PSU membrane. PSU membranes with 0.2 and 2 wt. %

mMWNT have been shown to increase AEF removal while increasing water quality of raw OPSW to levels that make them suitable for further membrane treatment (NF and RO) with no prior pre-treatment.

5.5 References

Afzal, A., Chelme-Ayala, P., Drzewicz, P., Martin, J.W., and Gamal El-Din, M. 2015. Effects of Ozone and Ozone/Hydrogen Peroxide on the Degradation of Model and Real Oil-Sands-Process-Affected-Water Naphthenic Acids. Ozone: Science and Engineering, 37: 45-54.

Allen, E.W. 2008. Process water treatment in Canada's oil sands industry: I. Target pollutants and treatment objectives. Journal of Environmental Engineering and Science, **7**: 123-138.

Alpatova, A., Kim, E-S, Dong, S., Sun, N., and Chelme-Ayala, P. 2014. Treatment of oil sands process-affected water with ceramic ultrafiltration membrane: Effects of operating conditions on membrane performance. Separation and Purification Technology, **122**: 170-182.

Anderson, J., Wiseman, S., Wang, N., Moustafa, A., Perez-Estrada, L., Gamal El-Din, M., Martin, J., Liber, K., and Giesy, J. 2012. Effectiveness of ozonation treatment in eliminating toxicity of oil sands process-affected water to Chironomus-dilutus. Environmental Science and Technology, **46**: 486-493.

ASTM International. 2014. Standard Test Method for Silt Density Index (SDI) of Water [online]. Available from http://dx.doi.org/10.1520/D4189 [accessed 1 May 2016].

Blanco, J-F., Sublet, J., Nguyen, Q.T., and Schaetzel, P. 2006. Formation and morphology studies of different polysulfones-based membranes made by wet phase inversion process. Journal of Membrane Science, **283**: 27-37..

Dong, S., Kim, E-S, Alpatova, A., Noguchi, H. Liu, Y., and Gamal El-Din, M. 2014. Treatment of oil sands process-affected water by submerged ceramic membrane microfiltration system. Separation and Purification Technology, **138**: 198-209.

Eaton, A.D., Clesceri, L., Greenberg, A.E., and Franson, M.A.H. 2016. Standard Methods for the Examination of Water and Wastewater. American Public Health Association, Washington, DC.

Farahani, M., Borghei, S., and Vantanpour, V. 2016. Recovery of cooling tower blowdown water for reuse: The investigation of different types of pretreatment prior to nanofiltration and reverse osmosis. Journal of Water Process Engineering, **10**: 188-199.

Gamal El-Din, M., Fu, H., Wan, N., Chelme-Ayala, P., Perez-Estrada, L., Drzewicz, P., Martin, J.W., Zubot, W., and Smith, D.W. 2011. Naphthenic acids speciation and removal during petroleum-coke adsorption and ozonation of oil sands process-affected water. Science of the Total Environment, **409**: 5119-5125.

Islam, M.S., Dong, T., Sheng, Z., Zhang, Y., Liu, Y., and Gamal El-Din, M. 2014. Microbial community structure and operational performance of a fluidized bed biofilm reactor treating oil sands process-affected water. International Biodeterioration & Biodegradation, **91**:111-118.

Kim, E-S, Liu, Y., and Gamal El-Din, M. 2011. The effects of pretreament on nanofiltration and reverse osmosis membrane filtration for desalination of oil sands process-affected water. Separation and Purification Technology, **81**: 418-428.

Kim, E-S, Liu, Y., and Gamal El-Din, M. 2012. Evaluation of Membrane Fouling for In-Line Filtration of Oil Sands Process-Affected Water: The Effects of Pretreatment Conditions. Environmental Science and Technology, **46**: 2877-2884.

Kim, E-S, Liu, Y., and Gamal El-Din, M. 2013. An in-situ integrated system of carbon nanotubes nanocomposite membrane for oil sands process-affected water treatment. Journal of Membrane Science, **29**: 418-427.

Klamerth, N., Moreira, J., Li, C., Singh, A., McPhedran, K.N., Chelme-Ayala, P., Belosevic, M., and Gamal El-Din, M. 2015. Effect of ozonation on the naphthenic acids' speciation and toxicity of pH-dependent organic extracts of oil sands process-affected water. Science of the Total Environment, **506-507**: 66-75.

Loganathan, K., Chelme-Ayala, P., and Gamal El-Din, M. 2015. Pilot-scale study on the reverse osmosis treatment of oil sands tailings pond water: Impact of pretreatment on process performance. Desalination, **360**: 52-60.

Masoudnia, K., Raisi, A., Aroujalian, A., and Fathizadeh, M. 2013. Treatment of Oily Wastewaters Using the Microfiltration Process: Effects of Operating Parameters and Membrane Fouling Study. Separation Science and Technology, **45**(10): 1544-1555.

Moustafa, A., Kim, E.S., Alpatova, A., Sun, N., Smith, S., Kang, S., and Gamal El-Din, M. 2014. Imact of polymeric membrane filtration of oil sands process water on organic compounds quantification. Water Science & Technology, **70**: 771-779.

Nahrstedt, A. and Carmago-Schmale, J. 2008. New insights into sild density index and modified fouling index measurements. Water Science & Technology: Water Supply, **8**: 401-411.

Peng, H., Volchek, K., MacKinnon, M., Wong, W., and Brown, C. 2004, Application of nanofiltration to water management options for oil sands operations. Desalination, **120**: 137-150.

Pourrezaei, P., Drzewicz, P., Yingnan, W., Gamal El-Din, M., Perez-Estrada, L., Martin, J., Anderson, J., Wiseman, S., Liber, K., and Geisy, J. 2011. The Impact of Metallic Coagulant on the Removal of Organic Compounds from Oil Sands Process-Affected Water. Environmental Science and Technology, **45**: 8452-8459.

Pourrezaei, P. Wang, Y.; Perez-Estrada, L.; Martin, J.; and Gamal El-Din, M. 2012. Coagulation/flocculation/sedimentation treatment of oil sands process-affected water. *In* Annual Conference of the Canadian Socieity for Civil Engineering 2012: Leadership in Sustainable Infrastructure, Edmonton, Alberta 2012. CSCE 2012.

Richards, H.L., Baker, P., and Iwuoha, E. 2012, Metal nanoparticle modifie polysulfone membranes for use in wastewater treatment: a critical review. Journal of Surface Engineered Materials and Advanced Technology, **2**: 183-193.

Shrestha, N., Chilkoor, G., Wilder, J., Gadhamshetty, V., and Stone, J. 2017. Potential water resource impacts of hydraulic fracturing from unconventional oil production in the Bakken shale. Water Research, **108**: 1-24.

Small, C.C., Ulrich, A.C., and Hashisho, Z. 2012. Adsorption of Acid Extractable Oil Sands Tailings. Journal of Environmental Engineering, **138**: 833-840.

Vantanpour, S., Madaeni, S., Morandian, R., Zinadini, S., and Astinchap, B. 2011. Fabrication and characterization of novel antifouling nanofiltration membrane prepared from oxidized multiwalled carbon nanotube/polyethersulfone nanocomposite. Journal of Membrane Science, **375**: 284-294.

Wei, C.H., Laborie, S., Aim, R.B., and Amy, G. 2012. Full utilization of silt density index (SDI) measurements for seawater pre-treatment. Journal of Membrane Science, **405-406**: 212-218.

Zaidi, A., Simms, K., and Kok, S. 1992. The use of micro/ultrafiltration for the removal of oil and suspended solids from oilfield brines. Water Science & Technology, **25**(10): 163-176.

Zhou, J., Wandera, D., and Husson, S. 2015. Mechanisms and control of fouling during ultrafiltration of high strength wastewater without pretreatment. Journal of Membrane Science, **488**: 103-110.

Zubot, W., MacKinnon, M.D., Chelme-Ayala, P., Smith, D.W., and Gamal El-Din, M. 2012. Petroleum coke adsorption as a water management option for oil sands process-affected water. Science of the Total Environment, **427-428**: 364-372.

6. ADSORPTION OF ORGANIC MATTER IN OIL SANDS PROCESS WATER (OSPW) BY CARBON XEROGEL[3]

6.1 Introduction

As one of the largest oil deposits in the world, the Alberta oil sands are composed of approximately 10% bitumen mixed with 5% water and 85% mineral solids (Allen 2008a; Zubot et al. 2012). The high content of mineral solids (mainly sand, clay and silt) renders it necessary to first extract the bitumen from the oil sands by the Clark caustic hot water extraction method which requires approximately 3 m^3 of water for every m^3 of oil sands processed, and results in the production of 4 m^3 of tailings (Holowenko et al. 2002). Water that has come into contact with oil sands or has been released from tailings is referred to as oil sands process water (OSPW) and is not released to the environment but kept in tailings ponds due to health and environmental concerns (Zubot et al. 2012). OSPW is a widely varying and complex mixture that may contain high concentrations of chloride, salts, polycyclic aromatic hydrocarbons (PAHs), naphthenic acids (NAs), trace heavy metals, BTEX (benzene, toluene, ethyl benzene, and xylenes), phenols and other inorganic and organic compounds (Gamal El-Din et al. 2011; Li et al. 2017).

NAs is a broad term that describes the family of saturated aliphatic and alicyclic carboxylic acids found naturally within the oil sands or other crude oil deposits (Quinlan and Tam 2015). NAs have the general empirical formula $C_nH_{2n+Z}O_x$, where "n" is the carbon number ($7 < n < 26$), "Z" is zero or a negative even integer ($0 \leq |Z| < 18$) representing the hydrogen deficiency resulting from rings or unsaturated bonding formation, and x represents the number of oxygen atoms, where x is 2 for classical NAs or $x \geq 3$ for oxy-NAs (Bertheussen et al. 2017). Although

[3] A version of this chapter will be submitted to the Water Research as "Benally, C., Messele, S., and Gamal El-Din, M.: Adsorption of organic matter in oil sands process water by carbon xerogel".

NAs account for less than 50% of the organic fraction of OSPW, some studies have indicated that NAs are a contributor to the acute and chronic toxicity of OSPW affecting aquatic and mammalian species (Jones et al. 2011; Klamerth et al. 2015; Li et al. 2017; MacKinnon and Boerger 1986). In addition, NAs are also one of the primary causes of corrosion to the equipment used during bitumen extraction; however they are needed during the extraction of bitumen from the sand (Derungs 1956; Fan 1991; Quinlan and Tam 2015).

Research on treatment methods for OSPW started as early as the 1970s and initially focused on solid-liquid separation aimed at enhancing settling rates of tailings and recovery of process water. Some remediation methods have included adsorption (Gamal El-Din 2011; Pourrezaei et al. 2014; Small et al. 2012; Zubot et al. 2011), coagulation and flocculation (Kim et al. 2011; Pourrezaei et al. 2011), membrane filtration (Alpatova et al. 2014; Dong et al. 2014; Kim et al. 2011; Kim et al. 2012; Kim et al. 2013; Peng et al. 2004; Zhu et al. 2017), and advanced oxidation processes (Afzal et al. 2015; Klamerth et al. 2015; Wang et al. 2016a). Reduction of NAs has become a more recent research area due in large part to studies that have shown that NAs, among other constituents in OSPW, contribute to the acute and sub-chronic toxicity of OSPW to aquatic and mammalian species.

Adsorption is an effective method that can be used to remove organic contaminants from an aqueous solution; this includes NAs (Zubot et al. 2012). Initially OSPW was treated by adsorption in order to remove oil and other organic foulants so that the water could be further used in the bitumen extraction process, but currently, adsorption of OSPW is conducted with the intent of removing or reducing the NAs concentration (Allen 2008b; Islam et al. 2014). Adsorbents tested for NAs removal studies include activated carbon (AC) (Iranmanesh et al. 2014; Islam et al. 2014; Islam et al. 2018), petroleum coke (Pourrezaei et al. 2014; Zubot et al.

2012), biochar (Bhuiyan et al. 2017; Frankel et al. 2016), and chitosan hydrogels (Quinlan et al. 2017).

AC is one of the most well-known adsorbent materials that have been applied to OSPW for AEF reduction (Bhuiyan et al. 2017). AC can have a high surface area if the pore structure is mainly microporous (Wu and Zhao 2011). While a high surface area is advantageous for adsorption, the presence of bulky organic contaminants can pose a problem when using an AC composed of mainly micropores, as some of the surface area thought to be available for adsorption on or within AC may not be accessible to the larger organic contaminants because their diameters might be larger than the diameter of pores in the AC (Wu and Zhao 2011). Carbon xerogels (CX) are polymer derived mesoporous materials which can be customized in order to accommodate larger sized adsorbates or specific conditions (Mahata et al. 2007). CX can have high surface area (400-1200 m^2/g), controllable pore size, and high adsorption capacity. These qualities make CX a potential adsorbent material for the removal of NAs in OSPW.

In this study the use of carbon xerogel (CX) as an adsorbent material used for the removal of AEF and NAs in OSPW was evaluated. The objectives of the present study were to: (1) determine the equilibrium time needed for adsorption of acid-extractable fraction (AEF) by CX, (2) gain an understanding of the effect of CX dose on adsorption of AEF in OSPW, (3) determine the adsorption capacity of CX, (4) gain an understanding of the kinetics involved in the removal of AEF and NAs by CX, and (5) determine the types of diffusion involved in the adsorption of AEF and NAs by CX using a diffusion model. To achieve these objectives, adsorption studies were performed by mixing raw OSPW with various doses of CX for different contact times. AEF removal was determined by first extracting AEF from raw and treated OSPW, and then analyzing AEF with Fourier transform infrared spectroscopy (FT-IR). The

adsorption capacity and mechanism of AEF adsorption was determined by fitting AEF concentration data to different adsorption isotherms and analyzing the resulting curves. In addition to removal of AEF, NAs removal was also examined by analysis of raw and treated OSPW using ultra-performance liquid chromatography coupled with time-of-flight mass spectrometer (UPLC-TOF-MS).

6.2 Experimental methods and materials

6.2.1 OSPW and chemicals

Raw OSPW was collected from an oil sands tailing pond in Fort McMurray, Alberta, Canada and stored in a cold room at 4°C. Dichloromethane (DCM) - HPLC grade and Optima® grade, hydrochloric acid (HCl), and sulfuric acid (H_2SO_4) were purchased from Fisher Scientific (Ottawa, ON, Canada). Resorcinol (99%), formaldehyde (37 wt.% in water, stabilized by 10-15 wt.% methanol), hydrochloric acid (>37%), sodium hydroxide (97%), were purchased from Fisher (New Jersey, USA). Milli-Q water was produced using a Milli-Q Ultrapure Water System (Millipore Corporation, Bedford, MA, USA).

6.2.2 Carbon xerogel synthesis

The carbon xerogels (CX) used for the adsorption experiments were prepared using a sol-gel preparation technique involving the polycondensation of formaldehyde and resorcinol (Job et al. 2004; Mahata et al. 2007). Two types of CX were prepared, denoted as CX5.5 and CX6.9. The ratio of resorcinol to formaldehyde was kept constant at 0.5 (Job et al. 2004). For the preparation of the CX samples, 25 g of resorcinol was dissolved in 40 mL of Milli-Q water. This solution was then adjusted to pH of 5.5 using 2 M NaOH for CX5.5, or to pH of 6.9 for CX6.9. Then 34 mL of formaldehyde was added to the resorcinol solution under constant mixing. The

resulting solution was then adjusted to pH of 5.5 (for CX5.5) or 6.9 (for CX6.9) using 2 M NaOH. The solutions were allowed to stir for 90 minutes to ensure that all components were completely mixed and then placed into an oven set at 60°C for 3 days in order for the gelation process to occur (Mahata et al. 2007). The gel then underwent a 7 day curing process in an oven with the following temperature profile: 60°C for 24 hours, 80°C for 24 hours, 100°C for 24 hours, 120°C for 24 hours, 105°C for 72 hours. The resulting material was a red-brown hardened gel that was opaque in color. Carbonization of the hardened gel was accomplished by pyrolysis in order to obtain mesoporous carbon samples (Mahata et al. 2007). The dried gels were heated in a Lindberg/Blue M^{TM} furnace (Thermo Fisher Scientific, USA) in an inert atmosphere (N_2 flow of 1 L/min) with the following heat temperature profile: room temperature to 200°C, hold at 200°C for 1 hour, 200°C to 700°C, hold at 700°C for 3 hours, 700°C to room temperature. The pyrolyzed gels were then crushed and sieved to the desired size of 0.6 to 1.4 mm.

6.2.3 Carbon xerogel characterization

The prepared carbon xerogel samples were characterized by the methods described in the text to follow[4]. Prepared carbon xerogel surface area and porous properties were determined by adsorption of nitrogen onto carbon xerogel at 77 K and by using a surface area analyzer (Autosorb-1MP Quanthachrome, USA). Both the surface area (S_{BET}) and the total pore volume (V_{total}) were calculated using the Brunauer-Emmett-Teller (BET) method (Bruanuer et al. 1938). The t-plot method (de Boer et al. 1966) was used to determine micropore surface area (S_{micro}), external surface area (S_{meso}) and micropore volume (V_{micro}). The method used by Barrett, Joyner and Halenda (Barrett et al. 1951) was used to determine the average pore diameter (D_p).

[4] Characterization of the carbon xerogel samples was performed by post-doctoral staff member, Dr. Selamawit Messele, in Dr. Gamal El-Din's research group at the University of Alberta.

6.2.4 Effect of adsorbent dose experiments

The effect of adsorbent loading was studied by varying the amount of carbon xerogel added to a specified volume of OSPW for 24 hours adsorption time. The following doses of each type of carbon xerogel (CX5.5 and CX6.9) were added to a specific amount of OSPW: 0.5 g/L, 1 g/L, 1.5 g/L, 2 g/L, 2.5 g/L, 3 g/L, 4 g/L, 5 g/L, 6 g/L. The loading experiments were conducted in duplicate. For each reactor, 50 mL of raw OSPW was transferred to an Erlenmeyer flask. The calculated amount of adsorbent material was weighed out and added to a reactor ready with raw OSPW and the start time was recorded. The reactor was covered and placed on a New Brunswick™ Innova® 2100 platform shaker (Eppendorf Inc., USA) set at 200 RPM for 24 hours. After 24 hours the OSPW and the carbon xerogel were filtered through a 0.45 μm filter to remove the adsorbent material from the OSPW. The filtered OSPW sample was collected and saved for FT-IR extraction/analysis and UPLC-MS-TOF analysis.

6.2.5 Equilibrium time experiments and kinetics experiments

Equilibrium time experiments (ETE) and kinetics experiments were conducted together. The data was used to determine the equilibrium time required in order for a sample of CX in OSPW to reach equilibrium with respect to adsorption of acid extractable fraction (AEF) and/or NAs. Additionally, the data could be used to study the kinetics of how AEF and NAs adsorption.

For the equilibrium time and kinetics experiments, the adsorbent used was CX5.5 and the adsorbent load was 3 g/L. The adsorption times for the reactors were as follows (with the subscript denoting the sampling time with appropriate time unit): t_{0min}, t_{5min}, t_{10min}, t_{15min}, $t_{0.5hr}$, t_{2hr}, t_{4hr}, t_{6hr}, t_{18hr}, and t_{24hr}. A separate reactor was required for each time as the sample volume of

raw OSPW used was at least 35 mL. Each experiment was conducted in duplicate. A control experiment was conducted without carbon xerogel.

For each reactor, 50 mL of raw OSPW was transferred to an Erlenmeyer flask. Approximately 150 mg (3 g/L) of adsorbent material was weighed out and added to a reactor ready with the OSPW, noting the start time. Each reactor was placed on a New Brunswick™ Innova® 2100 platform shaker (Eppendorf Inc., USA) set at 200 RPM for a specified amount of time after which the OSPW and the carbon xerogel were filtered through a 0.45 μm filter to remove the adsorbent material from the OSPW. The filtered OSPW sample was collected and saved for FT-IR extraction/analysis and UPLC-MS-TOF analysis.

6.2.6 FT-IR extraction and analysis

The AEF extraction method and FT-IR analysis method are found in detail elsewhere (Jivraj et al. 1996; Rogers et al. 2002; Zubot et al. 2012). These methods are described briefly in the following paragraphs.

The extraction of the OSPW and post adsorption OSPW samples was accomplished by first weighing the OSPW samples, adjusting the pH, extracting samples using dicholoromethane (DCM) and then evaporating the DCM from the acid-extractable fraction (AEF). Filtered raw OSPW and post adsorption OSPW samples were weighed out (approximate weight used was 50 g, however smaller sized aliquots such as 25 g or 35 g could be used) and then acidified to pH of 2.2 using a solution of 1 M H_2SO_4. The samples were extracted twice using 25 mL (or half the volume of the sample size) of DCM for each extraction. For each sample, the DCM with acid-extractable fraction (AEF) was collected in a clean glass tube. The DCM with AEF was dried

completely under filtered air flow at room temperature leaving behind only the AEF residue in the glass tube.

To perform FT-IR analysis of the AEF residue for each sample, the residue was first reconstituted with a known amount of Optima grade DCM. A small portion of the reconstituted AEF in DCM was carefully injected into a clean KBr cell and was analyzed by FT-IR spectrophotometer (Nicolet 8700, Thermo Scientific). The resulting FT-IR spectrums were analyzed by obtaining peak values at approximately 1743 cm^{-1} and 1706 cm^{-1}. Prior to analysis, a standard curve was generated on using known amounts of Fluka standard with the KBr cell. Using this data, and the peak values obtained from FT-IR analysis of AEF residue after extraction, it was possible to obtain a rough estimate of the AEF concentration in the raw and treated OSPW samples.

6.2.7 UPLC-TOF-MS analysis

Ultra-performance liquid chromatography coupled with time-of-flight mass spectrometer (UPLC-TOF-MS) was used to quantify NAs (Wang et al. 2016b). Six samples were chosen for analysis by UPLC-TOF-MS: raw OSPW, OSPW following adsorption with 3g/L dose of CX5.5 for time of 10 minutes, 30 minutes, 2 hours, 6 hours and 24 hours. Chromatographic separation of samples was conducted using a Waters UPLC Phenyl BEH column (1.7 µm, 150 mm x 1 mm) (Waters, AM, USA) (Huang et al. 2015). Samples were analyzed with high resolution TOF-MS with electrospray ionization (Synapt, G2, Waters, MA, USA) in negative mode and positive mode. Electrospray ionization (ESI) analysis in negative mode measured NAs, while ESI analysis in positive mode measured NAs as well as other species (Wang et al. 2016a). TOF analyzer was in high-resolution mode (Huang et al. 2015). For ESI in the negative mode an internal standard was employed which allowed calculation of NAs concentrations based upon

peak area. In the positive ESI mode, no internal standard was used due to lack of information about the molecular structures of species present in addition to NAs. As a result, NAs concentrations were not calculated from data resulting from positive ESI mode. More information regarding the method for UPLC-TOF-MS analysis can be found in previous studies (Huang et al. 2015; Wang et al. 2016a).

6.3 Results and discussion

6.3.1 Carbon xerogel properties

Table 6.1 gives common properties for the CX adsorbent material that was used for the adsorption experiments. The Brunauer, Emmet, and Teller (BET) surface area is shown in the first column for each type of CX. Of the two types of CX made, CX5.5 had the larger BET surface area at 573 ± 10 m^2/g. This result is high in comparison to BET surface area of 330 m^2/g obtained for CX made at pH 5.5 by Job et al. (2004). Approximately 87% of the pore volume contained in the sample of CX5.5 is due to the presence of mesopores. CX6.9 has a smaller BET surface area and about 42% of the pore volume contained in the sample is due to the presence of micropores. The total pore volume for CX5.5 is almost 6 times that for CX6.9. The pore size distributions of carbon xerogel (Figure S1 in the Appendix) show that both types of CX do contain both mesopores and micropores. CX5.5 has a broader range of mesopores (3– 32.5 nm) with most of the pores occurring in the region from 3-17.5 nm around a maximum of about 10 nm. CX6.9 has a much narrower pore size distribution in the mesopore region (2.5-5 nm) with a maximum of about 4 nm. Based upon these results alone one can conclude that the adsorbent material which will perform better for the adsorption of AEF from OSPW is CX5.5. This is due

to the fact that CX5.5 has a higher surface area, a higher total volume due to the presence of mesopores, and a wider pore size distribution when compared with CX6.9.

Table 6.1 Properties of carbon xerogel adsorbent material. S_{BET}: Total surface area; S_{micro}: Micropore surface area; V_{micro}: Micropore volume; V_{meso}: Mesopore volume; V_{total}: Total pore volume; D_p: Average pore diameter.

Sample	S_{BET} (m^2/g)	S_{micro} (m^2/g)	V_{micro} (cm^3/g)	V_{meso} (cm^3/g)	V_{total} (cm^3/g)	Dp (nm)
CX5.5	573	438	0.205	1.340 (87%)	1.545	11
CX6.9	391	256	0.116	0.157 (58%)	0.273	3

6.3.2 Effect of adsorbent dose

The effect of adsorbent dose on adsorption of AEF in OSPW is shown in Figure 6.1. For both CX5.5 and CX6.9, higher doses of adsorbent material resulted in higher AEF removal. This same trend was seen by Pourrezaei et al. (2014) for both AEF and chemical oxygen demand (COD) removal using PC. As well, Islam et al. (2018) found that higher doses of GAC resulted in higher removal of AEF and classical NAs. The trend seen is most likely because a higher adsorbent mass means that there is more surface area available for the AEF to readily adsorb onto, resulting in higher AEF removal (Khan et al. 2011).

There is a notable difference between the removal by CX5.5 and CX6.9. CX5.5 achieved 89% removal for 6 g/L dose and adsorption time of 24 hr, while CX6.9 only resulted in slightly more than 14% removal using the same dose and adsorption time. For doses higher than 1 g/L removal by CX5.5 continued to increase but at a decreasing rate. On the other hand, removal by CX6.9 increases very little initially and begins to plateau by dose of 4 g/L.

The low removal by CX6.9 can be linked directly to the CX properties (Table 6.1) and narrow pore size distribution (Figure S1). Lower removal of AEF by CX6.9 in comparison to CX5.5 was expected due to the higher pore size distribution, higher BET surface area and total pore volume for CX5.5 (Niasar et al. 2016). Due to the low AEF removal at all tested doses, it was concluded that CX6.9 was not an efficient adsorbent for the treatment of OSPW. Even with very high doses of CX6.9, it seems unlikely that AEF removal above 25% could be achieved using CX6.9. All further adsorption studies were conducted using only CX5.5.

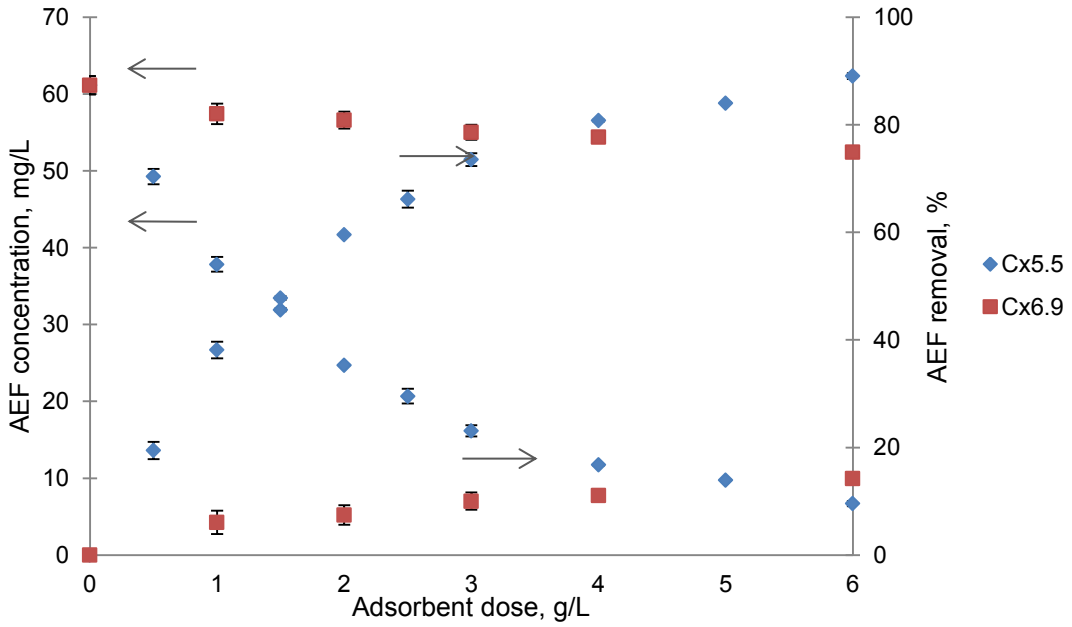

Figure 6.1 AEF concentration and removal in OSPW after 24 hour adsorption with different doses of CX5.5 or CX6.9.

6.3.3 AEF and NAs removal

Equilibrium time experiments were conducted to determine the amount of time needed for a sample of CX in OSPW to reach equilibrium with respect to adsorption of AEF. The results of the equilibrium time and kinetics experiments for adsorption of AEF by CX5.5 are shown in

Figure 2a. For a 3 g/L dose of CX5.5, AEF concentration decreases rapidly in the first 6 hours. From 6 h to 18 h, AEF concentration decreases in the treated OSPW but at a decreasing rate. Between 18 and 24 h the AEF concentration levels out, this is where AEF removal plateaus around 74.6%. By 18 hours, a sample of CX5.5 in OSPW has reached equilibrium with respect to removal of AEF. A similar trend was reported for the adsorption of AEF in OSPW onto granular activated carbon (Islam et al. 2018).

In addition to AEF concentration data, raw OSPW and treated OSPW samples post adsorption were analyzed by UPLC-TOF-MS with electrospray ionization (ESI) in the negative mode in order to obtain classical NAs concentration data. Figure 2b shows the total classical NAs concentration and removal curves as a function of time for OSPW that was treated by adsorption for up to 24 hours using a 3 g/L dose of CX5.5. The results are very similar to those obtained using the AEF concentration data for adsorption with CX5.5 (Figure 2a). The main difference being that classical NAs removal was nearly 89% for 24 hours adsorption, and AEF removal was 74.6% for the same adsorption time. In the first 2 hours of adsorption, there was a drastic reduction of total classical NAs concentration (~72%). By an adsorption time of 6 hours there was an 86.3% reduction in classical NAs. After this time the removal increases a few percent to a final removal of 88.8% for 24 hours adsorption time.

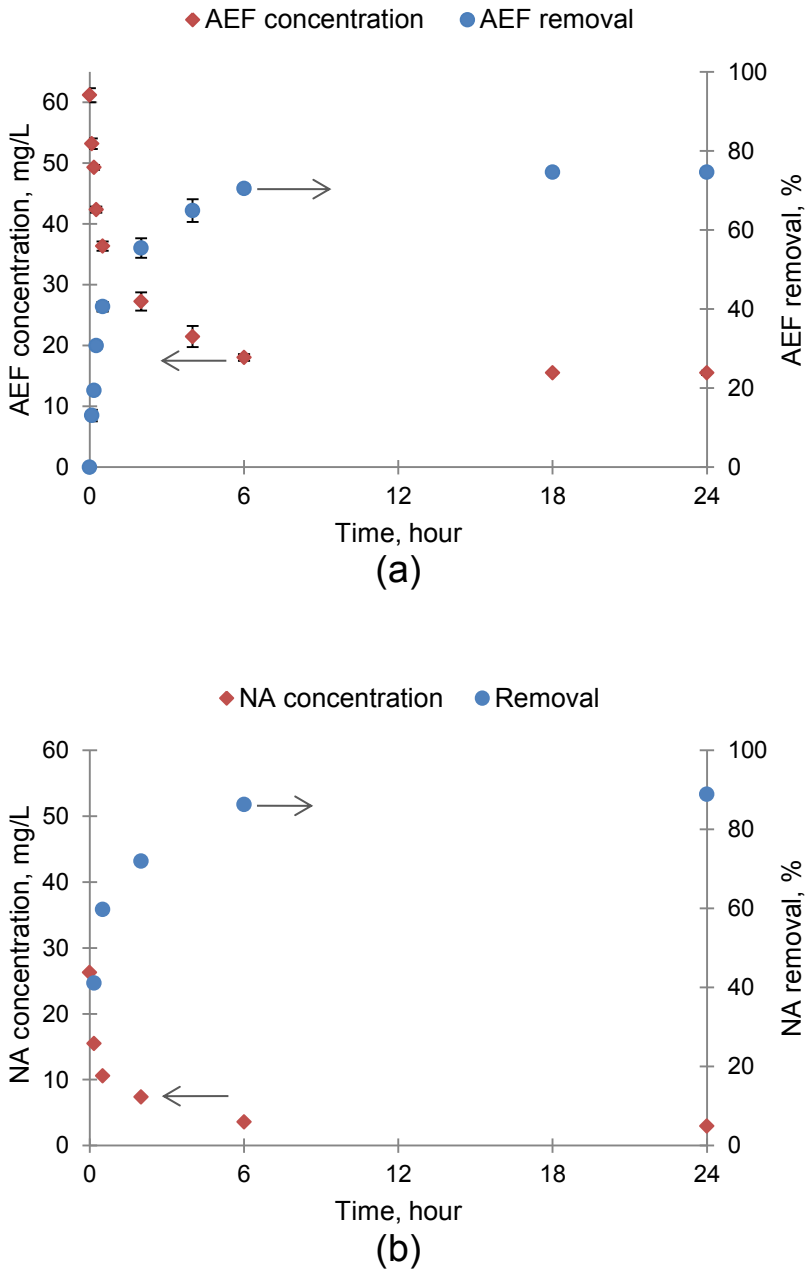

Figure 6.2 (a) AEF concentration and removal and (b) total classical NAs concentration and removal in OSPW after adsorption with 3g/L dose of CX5.5 for different adsorption time.

Figure S2 (Appendix) shows the classical NAs concentration profiles in OSPW as a function of carbon number and –Z number before and after treatment with 3 g/L CX5.5 for a 24 hour time adsorption time period. NAs found in raw OSPW (Figure S2a) were in the carbon

range of 9 to 21 and had –Z values ranging from 0 to 18. With respect to carbon number, the majority of NAs were found in the range of 12 to 18, with the peak value occurring for carbon number 14. With respect to –Z, the NAs distribution is bimodal with two distinct peaks. The larger peak occurs at –Z value of 4, however it is important to note that the second largest concentration of NAs occurs for –Z value of 6. After this, the NAs concentrations decrease for –Z values of 8 and 10. The lesser peak occurs at –Z value of 12, this is the third largest concentration of NAs with respect to –Z value. Therefore a majority of the classical NAs in the raw OSPW were bicyclic, tricyclic, and hexacyclic. The differences between the raw OSPW described here and elsewhere are due to the widely varying nature of OSPW in combination with differences in the bitumen ore, sampling dates, and changes in extraction methods (Gamal El-Din et al. 2011).

Post adsorption, the OSPW total classical NAs concentration was reduced from 26.3 mg/L to 2.94 mg/L. Classical NAs with carbon number 17 and above were almost completely removed (carbon number 19, 20 and 21 were removed in totality). For the NAs remaining post adsorption, the peak concentration occurred for carbon number 12. This means that more carbon number 14 was removed by adsorption than carbon number 12. This is supported by results shown in Figure S3a (Appendix), which shows the normalized classical NAs concentration profiles as a function of time for each carbon number. In general, the higher carbon numbers experience greater removal as demonstrated by the data for carbon number 12 and above. Classical NAs with carbon numbers 9 through 11 had the least removal by adsorption. NAs with higher carbon number have higher hydrophobicity which leads to greater adsorption (Zubot et al. 2011). These results are consistent with results reported by Islam et al. (2018), Pourrezaei et al. (2014), and Zubot et al. (2011).

Figure S3b shows the normalized classical NAs concentration profiles as a function of time for each –Z number. Results from Figure S2 in combination with data shown in Figure S3b indicate that CX5.5 was effective at adsorbing NAs with higher cyclicity. These findings are consistent with previous results for adsorption treatment of OSPW (Gamal El-Din et al. 2011; Pourrezaei et al. 2014; Zubot et al. 2011). With respect to –Z, the classical NAs distribution was no longer bimodal post adsorption. For values of –Z greater than or equal to 8, classical NA concentrations were present in amounts less than 0.2 mg/L. A peak concentration of 1.04 mg NAs/L occurred at –Z value of 4, this was also the –Z value with the highest concentration in raw OSPW. Classical NAs with –Z value of 2 were the least removed. Unlike the results obtained for NAs removal as a function of carbon number, there were no values of –Z that were completely removed by adsorption. This indicates that carbon number has a greater influence on adsorption of NAs than –Z. These results are consistent with results found by Pourezzaei et al. (2014).

The removal of classical NAs as a function of carbon number and –Z number in raw and treated OSPW for different adsorption time is shown in Figure 6.3. Greater adsorption time leads to greater NAs removal, as also shown by Figure 2b. The removal results for 6 hours adsorption time are not far below the final removal after 24 hours adsorption for both carbon number and –Z number. For 24 hours adsorption time, only carbon numbers 13 through 21 experience at least 80% removal. NAs with carbon number less than 12 have removal values that vary between 38% and 47% with no clear removal trend. For 24 hours adsorption time, NAs with –Z values of 4 to 18 all result in at least 80% removal. There is

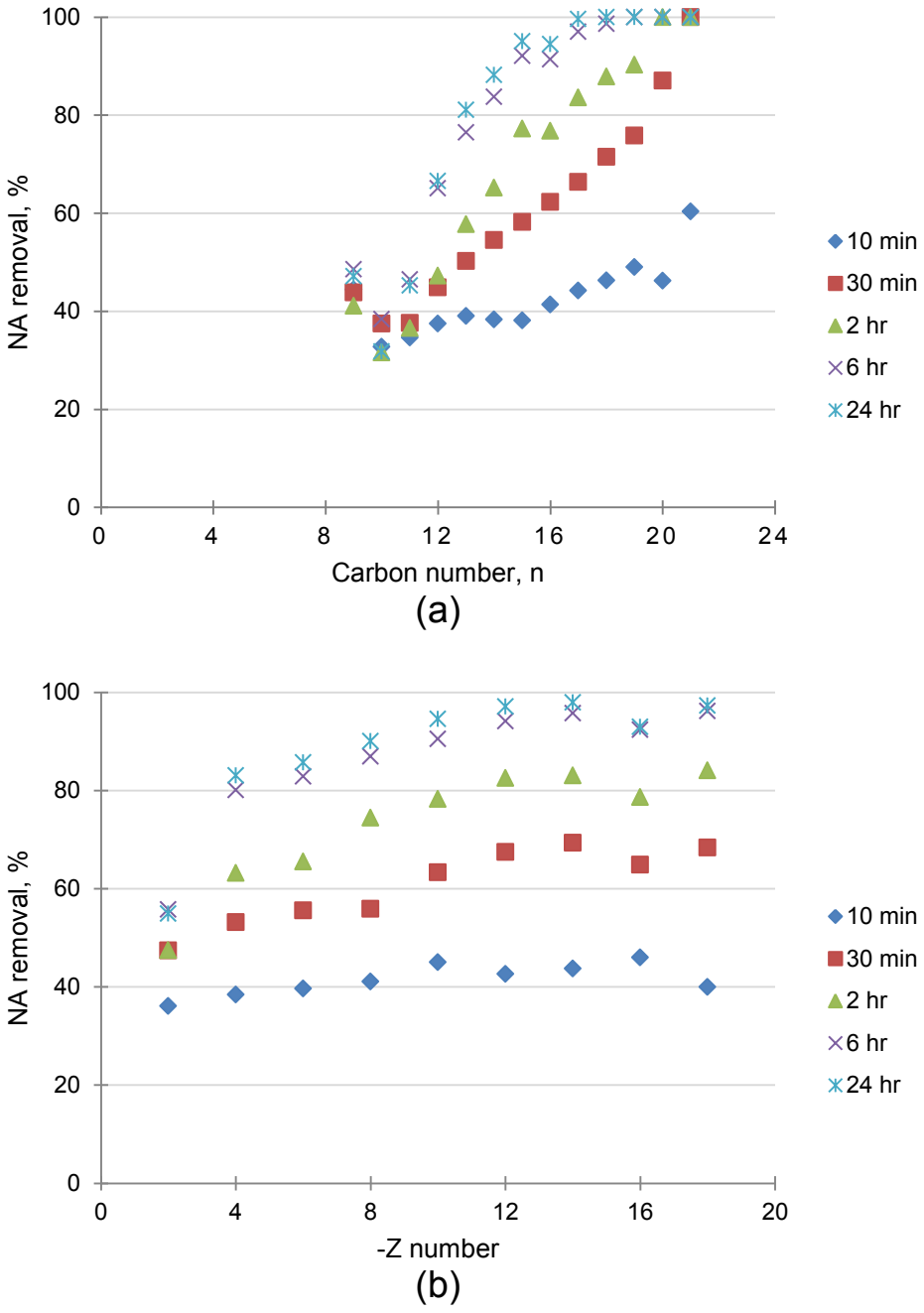

Figure 6.3 Classical NAs removal (%) in OSPW after adsorption with 3 g/L dose of Cx5.5 for various times shown as a function of (a) carbon number and (b) -Z number. Data analysis was performed using high resolution TOF-MS with electrospray ionization in negative mode.

a wider range of resulting NAs removal as a function of carbon number (38.4%-100%) compared to –Z number (54.9%-97.9%). This further supports the previous statement that carbon number has a greater influence on NAs adsorption than –Z number.

6.3.4 Adsorption capacity of CX5.5

The equilibrium adsorption capacity of CX5.5 as a function of equilibrium AEF concentration is shown in Figure S4 (Appendix). The equilibrium adsorption capacity for CX5.5 was at a minimum for the lowest resulting equilibrium AEF concentration, which occurred with the highest CX5.5 dose (6 g/L). And conversely, the highest resulting equilibrium adsorption capacities occurred for the highest equilibrium AEF concentrations, which occurred with the lowest CX5.5 doses (0.5 and 1 g/L). The same trend of an increasing adsorbent dose resulting in a decreasing adsorption capacity was also reported by Pourrezaei et al. (2014), Khan et al. (2011), and Islam et al. (2018). At low adsorbent dose, the adsorption sites become saturated and after a point are no longer able to adsorb organic material, this leads to the lower removal efficiencies (Xing et al. 2008). When higher amounts of adsorbent were present, some adsorption sites remained unsaturated during the adsorption process thus lowering the adsorption capacity but increasing removal efficiency (Khan et al. 2011).

The adsorption capacities of AEF by CX5.5 ranged from 6.7 mg/g to approximately 25 mg/g for CX5.5 doses from 0.5 g/L to 6 g/L respectively. For GAC doses from 0.05 g/L to 2 g/L, the resulting adsorption capacities for AEF ranged from about 30 mg/g to 65 mg/g (Islam et al. 2018). For a 50 g/L dose of non-activated PC, GAC and PAC, the resulting AEF adsorption equilibrium capacities were 1.02 mg/L, 50.5 mg/g and 71.0 mg/g respectively (Pourrezaei et al. 2014). In general, the adsorption capacities for CX5.5 fall between the resulting adsorption capacities for PC and GAC/PAC, however a direct comparison of resulting adsorption capacities is not possible since different sources of raw OSPW were used and since different doses of adsorbent material were used by Islam et al. (2018) and Pourrezaei et al. (2014). Zubot et al. (2012) demonstrated that very high dose of up to 40 wt% PC in OSPW (~400 g/L) can lead to

very low AEF adsorption capacities ranging from 0.1 to 0.43 mg/g. In general, the adsorption capacity results obtained for CX5.5 fall in the general range to be expected considering the fact that the BET surface area for CX5.5 was higher than that for PC (7.7 m^2/g) but lower than that for PAC (800 m^2/g) and GAC (912 m^2/g) (Pourrezaei et al. 2014).

Comparison of equilibrium adsorption capacities of AEF and NAs by CX5.5 (3 g/L dose) is shown in Figure S5 (Appendix). The equilibrium adsorption capacity obtained by FT-IR AEF concentration data was 15 mg AEF/g CX5.5 and by overall MS-TOF classical NAs concentration data was 7.8 mg NAs/g CX5.5. The adsorption capacity obtained using the NAs concentration data was approximately half of that obtained using the AEF concentration data. This is to be expected since the initial concentrations of AEF and classical NAs in the raw OSPW were 61.2 mg/L and 26.3 mg/L respectively.

The equilibrium adsorption capacities of classical NAs by CX5.5 in OSPW were determined for each carbon number and –Z number, Figure 6.4. In the case of carbon number, highest adsorption capacity occurs for carbon number 14. With respect to –Z number, the adsorption capacities have a bimodal distribution (peak values at –Z of 4 and 12). The equilibrium adsorption capacity of NAs by carbon number and –Z number follow the same trend that was obtained for the raw OSPW classical NAs concentration data (Figure S2a). This is a strong indication that adsorption capacity of NAs onto CX5.5 is highly dependent on initial NAs concentration in OSPW. These results are also supported by the amount of classical NAs adsorbed onto CX5.5 (q_t) as a function of time and carbon number (Figure S6 in Appendix). The resulting curves follow the same trends found for the initial NAs concentrations in raw OSPW. As well, Islam et al. (2018) found that differences in adsorption capacities obtained for adsorption of NAs onto GAC were a result of initial concentrations found in the raw OSPW.

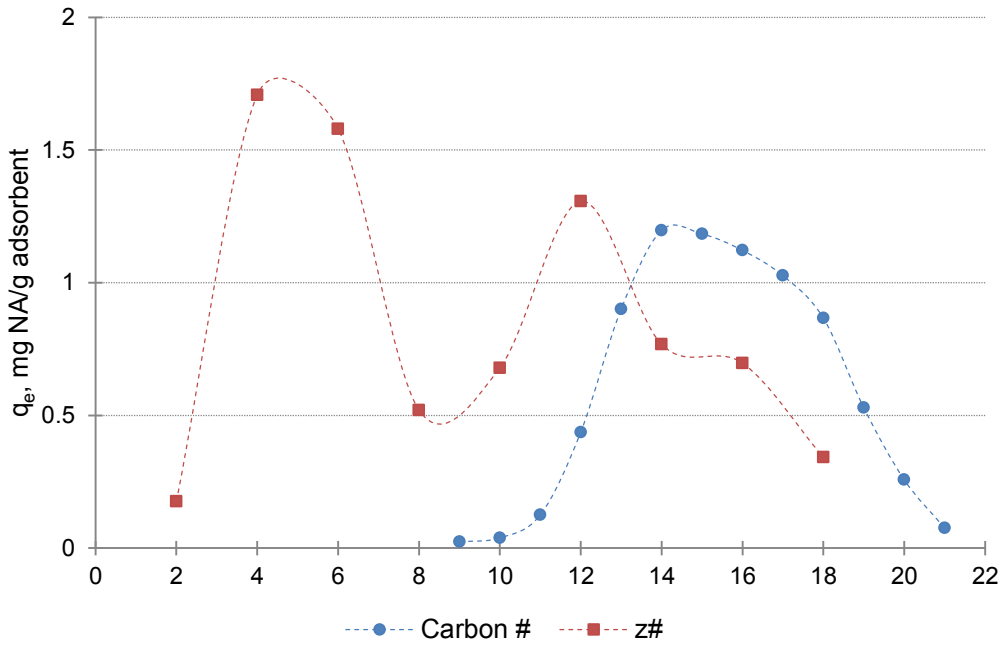

Figure 6.4 Equilibrium adsorbent capacities of classical NAs by CX5.5 (3g/L dose) in OSPW for different carbon number and -Z number.

While q_e as a function of carbon number (Figure 6.4) follows a trend very similar to the initial NAs concentration data presented in Figure S2a, it is not always the case that a carbon number with a higher initial NAs concentration than a different carbon number would result in an adsorption capacity that was higher as well. The initial NAs concentrations for carbon numbers 13 and 17 were 3.3 mg/L and 3.1 mg/L respectively. Carbon number 13 has a higher initial concentration but a lower adsorption capacity (0.90 mg/g) than carbon number 17 (1.0 mg/g). This phenomenon occurred for carbon numbers 12 and 19, 11 and 20, and 10 and 21. These results indicate that adsorption capacity is not only a function of initial NAs concentration but also a function of carbon number to some exent. For carbon numbers having similar intial concentrations, the higher adsorption capacity resulted for the NAs having a higher carbon number.

6.3.5 Kinetics of adsorption

Kinetics of adsorption is the study of how fast the adsorbate attaches to the adsorbent surface and is important to understand in order to design a full-scale batch process with optimum operating conditions (Kalavathy et al. 2005). Kinetics of adsorption data was analyzed using two kinetic models: pseudo-first order and pseudo-second order models.

The AEF concentration data and the classical NAs concentration data were treated with the pseudo-first order (PFO) model given by equation 3.8 in Chapter 3. The rate constant k_{PFO} is obtained from the slope of the plot of log $(q_e - q_t)$ vs. t. The resulting plot should be linear if the data is best described by the PFO kinetic model. AEF and NAs concentration data were also modeled using the pseudo-second order (PSO) kinetics given by equation 3.12 in Chapter 3. The pseudo-second order constant is determined by plotting t/q_t versus t.

The PFO kinetic model using the AEF concentration data is shown in Figure 6.5a. As seen, the entire data set is not linear but consists of two different linear regions, called Phase A and Phase B. Each of the regions was modeled separately to obtain the highest correlation coefficient values. The kinetic parameters for the PFO model of AEF adsorption are shown in Table 6.2. For comparison with the AEF PFO kinetics results, the classical NAs concentration data was used to model the adsorption of classical NAs onto CX5.5. The PFO modeling of adsorption of classical NAs is shown in Figure 6.6a with corresponding kinetic parameters also found in Table 6.2. As with AEF data, the two apparent phases for the NAs concentration data are modeled separately using the PFO model (Figure 6.6a).

The Pseudo-Second Order (PSO) kinetic model of the AEF concentration data is shown in Figure 6.5b with the corresponding kinetic parameters summarized in Table 6.2. The resulting

PSO modeling for adsorption of classical NAs is shown in Figure 6.6b and all of the corresponding rate constants are found in Table 6.2.

With respect to correlation coefficients, the PSO kinetic model resulted in coefficient values that were 1.0 for both AEF and NAs. Correlation coefficient values for the PFO model ranged from 0.93-1.0 for the different phases. If the data were not modeled in separate phases, the correlation coefficients would be farther off from 1.0. Although the PSO kinetic model resulted in correlation coefficients of 1.0, this by itself is not enough to determine which model best represented the data. If one takes into consideration the % error that can be calculated by comparing the experimental equilibrium adsorption capacity, q_e, with the equilibrium adsorption capacity obtained by use of the model in question, q_{mod}, then it becomes more clear which model is more representative of the kinetics of adsorption onto CX5.5. For the PFO kinetic model the error for the AEF data is 4.61% and 56.1% for phase A and phase B, and for the NAs data the error is 10.3% and 56.7% for phase A and phase B. For the PSO kinetic model the error for the AEF data is 2.63% and for the NAs data the error is 1.16%. Thus, the PSO kinetic model is more representative of adsorption of AEF and NAs onto CX5.5. This result is in agreement with published findings by Islam et al. (2008) when comparing PFO and PSO modeling of OSPW AEF and NAs adsorption data onto GAC.

Using the NAs concentration data it was possible to take a closer look at the adsorption kinetics of classical NAs with specific carbon numbers and –Z numbers. Initially, a lower carbon number resulting in a low adsorption capacity (n = 12) and a higher carbon number (n=15) resulting in a higher adsorption capacity were chosen for analysis. As well, the two –Z values (-Z = 4 and 12) resulting in the two peak NAs uptake values were chosen for analysis. The resulting PFO and PSO models for carbon number 12 and 15 are presented in Figure S7 (Appendix), and

those for –Z of 4 and –Z of 12 are shown in Figure S8 (Appendix). Comparison of correlation coefficients and calculated $q_{e,mod}$ values for each kinetic model (Tables 6.2) show that the kinetics of adsorption for each carbon number (12 amd 15) and –Z number (4 and 12) followed PSO kinetics. For the PSO kinetics model, it should be noted that the rate of adsorption for NAs with carbon number 12 was 6.05 g/mg/hr. This rate constant is much higher than that obtained using total NAs concentration data (0.418 g/mg/hr) or NAs with carbon number 15 concentration data (2.41 g/mg/hr).

To further understand why the PSO rate constant for NAs with carbon number 12 was so high, additional PSO rate constants at different carbon number (13, 17, and 18) were determined and are shown in Table 6.2. As carbon number increases or decreases away from carbon number 14, the rate constant increases. This same trend is shown by Islam et al. (2018) for PSO rate constants found for different carbon number in raw NAs. In general, the PSO rate constant seems to be inversely proportional to the initial concentration of NAs for different carbon number, also shown in Table 6.2. There is a lower rate constant for those NAs that are initially present in higher concentration. A similar trend in the relation between initial adsorbate concentration and PSO rate constants was observed by Wang et al. (2018) for the adsorption of different nitrosamines by nanoscale zero-valent iron/GAC composites.

To determine if a relationship existed between carbon number or –Z number and the adsoprtion rate constants obtained for the PSO kinetic model the effect of initial NAs concentration on the resulting equilibrium adsorption capacity had to be reduced. Two carbon numbers, 13 and 17, with very similar initial NAs concentrations and two –Z numbers, 10 and 16, with similar initial NAs concentrations were chosen for analysis. Table 6.2 shows the resulting rate constants for the PSO model model per n or -Z value.

The concentration of NAs with carbon number 13 was slightly higher than NAs with carbon number 17 and the rate of adsorption was 1.4 times higher for carbon number 17. Part of this may be due to the phenomenon previously discussed, higher initial concentration results in a higher PSO rate constant, but it also seems that NAs with higher carbon number may have had a role. NAs with higher carbon numbers were more completely removed, even when they had a smaller initial concentration, as shown by the classical NAs concentration removal data (Figure 6.3). As discussed in section 6.3.3, NAs with higher carbon number are more completely removed (Pourrezaei et al. 2014; Zubot et al. 2011).

The concentration of NAs with –Z number 16 was slightly higher than that of NAs with –Z of 10, however in this case the rate constant of NAs with –Z of 16 was 1.3 times higher than that for NAs with –Z of 10. With the effect of the initial NAs concentration reduced, it can be seen that NAs with higher –Z number result in a higher PSO rate constant. Despite having the higher PSO rate constant, 92.9% of NAs with –Z value of 16 were removed after 24 hours, while 94.6% of NAs with –Z value of 10 were removed after 24 hours. This shows that with respect to –Z value, carbon number has a greater influence on adsorption of NAs than –Z as mentioned in section 6.3.3.

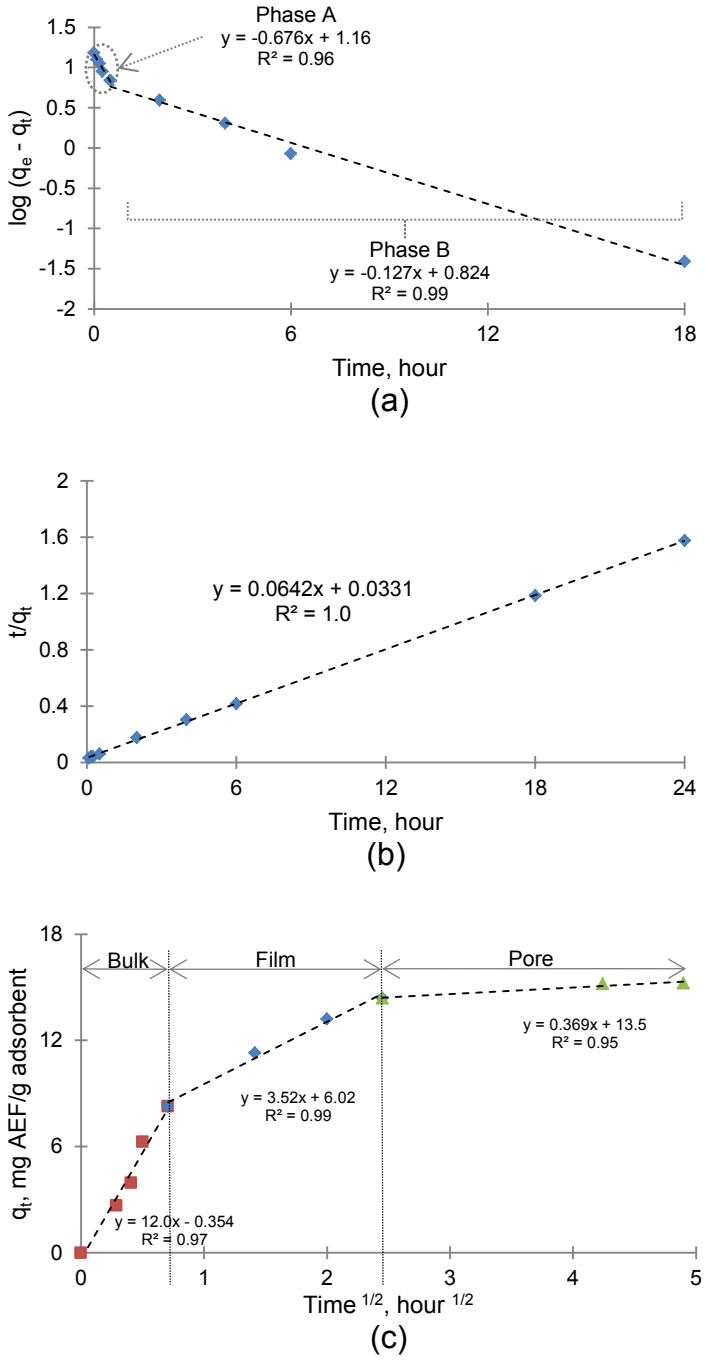

Figure 6.5 (a) Two phase pseudo-first order kinetic model with regions A and B, (b) pseudo-second order kinetic model, and (c) intraparticle diffusion model for the adsorption of AEF onto CX5.5 for 3 g/L dose and various adsorption time.

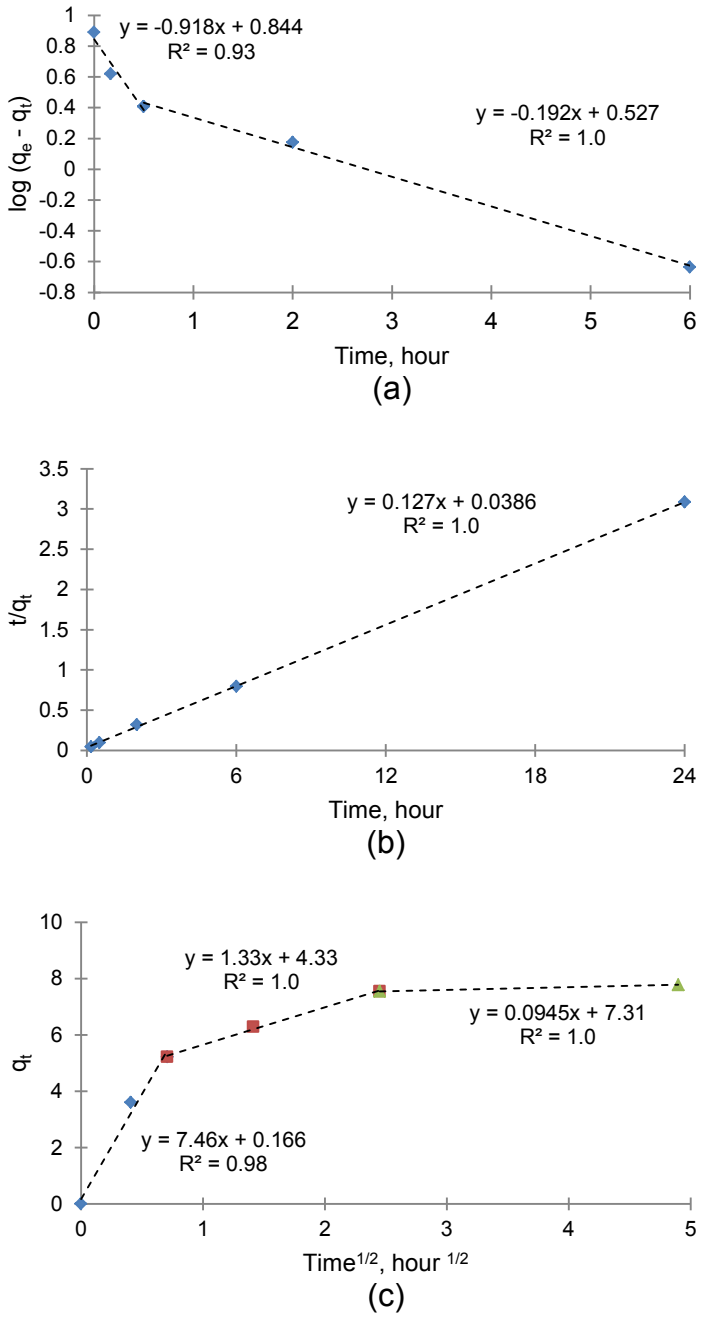

Figure 6.6 (a) Two phase pseudo-first order kinetic model, (b) pseudo-second order kinetic model, and (c) intraparticle diffusion model for the adsorption of NA onto Cx5.5 at a dose of 3 g/L for various adsorption time.

Table 6.2 Summary of modeling parameters for total AEF, total NAs, and NAs with specific carbon number and –Z number. Note: exp means experimental and mod means generated from the kinetic model, and * indicates PFO parameters shown are for the entire data set, not separate phases.

Model & Parameters	Total AEF	Total NAs	NAs with n:					NAs with -Z:			
			18	17	15	13	12	4	10	12	16
$q_{e,exp}$ (mg/g)	15.2	7.78			1.18		0.436	1.71		1.31	
Initial conc. (mg/L)	61.2	26.3	2.60	3.09	3.73	3.33	1.97	6.17	2.15	4.04	2.25
Pseudo-1st order					*All data*		*All data*	*All data*		*All data*	
Phase A					*		*	*		*	
k_{PFO}	1.56	2.11			0.519		0.539	0.484		0.509	
R^2	0.96	0.93			0.96		0.93	0.95		0.92	
$q_{e,mod}$ (mg/g)	14.5	6.98			0.784		0.278	1.11		0.764	
Phase B											
k_{PFO}	0.292	0.443									
R^2	0.99	1									
$q_{e,mod}$ (mg/g)	6.67	3.37									
Pseudo-2nd order											
k_{PSO} (g/mg/hr)	0.124	0.418	5.29	3.40	2.41	2.41	6.05	1.56	4.73	2.78	6.22
R^2	1.0	1.0	1.0	1.0	1.0	1.0	1.0	1.0	1.0	1.0	1.0
$q_{e,mod}$ (mg/g)	15.6	7.87									
Intraparticle diffusion											
Bulk											
$k_{i\text{-}bulk}$ (mg/g/hour$^{1/2}$)	12	7.46	0.881	0.973	1.03	0.804	0.426	1.57	0.650	1.29	0.696
C	-0.354	0.166	0.0124	0.0174	0.0161	0.0315	0.0214	0.0450	0.0173	0.0143	0.0182
R^2	0.97	0.98	0.99	0.99	0.99	0.95	0.92	0.97	0.98	0.99	0.98
Film											
$k_{i\text{-}film}$(mg/g/hour$^{1/2}$)	3.52	1.33	0.132	0.178	0.238	0.170	0.0789	0.319	0.110	0.202	0.117
C	6.02	4.33	0.543	0.575	0.579	0.423	0.223	0.858	0.386	0.785	0.41
R^2	0.99	1.0	0.95	0.97	0.97	0.98	0.91	1.0	0.97	0.97	0.99
Pore											
$k_{i\text{-}pore}$ (mg/g/hour$^{1/2}$)	0.369	0.0945	0.0054	0.0116	0.0157	0.0213	0.00420	0.0257	0.0124	0.0169	0.00200
C	13.5	7.31	0.840	0.969	1.11	0.796	0.416	1.58	0.619	1.22	0.687
R^2	0.95	1.0	1.0	1.0	1.0	1.0	1.0	1.0	1.0	1.0	1.0

6.3.6 Adsorption mechanisms

The Weber and Morris intraparticle diffusion model can be used to determine diffusion mechanism and rate-determining steps during adsorption and is given by equation 3.7 in Chapter 3. If the plot of q_t versus $t^{1/2}$ passes though the origin then this indicates that the intraparticle diffusion is the sole rate limiting step (Nethaji et al. 2013). If the plot passes instead though an intercept, C, then the rate limiting step is a result of additional steps. The intercept, C, is an indicator of the boundary layer effect. A larger intercept indicates that a particular step plays a more significant role in the determination of the rate limiting step (Kalavathy et al. 2005). In general adsorption is thought to consist of three steps (1) mass transfer across the film boundary layer surrounding the adsorbent, (2) internal or external adsorption on the adsorbent surface with physical or chemical binding, considered extremely rapid; (3) adsorbate diffusion to adsorption sites by pore diffusion or solid surface diffusion mechanisms (Cheung et al. 2007).

The intraparticle diffusion model for adsorption of AEF onto CX5.5 is shown in Figure 6.5c. The plot is multilinear with three linear regions, which suggests that three steps govern the adsorption of AEF onto CX5.5. Table 6.2 summarizes the rate constants calculated for each region in Figure 6.5c. Each region represents one of three types of diffusion: bulk, film and pore. The first region shown on the far left side represents bulk diffusion, this region has the highest rate constant of 12 mg/g/h$^{1/2}$. The second region, shown in the middle, represents film diffusion. This is mass transfer through the film surrounding the adsorbent material which takes more time when compared with mass transfer though the bulk liquid. The third region shown on the right hand side represents pore diffusion. This is mass transfer within the pores of the adsorbent material. The pore diffusion region encompasses the most amount of time and has the lowest rate constant for all three regions, 0.369 mg/g/h$^{1/2}$. In addition, the pore diffusion region has the

highest intercept of all three regions, indicating that this step plays a more significant role in determination of the rate limiting step. Once the mass travels though the bulk liquid, it begins to slow down as it travels into and through the film surrounding the adsorbent. The mass slows down even more once it encounters the actual adsorbent material and begins to traverse first though the larger macropores and down into the mesopores. Pore diffusion is the rate limiting step for the adsorption of AEF by CX5.5.

A similar trend was seen when IPD model was applied to the total classical NAs concentration data. There are three distinct phases present (Figure 6.6c), with the values of the IPD rate constants for each region (Table 6.2) following the same trend as seen for the AEF concentration data: $k_{i\text{-}bulk} > k_{i\text{-}film} > k_{i\text{-}pore}$. Again, the pore diffusion region has the highest intercept of all three regions for the total NAs concentration data.

The IPD model was applied to specific NAs with certain carbon number and certain –Z numbers. The results are shown in Table 6.2. Unlike the PSO rate constants, the IPD rate constants for the bulk and film regions are directly proportional to the initial concentration of the NAs since they generally followed the same trend as the initial concentration data. Deviation from the initial concentration data trend was found for NAs with higher carbon number (17 and 18). For higher carbon number the IDP rate constant for the bulk diffuion region tended to be higher that that of lower carbon number with a similar starting concentration for NAs. For carbon number 17 the IDP rate constant for the film diffusion region had a higher IDP rate constant when compared with carbon number 13, which had a slighly higher starting initial concentration. These deviations support the earlier claim that NAs with higher carbon number has some influence on removal of those particular NAs.

The IDP rate constant for the pore diffusion region also showed high dependence on the initial concentration of the NAs, however there were also some deviations based upon carbon number and –Z number. NAs with carbon number 13 had the highest IDP rate constant but had the second highest initial concentration. In addition, NAs with –Z of 16 had the lowest IDP rate constant in the pore diffusion region but had the second lowest initial concentration. In the pore diffusion region, this may suggest that although initial NAs concentration was a major factor in determination of the IPD rate constant, smaller NAs (carbon number) that were less bulky (-Z number) tended to diffuse faster within the pores of the carbon xerogel. In addition to being more bulky, higher –Z number might have a lower IDP rate constant due to π-π dispersion interactions, as discussed in Chapter 3 (Moreno-Castilla 2004).

6.4 Conclusions

The results of this study demonstrated that a mesoporous carbonaceous material can successfully be used to adsorb persistent and toxic organic contaminants from OSPW. Of the two different types of CX used, CX made at pH 5.5 removed a substantially larger amount of AEF than CX made at pH 6.9. The adsorption equilibrium was reached by about 12 hours for both AEF and total classical NAs. After 24 hours of adsorption, 74.6% of AEF was removed and 88.8% of total classical NAs were removed. Upon closer examination of classical NAs removal, it was found that the larger the carbon number, the higher the removal was. Carbon number had more influence on NAs removal when compared with –Z number. It was found that while using a larger dose of CX5.5 increased removal of AEF, this resulted in a decreased adsorption capacity for CX5.5, thus lowering the efficiency of the adsorption process. For a 3 g/L dose of CX 5.5, the equilibrium adsorption capacity was found to be 15 mg AEF/g CX5.5 and 7.8 mg NAs/g CX5.5. Adsorption of AEF and total classical NAs onto CX5.5 followed pseudo-second

order kinetics. With respect to diffusion of AEF and NAs, there were three distinct regions: bulk diffusion, film diffusion and pore diffusion. The rate limiting step in all cases analyzed was pore diffusion.

6.5 References

Afzal, A., Chelme-Ayala, P., Drzewicz, P., Martin, J.W., and Gamal El-Din, M. 2015. Effects of Ozone and Ozone/Hydrogen Peroxide on the Degradation of Model and Real Oil-Sands-Process-Affected-Water Naphthenic Acids. Ozone: Science and Engineering, 37: 45-54.

Allen, E.W. 2008a. Process water treatment in Canada's oil sands industry: I. Target pollutants and treatment objectives. Journal of Environmental Engineering and Science, **7**: 123-138.

Allen, E.W. 2008b. Process water treatment in Canada's oil sands industry: II. A review of emerging technologies. Journal of Environmental Engineering and Science: **7**: 499-524.

Alpatova, A., Kim, E-S, Dong, S., Sun, N., and Chelme-Ayala, P. 2014. Treatment of oil sands process-affected water with ceramic ultrafiltration membrane: Effects of operating conditions on membrane performance. Separation and Purification Technology, **122**: 170-182.

Barrett, E.P., Jovner, L.G., and Halenda, P.P. 1951. The determination of pore volume and area distributions in porous substances. I. Computations from nitogen isotherms. Journal of the American Chemical Society, **73**: 373-380.

Bertheussen, A., Simon, S., and Sjöblom, J. 2017. Equilibrium partitioning of naphthenic acids and bases and their consequences on interfacial properties. Colloids and Surfaces A, **529**: 45-56.

Bhuiyan, T.I., Tak, J.K., Sessarego, S., Harfield, D., and Hill, J.M. 2017. Adsorption of acid-extractable organics from oil sands process-affected water onto biomass-based biochar: Metal content matters. Chemosphere, **168**; 1337-1344.

Brunauer, S., Emmett, P.H., and Teller, E. 1938. Adsorption of gases in multimolecular layers. Journal of the American Chemical Society, **60**(2): 309-319.

Cheung, W.H., Szeto, Y.S., and McKay, G. 2007. Intraparticle diffusion processes during acid dye adsorption onto chitosan. Bioresource Technology, **98**: 2897-2904.

de Boer, J.H., Lippens, B.C., Linsen, B.G., Broekhoff, J.C.P., van den Heuvel, A., and Osinga, Th.J. 1966. The t-curve of multimolecular N_2-adsorption. Journal of Colloid and Interface Science, **21**: 405-414.

Derungs, W.A. 1956. Naphthenic Acid Corrosion – An Old Energy of the Petroleum Industry. Corrosion, **12**: 41-46.

Dong, S., Kim, E-S, Alpatova, A., Noguchi, H. Liu, Y., and Gamal El-Din, M. 2014. Treatment of oil sands process-affected water by submerged ceramic membrane microfiltration system. Separation and Purification Technology, **138**: 198-209.

Fan, T-P. 1991. Characterization of Naphthenic Acids in Petroleum by Fast Atom Bombardment Mass Spectrometry. Energy and Fuels, **5**(3): 371-375.

Frankel, M.L., Bhuiyan, T.I., Veksha, A., Demeter, M.A., Layzell, D.B., Helleur, R.J., Hill, J.M., and Turner, R.J. 2016. Removal and biodegradation of naphthenic acids by biochar and attached environmental biofilms in the presence of co-contamination metals. Bioresource Technology, **216**: 352-361.

Gamal El-Din, M., Fu, H., Wan, N., Chelme-Ayala, P., Perez-Estrada, L., Drzewicz, P., Martin, J.W., Zubot, W., and Smith, D.W. 2011. Naphthenic acids speciation and removal during petroleum-coke adsorption and ozonation of oil sands process-affected water. Science of the Total Environment, **409**: 5119-5125.

Holowenko, F.M., MacKinnon, M.D., and Fedorak, P.M. 2002. Characterization of naphthenic acids in oil sands wastewaters by gas chromatrography-mass spectrometry. Water Research, **36**: 2843-2855.

Huang, R., Sun, N., Chelme-Ayala, P., McPhedran, K.N., Changalov, M., and Gamal El-Din, M. 2015. Fractionation of oil sands-process affected water using pH-dependent extractions: A study of dissociation constants for naphthenic acids species. Chemosphere, **127**: 291-296.

Iranmanesh, S., Harding, T., Abedi, J., Seyedeyn-Azad, F., and Layzell, D.B. 2014. Adsorption of naphthenic acids on high surface area activated carbons. Journal of Environmental Science and Health, Part A, **49**(8): 913-922.

Islam, M.S., Dong, T., Sheng, Z., Zhang, Y., Liu, Y., and Gamal El-Din, M. 2014. Microbial community structure and operational performance of a fluidized bed biofilm reactor treating oil sands process-affected water. International Biodeterioration & Biodegradation, **91**:111-118.

Islam, M.S., McPhedran, K.N., Messele, S.A., Liu, Y., and Gamal El-Din, M. 2018. Isotherm and kinetic studies on adsorption of oil sands process-affected water organic compounds using granular activated carbon. Chemosphere, **202**: 716-725.

Islam, M.S., Zhang, Y., McPhedran, K., Liu, Y., and Gamal El-Din, M. 2016. Mechanistic investigation of industrial wastewater naphthenic acids removal using granular activated carbon (GAC) biofilm based processes. Science of the Total Environment, **541**: 238-246.

Jivraj, M.N., MacKinnon, M., and Fung, B. 1996. Naphthenic acid extraction and quantitative analysis with FT-IR spectroscopy. Syncrude Internal Report, Syncrude Canada Ltd, Edmonton, Alberta, Canada.

Job, N, Pirard, R., Marien, J., and Pirard, J-P. 2004. Porous carbon xerogels with texture tailored by pH control during sol-gel process. Carbon, **42**: 619-628.

Jones, D., Scarlett, A., West, C.E., and Rowland, S.J. 2011. Toxicity of individual naphthenic acids to Vibrio fisheri. Environmental Science & Technology, **45:** 9776-9782.

Kalavathy, M.H., Karthikeyan, T., Rajgopal, S., and Miranda L.R. 2005. Kinetic and isotherm studies of Cu(II) adsorption onto H3PO4-activated rubber wood sawdust. Journal of Colloid and Interface Science, **292**: 354-362.

Khan, M.A., Lee, S-H, Kang, S., Paeng, K-J, Lee, G., Oh, S-E, and Jeon, B-H. 2011. Adsorption studies for the removal of methyl tert-butyl ether on various commercially available GACs from an aqueous medium. Separation Science and Technology, **47**(7): 1121-1130.

Kim, E-S, Liu, Y., and Gamal El-Din, M. 2011. The effects of pretreament on nanofiltration and reverse osmosis membrane filtration for desalination of oil sands process-affected water. Separation and Purification Technology, **81**: 418-428.

Kim, E-S, Liu, Y., and Gamal El-Din, M. 2012. Evaluation of Membrane Fouling for In-Line Filtration of Oil Sands Process-Affected Water: The Effects of Pretreatment Conditions. Environmental Science and Technology, **46**: 2877-2884.

Kim, E-S, Liu, Y., and Gamal El-Din, M. 2013. An in-situ integrated system of carbon nanotubes nanocomposite membrane for oil sands process-affected water treatment. Journal of Membrane Science, **29**: 418-427.

Klamerth, N., Moreira, J., Li, C., Singh, A., McPhedran, K.N., Chelme-Ayala, P., Belosevic, M., and Gamal El-Din, M. 2015. Effect of ozonation on the naphthenic acids' speciation and toxicity of pH-dependent organic extracts of oil sands process-affected water. Science of the Total Environment, **506-507**: 66-75.

Li, C., Fu, L., Stafford, J., Belosevic, M., and Gamal El-Din, M. 2017. The toxicity of oil sands process-affected water (OSPW): A critical review. Science of the Total Environment, **601-602**: 1785-1802.

MacKinnon, M.D., and Boerger, H. 1986. Description of two treatment methods for detoxifying oil sands process water. Water Pollution Research Journal of Canada, **21**: 496–512.

Mahata, N., Silva, A.R., Pereira, M.F.R., Freire, C., de Castro, B., and Figueiredo, J.L. 2007. Anchoring of a [Mn(*salen*)Cl] complex onto mesoporous carbon xerogels. Journal of Colloid and Interface Science, **311**: 152-158.

Moreno-Castilla, C. 2004. Adsorption of organic molecules from aqueous solutions on carbon materials. Carbon, **42**: 83-94.

Nethaji, S., Sivasamy, A., and Mandal, A.B. 2013. Adsorption isotherms, kinetics and mechanism for the adsorption of cationic and anionic dyes onto carbonaceous particles prepared from *Junglans regia* shell biomass. International Journal of Environmental Science and Technology, **10**: 231-242.

Niasar, H.S., Li, H., Kasanneni, T.V.R., Ray, M.B., and Xu, C. 2016. Surface amination of activated carbon and petroleum coke for the removal of naphthenic acids and treatment of oil sands process-affected water (OSPW). Chemical Engineering Journal, **293**: 189-199.

Peng, H., Volchek, K., MacKinnon, M., Wong, W., and Brown, C. 2004, Application of nanofiltration to water management options for oil sands operations. Desalination, **120**: 137-150.

Pourrezaei, P., Alpatova, A., Chelme-Ayala, P., Perez-Estrada, L.A., Jensen-Fontaine, M., Le, X.C., and Gamal El-Din, M. 2014. Imact of petroleum coke characteristics on the adsorption of the organic fractions from oil sands process-affected water. International Journal of Environmental Science and Technology, **11**: 2037-2050.

Pourrezaei, P., Drzewicz, P., Yingnan, W., Gamal El-Din, M., Perez-Estrada, L., Martin, J., Anderson, J., Wiseman, S., Liber, K., and Geisy, J. 2011. The Impact of Metallic Coagulant on the Removal of Organic Compounds from Oil Sands Process-Affected Water. Environmental Science and Technology, **45**: 8452-8459.

Quinlan, P.J., Grishkewich, N., Tam, K.C. 2017. Removal of 2-naphtheoxyacetic acid from aqueous solution using quaternized chitosan beads. The Canadian Journal of Chemical Engineering, **95**: 21-32.

Quinlan, P.J., and Tam, K.C. 2015. Water treatment technologies for the remediation of naphthenic acids in oil sands process-affected water. Chemical Engineering Journal, **279**: 696-714.

Rogers, V.V., Liber, K., and MacKinnon, M. 2002. Isolation and characterization of naphthenic acids from Athabasca oil sands tailing pond water. Chemosphere, **48**: 519-527.

Small, C.C., Ulrich, A.C., and Hashisho, Z. 2012. Adsorption of Acid Extractable Oil Sands Tailings. Journal of Environmental Engineering, **138**: 833-840.

Wang, C., Klamerth, N., Huang, R., Elnakar, H., and Gamal El-Din, M. 2016a. Oxidation of oil sands process-affected water by potassium ferrate (VI). Environmental Science and Technology, **50** (8): 4238-4247.

Wang, C., Klamerth, N., Messele, S.A., Singh, A., Belosevic, M., and Gamal El-Din, M. 2016b. Comparison of UV/hydrogen peroxide, potassium ferrate (VI), and ozone in oxidizing the organic fraction of oil sands process-affected water (OSPW). Water Research, **100**: 476-485.

Wang, W., Wang, J., Guo, Y., Zhu, C., Pan, F., Wu, R., and Wang, C. 2018. Removal of multiple nitrosamines from aqueous solution by nanoscale zero-valent iron supported on granular activated carbon: Influencing factors and reaction mechanism. Science of the Total Environment, **639**: 934-943.

Wu, Z., and Zhao, D. 2011. Ordered mesoporous materials as adsorbents. Chemical Communications, **47**: 3332-3338.

Xing, W., Ngo, H.H., Kim, S.H., Guo, W.S., and Hagare, P. 2008. Adsorption and bioadsorption of granular activated carbon (GAC) for dissolved organic carbon (DOC) removal in wastewater. Bioresource Technology, **99**: 8674-8678.

Zhu, S., Li, M., and Gamal El-Din, M. 2017. Forward osmosis as an approach to manage oil sands tailings water and on-site basal depressurization water. Journal of Hazardous Materials, **327**: 18-27.

Zubot, W., MacKinnon, M.D., Chelme-Ayala, P., Smith, D.W., and Gamal El-Din, M. 2012. Petroleum coke adsorption as a water management option for oil sands process-affected water. Science of the Total Environment, **427-428**: 364-372.

7. CONCLUSIONS AND RECOMMENDATIONS

7.1 Thesis overview

In Northern Alberta, water and wastewater management is a growing concern due to the existence of the large bitumen deposits and the resulting oil sands industry. OSPW is generated as a result of the Clark caustic hot water extraction process used for the extraction of bitumen. OSPW is a widely varying and complex mixture that can contain high concentrations of chloride, salts, organic material and other inorganic compounds. Studies have shown that OSPW can pose a great threat to aquatic and mammalian species and this is often attributed to the presence of the organic fraction. Due to the acute toxicity of OSPW, its release to the environment is not permissible under Alberta's zero discharge approach, so it is sequestered in tailings ponds. Over time, the amount of OSPW has continually increased due to the addition of freshwater for the extraction processes. In order to reduce the amount of freshwater needed, a portion of OSPW has been recycled for extraction processes, however, this has led to further decrease of OSPW water quality.

Storage of OSPW in tailings ponds has been the norm for dealing with this process water, however environmental impacts can be seen in the surrounding land, air and water. OSPW tailings ponds can emit chemical and greenhouse gases. As the tailings ponds grow, the natural habitats of many animals may be impacted negatively. Although the oil sands industry has made significant efforts to reduce the impacts of its operation, a holistic approach to manage the process water and tailings ponds has not been reported so far. All of these factors combined have made it clear that there needs to be some forward movement with respect to the development of feasible reclamation techniques for the treatment of OSPW.

Several types of treatment methods have been applied to OSPW at the bench scale level. These include coagulation flocculation sedimentation (CFS), membrane filtration (MF, UF, NF, RO), advanced oxidation processes, adsorption, biological treatment, and combinations of the mentioned. The complex nature of OSPW forces the use of treatment trains involving several treatment methods.

A first step involves removal of suspended solids and reduction of turbidity, clarification of the water. This can be accomplished by methods such as CFS, membrane filtration, granular media filtration. Pre-treatment can aid in further treatment of the OSPW by other methods such as high pressure membrane filtration or AOP. Such a process includes low pressure membrane filtration (MF or UF) which can help to clarify OSPW at relatively low cost. Research has been conducted in this area, combining low and high pressure membrane filtration. Due to the lower cost of low pressure membrane filtration, a closer look at the application of low pressure membranes (UF) was the focus of one portion of this work contained in this thesis. More specifically, carbon containing nanocomposite membranes were developed and used to treat of OSPW.

After clarification of OSPW, secondary and tertiary treatment technologies can used to remove dissolved organic constituents in OSPW. These include treatment methods such as adsorption, high pressure membrane filtration, AOPs, and biological treatments. Adsorption is an effective method that can be used to remove organic contaminants from OSPW. AC is the most common adsorbent that has been successfully used for adsorption studies involving the removal of organic material from wastewaters. This is mainly due to its large surface area that results from many micropores. With organic contaminants that are bulky in nature, some of the surface area may not be effectively utilized. In addition, AC is not cost effective. On the opposite end,

use of a cheap and readily available material such as petroleum coke, does not result in the same type of organic material removal afforded by use of AC as an adsorbent material. This is mainly due to the very small surface area. In the middle of both extremes are mesoporous adsorbents. One such material is carbon xerogel which be that can be modified to change the porous nature or the surface chemistry in order to accommodate bulkier contaminants. Carbon xerogel has surface areas that are much higher than that of petroleum coke but not as high as AC. The focus of one portion of the work contained in this thesis examined the use of carbon xerogels for adsorption of organic fraction from OSPW.

7.2 Conclusions

Based on the experimental results and analysis presented in this this thesis, the following main conclusions were made:

1. Addition of mMWNT to PSU resulted in increased hydrophilicity of selective membrane surface due to the presence of the carboxyl groups on the MWNT.
2. Small addition of mMWNT (up to 1 wt. % mMWNT) resulted in decreased average pore size on the selective membrane surface, after which further addition of mMWNT resulted in an increased selective surface average pore size. Pure water flux followed the same general trend, decreasing with small additions of mMWNT (up to 0.5 wt. %), followed by an increasing pure water flux with higher addition of mMWNT (1 wt. % to 5 wt. %).
3. All nanocomposite membranes had a higher rejection of 100 kDa PEG than plain PSU membrane. The highest rejection, 92.3%, occurred with mMWNT-0.2, however a fairly high rejection combined with high PEG flux resulted for mMWNT-2.

4. Addition of mMWNT resulted in a reduced tendency for membrane fouling to occur, as shown by the decreased fouling ratios and increased flux recovery ratios for the nanocomposite membranes as compared with plain PSU membrane.
5. The dominant fouling mechanisms during filtration of OSPW were found to be standard blocking and cake filtration. The standard blocking model resulted in the highest correlation value for membrane mMWNT-0, while the cake filtration model gave the highest correlation values for all nanocomposite membranes
6. With respect to water quality, all fabricated membranes effectively reduced turbidity to values below 2 NTU. TS was found to be affected by filtration time, lower filtration led to a higher reduction of TS in the analyzed permeates, while longer filtration time led to higher TS in the resulting permeates. Addition of 0.2 and 2 wt. % mMWNT within the PSU membrane matrix led to OSPW filtration permeates which had SDI_{15} values which were 32.7% and 6.7% less than the SDI_{15} for plain PSU.
7. Addition of 0.2 and 2 wt. % mMWNT within the PSU membrane matrix led to increased AEF removals that were 11.9% and 13.9% higher than AEF removal by plain PSU membrane.
8. PSU membranes with 0.2 and 2 wt. % mMWNT have been shown to increase AEF removal while increasing water quality of raw OPSW to levels that make them suitable for further membrane treatment (NF and RO) with no prior pre-treatment.
9. Of the two different types of CX used, CX made at pH 5.5 removed a substantially larger amount of AEF than CX made at pH 6.9.
10. The adsorption equilibrium was reached by about 12 hours for adsorption of both AEF and total classical NAs onto CX5.5.

11. After 24 hours of adsorption by CX, 74.6% of AEF was removed and 88.8% of total classical NAs were removed.
12. With respect to classical NAs removal, it was found that the larger the carbon number, the higher the removal was.
13. Carbon number had more influence on NAs removal by CX when compared with –Z number.
14. It was found that while using a larger dose of CX5.5 increased removal of AEF, this resulted in a decreased adsorption capacity for CX5.5, thus lowering the efficiency of the adsorption process.
15. Adsorption of AEF and total classical NAs onto CX5.5 followed pseudo-second order kinetics.
16. With respect to diffusion of AEF and NAs, there were three distinct regions: bulk diffusion, film diffusion and pore diffusion. The rate limiting step in all cases analyzed was pore diffusion.

7.3 Recommendations

Based on the conclusions of the research presented, the following recommendations can be made for future experiments:

- With respect to membrane development, it would be of interest to look at the inclusion of other types of carbonaceous materials, less costly than carbon nanotubes, within the membrane matrix.

- For a polymeric membrane containing carbonaceous material, it would be interesting to try and determine at what level the carbonaceous material was adsorbing the organic constituents contained in OSPW.
- With respect to the adsorption work performed, it would be interesting to analyze the oxy-NAs in terms of removal, adsorption kinetics, and diffusion.
- The adsorption work presented classical NAs concentration data obtained using electrospray ionization (ESI) analysis in negative mode. Samples of treated OSPW could be subjected to ESI analysis in positive mode. The results could be analyzed. Assess the performance of mesoporous carbonaceous material such as CX in passive or semi-passive treatment approaches such as wetland or pit lakes. CX could be used as a pre- or post-passive treatment method to remove the persistent organic fraction of OSPW.

BIBLIOGRAPHY

Afzal, A., Chelme-Ayala, P., Drzewicz, P., Martin, J.W., and Gamal El-Din, M. 2015. Effects of Ozone and Ozone/Hydrogen Peroxide on the Degradation of Model and Real Oil-Sands-Process-Affected-Water Naphthenic Acids. Ozone: Science and Engineering, 37: 45-54.

Ahmad, M., Lee, S.S., Dou, X., Mohan, D., Sung, J., Yang, J.E., and Ok, Y.K. 2012. Effects of pyrolysis temperature on soybean stover- and peanut shell-derived biochar properties and TCE adsorption in water. Bioresource Technology, **118**: 536-544.

Allen, E.W. 2008a. Process water treatment in Canada's oil sands industry: I. Target pollutants and treatment objectives. Journal of Environmental Engineering and Science, **7**: 123-138.

Allen, E.W. 2008b. Process water treatment in Canada's oil sands industry: II. A review of emerging technologies. Journal of Environmental Engineering and Science: **7**: 499-524.

Alpatova, A., Kim, E-S., Sun, X., Hwang, G., Liu, Y. and Gamal El-Din, M. 2013. Fabrication of porous polymeric nanocomposite membranes with enhanced anti-fouling properties: Effect of casting composition. Journal of Membrane Science, **444**: 449-460.

Alpatova, A., Kim, E-S., Dong, S., Sun, N., Chelme-Ayala, P., and Gamal El-Din, M. 2014. Treatment of oil sands process-affected water with ceramic ultrafiltration membrane: Effects of operating conditions on membrane performance. Separation and Purification Technology. **122**: 170-182.

Alpatova, A., Meshref, M., McPhedran, K., and Gamal El-Din, M. 2015. Composite polyvinylidene fluoride (PVDF) membrane impregnated with Fe_2O_3 nanoparticles and

multiwalled carbon nanotubes for catalytic degradation of organic contaminants. Journal of Membrane Science, **490**: 227-235.

Anderson, J., Wiseman, S., Wang, N., Moustafa, A., Perez-Estrada, L., Gamal El-Din, M., Martin, J., Liber, K., and Giesy, J. 2012. Effectiveness of ozonation treatment in eliminating toxicity of oil sands process-affected water to Chironomus-dilutus. Environmental Science and Technology, **46**: 486-493.

ASTM International. 2014. Standard Test Method for Silt Density Index (SDI) of Water [online]. Available from http://dx.doi.org/10.1520/D4189 [accessed 1 May 2016].

AWWA. 1999. Water Quality and Treatment: A Handbook of Community Water Supplies, 5th edition. McGraw-Hill, New York, NY.

Ballinas, L., Torras, C., Fierro, V., and Garcia-Valls, R. 2004. Factors influencing activated carbon polymeric composite membrane structure and performance. Journal of Physics and Chemistry of Solids, **65**: 633-637.

Banerjee, S., Hemraj-Benny, T., and Wong, S.S. 2005. Covalent surface chemistry of single-walled carbon nanotubes. Advanced Materials, **17**(1): 17-29.

Bansal and Goyal. 2005. Activated Carbon Adsorption. Taylor & Francis Group. New York, NY.

Barrett, E.P., Jovner, L.G., and Halenda, P.P. 1951. The determination of pore volume and area distributions in porous substances. I. Computations from nitogen isotherms. Journal of the American Chemical Society, **73**: 373-380.

Bertheussen, A., Simon, S., and Sjöblom, J. 2017. Equilibrium partitioning of naphthenic acids and bases and their consequences on interfacial properties. Colloids and Surfaces A, **529**: 45-56.

Bhuiyan, T.I., Tak, J.K., Sessarego, S., Harfield, D., and Hill, J.M. 2017. Adsorption of acid-extractable organics from oil sands process-affected water onto biomass-based biochar: Metal content matters. Chemosphere, **168**; 1337-1344.

Blanchard, G., Maunaye, M., and Martin, G. 1984. Removal of heavy metals from waters by means of natural zeolites. Water Research, **18**(12): 1501-1507.

Blanco, J-F., Sublet, J., Nguyen, Q.T., and Schaetzel, P. 2006. Formation and morphology studies of different polysulfones-based membranes made by wet phase inversion process. Journal of Membrane Science, **283**: 27-37.

Brunauer, S., Emmett, P.H., and Teller, E. 1938. Adsorption of gases in multimolecular layers. Journal of the American Chemical Society, **60**(2): 309-319.

Carabineiro, S.A.C., Thavorn-amornsri, T., Periera, M.F.R., Serp, P., and Figueiredo, J.L. 2012. Comparison between activated carbon, carbon xerogel and carbon nanotubes for the adsorption of the antibiotic ciprofloxacin. Catalysis Today, **186**: 29-34.

Celik, E., Park, H., Choi, H., and Choi, H. 2011. Carbon nanotube blended polyethersulfone membranes for fouling control in water treatment. Water Research, **45**: 274-282.

Chen, H. and Hashisho, Z. 2012. Fast preparation of activated carbon from oil sands coke using microwave –assisted activation. Fuel, **95**: 178-182.

Cheryan, M. 1998. Ultrafiltration and Microfiltration Handbook. Technomic Publishing Company, Lancaster, P.A.

Cheung, W.H., Szeto, Y.S., and McKay, G. 2007. Intraparticle diffusion processes during acid dye adsorption onto chitosan. Bioresource Technology, **98**: 2897-2904.

Choi, J-H., Jegal, J., and Kim, W-N. 2006. Fabrication and characterization of multi-walled carbon nanotubes/polymer blend membranes. Journal of Membrane Science, **284**: 406-415.

Clemente, J.S., and Fedorak, P.M. 2005. A review of the occurrence, analysis, toxicity, and biodegradation of naphthenic acids. Chemosphere, **60**: 585-600.

Coleman, J., Khan, U., Blau, W., and Gun'ko, Y. 2006. Small but strong: a review of mechanical properties of carbon nanotube-polymer composites. Carbon, **44**: 1624-1652.

Coughlin, R.W., and Ezra, F.S. 1968. Role of surface acidity in the adsorption of organic pollutants on the surface of carbon. Environmental Science and Technology, **2**: 291-297.

Crittenden, J.C. 2005. MWH's water treatment: principles and design, 2nd edition. John Wiley & Sons, Hoboken, N.J.

de Boer, J.H., Lippens, B.C., Linsen, B.G., Broekhoff, J.C.P., van den Heuvel, A., and Osinga, Th.J. 1966. The t-curve of multimolecular N_2-adsorption. Journal of Colloid and Interface Science, **21**: 405-414.

Deanin, R.D. 1972. Polymer structure, properties, and applications. Cahners Books, Boston, M.A.

Derungs, W.A. 1956. Naphthenic Acid Corrosion – An Old Energy of the Petroleum Industry. Corrosion, **12**: 41-46.

Dhakras, P.A. 2011. Nanotechnology applications in water purification and waste water treatment: a review. *In* Proceedings of the International Conference on Nanoscience,

Engineering and Technology (ICONSET), Calicut, India. November 28-30, 2011, pp. 285-291.

Dong, S., Kim, E-S, Alpatova, A., Noguchi, H. Liu, Y., and Gamal El-Din, M. 2014. Treatment of oil sands process-affected water by submerged ceramic membrane microfiltration system. Separation and Purification Technology, **138**: 198-209.

Drzewicz, P., Afzal, A., Gamal El-Din, M., Martin, J.W. 2010. Degradation of a Model Naphthenic Acid, Cyclohexanoic Acid, by Vacuum UV (172 nm) and UV (254 nm)/H2O2. Journal of Physical Chemistry A, **114**: 12067-12074.

Eaton, A.D., Clesceri, L., Greenberg, A.E., and Franson, M.A.H. 2016. Standard Methods for the Examination of Water and Wastewater. American Public Health Association, Washington, DC.

Eykamp, W. 1995. Microfiltration and ultrafiltration. *In* Membrane Separations and Technology, Principles and Applications. *Edited by* R.D. Noble and S.A. Stern. Elsevier Science B.V., Amsterdam.

Fan, T-P. 1991. Characterization of Naphthenic Acids in Petroleum by Fast Atom Bombardment Mass Spectrometry. Energy and Fuels, **5**(3): 371-375.

Farahani, M., Borghei, S., and Vantanpour, V. 2016. Recovery of cooling tower blowdown water for reuse: The investigation of different types of pretreatment prior to nanofiltration and reverse osmosis. Journal of Water Process Engineering, **10**: 188-199.

Ferlita, R., Phipps, D., Safarik, J., and Yeh, D. Cryo-Snap: 2008. A simple modified freeze-fracture method for SEM imaging of membrane cross-sections. Environmental Progress, **27**: 204-209.

Frank, R.A., Roy, J.W., Bickerton, G., Rowland, S.J., Headley, J.V., Scarlett, A.G., West, C.E., Peru, K.M., Parrot, J.L., Conly, F.M., and Hewitt, L. M. 2014. Profiling Oil Sands Mixtures from Industrial Developments and Natural Groundwaters for Source Identification. Environmental Science and Technology, **48**: 2660-2670.

Frankel, M.L., Bhuiyan, T.I., Veksha, A., Demeter, M.A., Layzell, D.B., Helleur, R.J., Hill, J.M., and Turner, R.J. 2016. Removal and biodegradation of naphthenic acids by biochar and attached environmental biofilms in the presence of co-contamination metals. Bioresource Technology, **216**: 352-361.

Gamal El-Din, M., Fu, H., Wan, N., Chelme-Ayala, P., Perez-Estrada, L., Drzewicz, P., Martin, J.W., Zubot, W., and Smith, D.W. 2011. Naphthenic acids speciation and removal during petroleum-coke adsorption and ozonation of oil sands process-affected water. Science of the Total Environment, **409**: 5119-5125.

Headley, J.V., Peru, K.M., Fahlman, B., Colodey, A. and McMartin, D.W. 2013. Selective solvent extraction and characterization of the acid extractable fraction of Athabasca oils sands process waters by Orbitrap mass spectrometry. International Journal of Mass Spectrometry **345-347**: 104-108.

Ho, Y-S. 2006. Review of second-order models for adsorption systems. Journal of Hazardous Materials, **B136**: 681-689.

Ho, Y-S., and McKay, G. 1998. Sorption of dye from aqueous solution by peat. Chemical Engineering Journal, **70**: 115-124.

Ho, Y-S., and McKay, G. 1999. Pseudo-second order model for sorption processes. Process Biochemistry, **34**: 451-465.

Ho, Y-S., and McKay, G. 2000. The kinetics of sorption of divalent metal ions onto sphagnum moss peat. Water Research, **34**: 735-742.

Hodson, P.V. 2013. History of environmental contamination by oil sands extraction. Proceedings of the National Academy of Sciences, **111**(5): 1569-1570.

Hofs, B., Ogier, J., Vries, D., Beerendonk, E.F., and Cornelissen, E.R. 2011. Comparison of ceramic and polymeric membrane permeability and fouling using surface water. Separation and Purification Technology, **79**: 365-374.

Holowenko, F.M., MacKinnon, M.D., and Fedorak, P.M. 2002. Characterization of naphthenic acids in oil sands wastewaters by gas chromatrography-mass spectrometry. Water Research, **36**: 2843-2855.

Huang, R., Sun, N., Chelme-Ayala, P., McPhedran, K.N., Changalov, M., and Gamal El-Din, M. 2015. Fractionation of oil sands-process affected water using pH-dependent extractions: A study of dissociation constants for naphthenic acids species. Chemosphere, **127**: 291-296.

Inyang, M. and Dickenson, E. 2015. The potential role of biochar in the removal of organic and microbial contaminants from potable and reuse water: A review. Chemosphere, **134**: 232-240.

Iranmanesh, S., Harding, T., Abedi, J., Seyedeyn-Azad, F., and Layzell, D.B. 2014. Adsorption of naphthenic acids on high surface area activated carbons. Journal of Environmental Science and Health, Part A, **49**(8): 913-922.

Iritani, E. 2013. A review on modeling of pore-blocking behaviors of membranes during pressurized membrane filtration. Drying Technology, **31**: 146-162.

Islam, M.S., Dong, T., Sheng, Z., Zhang, Y., Liu, Yang, and Gamal El-Din, M. 2014a. Microbial community structure and operational performance of a fluidized bed biofilm reactor treating oil sands process-affected water. International Biodeterioration and Biodegradation, **91**: 111-118.

Islam, M.S., Dong, T., McPhedran, K ,Sheng, Z., Zhang, Y, Liu, Yang, and Gamal El-Din, M. 2014b. Impact of ozonation pre-treatment of oil sands process-affected water on the operational performance of a GAC-fluidized bed biofilm reactor. . Biodegradation, **25**: 811-823.

Islam, M.S., McPhedran, K.N., Messele, S.A., Liu, Y., and Gamal El-Din, M. 2018. Isotherm and kinetic studies on adsorption of oil sands process-affected water organic compounds using granular activated carbon. Chemosphere, **202**: 716-725.

Islam, M.S., Zhang, Y., McPhedran, K , Liu, Yang, and Gamal El-Din, M. 2015. Granular activated carbon for simultaneous adsorption and biodegradation of toxic oil sands process-affected water organic compounds. Journal of Environmental Management, **152**: 49-57.

Islam, M.S., Zhang, Y., McPhedran, K , Liu, Yang, and Gamal El-Din, M. 2016. Mechanistic investigation of industrial wastewater naphthenic acids removal using granular activated carbon (GAC) biofilm based processes. Science of the Total Environment, **541**: 238-246.

Jivraj, M.N., MacKinnon, M., and Fung, B. 1995. Naphthenic acid extraction and quantitative analysis with FT-IR spectroscopy. Syncrude Internal Report, Syncrude Canada Ltd, Edmonton, Alberta, Canada.

Job, N, Pirard, R., Marien, J., and Pirard, J-P. 2004. Porous carbon xerogels with texture tailored by pH control during sol-gel process. Carbon, **42**: 619-628.

Jones, D., Scarlett, A., West, C.E., and Rowland, S.J. 2011. Toxicity of individual naphthenic acids to Vibrio fisheri. Environmental Science & Technology, **45:** 9776-9782.

Kalavathy, M.H., Karthikeyan, T., Rajgopal, S., and Miranda L.R. 2005. Kinetic and isotherm studies of Cu(II) adsorption onto H3PO4-activated rubber wood sawdust. Journal of Colloid and Interface Science, **292**: 354-362.

Kang, S., Herzberg, M., Rodrigues, D., and Elimelech, M. 2008. Antibacterial effects of carbon nanotubes: size does matter. Langmuir, **24**: 6409-6413.

Khan, M.A., Lee, S-H, Kang, S., Paeng, K-J, Lee, G., Oh, S-E, and Jeon, B-H. 2011. Adsorption studies for the removal of methyl tert-butyl ether on various commercially available GACs from an aqueous medium. Separation Science and Technology, **47**(7): 1121-1130.

Kim, E-S., and Deng, B. 2011. Fabrication of polyamide thin-film nano-composite (PA-TFN) membrane with hydrophilized ordered mesoporous carbon (H-OMC) for water purifications. Journal of Membrane Science, **375**(1-2): 46-54.

Kim, E-S, Liu, Y., and Gamal El-Din, M. 2011. The effects of pretreament on nanofiltration and reverse osmosis membrane filtration for desalination of oil sands process-affected water. Separation and Purification Technology, **81**: 418-428.

Kim, E-S., Hwang, G., Gamal El-Din, M., and Liu, Y. 2012. Development of nanosilver and multi-walled carbon nanotubes thin-film nanocomposite membrane for enhanced surface water treatement. Journal of Membrane Science, **394-395**: 37-48.

Kim, E-S, Liu, Y., and Gamal El-Din, M. 2012. Evaluation of Membrane Fouling for In-Line Filtration of Oil Sands Process-Affected Water: The Effects of Pretreatment Conditions. Environmental Science and Technology, **46**: 2877-2884.

Kim, E-S, Liu, Y., and Gamal El-Din, M. 2013. An in-situ integrated system of carbon nanotubes nanocomposite membrane for oil sands process-affected water treatment. Journal of Membrane Science, **29**: 418-427.

Klamerth, N., Moreira, J., Li, C., Singh, A., McPhedran, K.N., Chelme-Ayala, P., Belosevic, M., and Gamal El-Din, M. 2015. Effect of ozonation on the naphthenic acids' speciation and toxicity of pH-dependent organic extracts of oil sands process-affected water. Science of the Total Environment, **506-507**: 66-75.

Kramer, F.C., Shang, R., Heijman, S.G.J., Scherrenberg, S.M., van Lier, J.B., and Rietveld, L.C. 2015. Direct water reclamation from sewage using ceramic ultra- and nanofiltration. Separation and Purification Technology, **147**: 329-336.

Laninovic, V. 2005. Relationship between type of nonsolvent additive and properties of polyethersulfone membranes. Desalination, **186**: 39-46.

Largitte, L. and Pasquier, R. 2016. A review of the kinetics adsorption models and their application to the adsorption of lead by an activated carbon. Chemical Engineering Research and Design, **109**: 495-504.

Le, N.L., and Nunes, S.P. 2016. Materials and membrane technologies for water and energy sustainability. Sustainable Materials and Technologies, **7**: 1-28.

Lee, S.Y., Kim, H.J., Patel, R., Im, S.J, Kim, J.H., and Min, B.R. 2007. Silver nanoparticles immobilized on thin film composite polyamide membrane: chacterization, nanofiltration, antifouling properties. Polymers for Advanced Technologies, **18**(7): 562-568.

Lewis, S.R., Datta, S., Gui, M., Coker, E.L., Huggins, F.E., Daunert, S., Bachas, L., and Bhattacharyya, D. 2011. Reactive nanostructured membranes for water purification. PNAS, **108**(21): 8577-8582.

Li, C., Fu, L., Stafford, J., Belosevic, M., and Gamal El-Din, M. 2017. The toxicity of oil sands process-affected water (OSPW): A critical review. Science of the Total Environment, **601-602**: 1785-1802.

Li, Q., Mahendra, S., Lyon, D.Y., Brunet, L., Liga, M.V., Li, D., and Alvarez, P.J.J. 2008. Antimicrobial nanomaterials for water disinfection and microbial control: Potential applications and implications. Water Research, **42**(18): 4591-4602.

Lind, M.L., Ghosh, A.K., Jawor, A., Huang, X., Hou, W., Yang, Y., and Hoek, E.M.V. 2009. Influence of zeolite crystal size on zeolite-polyamide thin film nanocomposite membranes. Langmuir, **25**(17): 10130-10145.

Loganathan, K., Chelme-Ayala, P., and Gamal El-Din, M. 2015. Pilot-scale study on the reverse osmosis treatment of oil sands tailings pond water: Impact of pretreatment on process performance. Desalination, **360**: 52-60.

MacKinnon, M.D., and Boerger, H. 1986. Description of two treatment methods for detoxifying oil sands process water. Water Pollution Research Journal of Canada, **21**: 496–512.

Mahata, N., Silva, A.R., Pereira, M.F.R., Freire, C., de Castro, B., and Figueiredo, J.L. 2007. Anchoring of a [Mn(*salen*)Cl] complex onto mesoporous carbon xerogels. Journal of Colloid and Interface Science, **311**: 152-158.

Mandaeni, S.S. 1999. The Application of Membrane Technology for Water Disinfection. Water Research, **33**(2): 301-308.

Masoudnia, K., Raisi, A., Aroujalian, A., and Fathizadeh, M. 2013. Treatment of Oily Wastewaters Using the Microfiltration Process: Effects of Operating Parameters and Membrane Fouling Study. Separation Science and Technology, **45**(10): 1544-1555.

Metcalf & Eddy, Inc. 2003. Wastewater Engineering Treatment and Reuse, 4th edition. McGraw-Hill, New York, NY.

Moreno-Castilla, C. 2004. Adsorption of organic molecules from aqueous solutions on carbon materials. Carbon, **42**: 83-94.

Moustafa, A., Kim, E.S., Alpatova, A., Sun, N., Smith, S., Kang, S., and Gamal El-Din, M. 2014. Imact of polymeric membrane filtration of oil sands process water on organic compounds quantification. Water Science & Technology, **70**: 771-779.

Mulder, M. 1997. Basic Principles of Membrane Technology. Kluwer Academic Publishers, Dordrecht, Netherlands.

Nahrstedt, A. and Carmago-Schmale, J. 2008. New insights into sild density index and modified fouling index measurements. Water Science & Technology: Water Supply, **8**: 401-411.

Nethaji, S., Sivasamy, A., and Mandal, A.B. 2013. Adsorption isotherms, kinetics and mechanism for the adsorption of cationic and anionic dyes onto carbonaceous particles prepared from *Junglans regia* shell biomass. International Journal of Environmental Science and Technology, **10**: 231-242.

Ng, L.Y., Mohammad, A.W., Leo, C.P., and Hilal, N. 2013. Polymeric membranes incorporated with metal/metal oxide nanoparticles: A comprehensive review. Desalination, **308**: 15-33.

Niasar, H.S., Li, H., Kasanneni, T.V.R., Ray, M.B., and Xu, C. 2016. Surface amination of activated carbon and petroleum coke for the removal of naphthenic acids and treatment of oil sands process-affected water (OSPW). Chemical Engineering Journal, **293**: 189-199.

Ohya, H., Kim, J., Chinen, A., Aihara, M., Semenova, S., Negishi, Y., Mori, O., and Yasuda, M. Effects of pore size on separation mechanisms of microfiltration of oily water using porous glass tubular membrane. Journal of Membrane Science, **145**: 1-14.

Parajulee, A. and Wania, F. 2014. Evaluating officially reported polycyclic aromatic hydrocarbon emissions in the Athabasca oil sands region with a multimedia fate model. Proceedings of the National Academy of Sciences, **111**(9): 3344-3349. doi: 10.7073/pnas.1319780111.

Peng, H., Volchek, K., MacKinnon, M., Wong, W.P., and Brown, C.E. 2004. Application of nanofiltration to water management options for oil sands operations. Desalination, **170**(2): 137-150.

Penner, T.J. and Foght, J.M. 2010. Mature fine tailings from oil sands processing harbour diverse methanogenic communities. Canadian Journal of Microbiology, **56**(6): 459-470.

Plazinski, W., Dziuba, J., and Rudzinski, W. 2013. Modeling of sorption kinetics: the pseudo-second order equation and the sorbate intraparticle diffusivity. Adsorption, **19**: 1055-1064.

Pourrezaei, P., Alpatova, A., Chelme-Ayala, P., Perez-Estrada, L.A., Jensen-Fontaine, M., Le, X.C., and Gamal El-Din, M. 2014a. Impact of petroleum coke characteristics on the adsorption of the organic fractions from oil sands process-affected water. International Journal of Environmental Science and Technology, **11**: 2037-2050.

Pourrezaei, P., Alpatova, A., Chelme-Ayala, Khosravi, K., Drzewicz, P., Chen, Y., Chelme-Ayala, P., and Gamal El-Din, M. 2014b. Removal of organic compounds and trace metals from oil sands process-affected water using zero valent iron enhanced by petroleum coke. Journal of Environmental Management, **139**: 50-58.

Pourrezaei, P., Drzewicz, P., Yingnan, W., Gamal El-Din, M., Perez-Estrada, L., Martin, J., Anderson, J., Wiseman, S., Liber, K., and Geisy, J. 2011. The Impact of Metallic Coagulant on the Removal of Organic Compounds from Oil Sands Process-Affected Water. Environmental Science and Technology, **45**: 8452-8459.

Pourrezaei, P. Wang, Y.; Perez-Estrada, L.; Martin, J.; and Gamal El-Din, M. 2012. Coagulation/flocculation/sedimentation treatment of oil sands process-affected water. *In* Annual Conference of the Canadian Socieity for Civil Engineering 2012: Leadership in Sustainable Infrastructure, Edmonton, Alberta 2012. CSCE 2012.

Qui, H., LV, L., Pan, B., Zhang, Q-j, Zhang, W-m, and Zhang, Q-x. 2009. Critical review in adsorption kinetic models. Journal of Zheijiang University SCIENCE A, **10**(5): 716-724.

Qui, S., Wu, L., Pan, X., Zhang, L., Chen, H., and Gao, C. 2009. Preparation and properties of functionalized carbon nanotube/PSF blend ultrafiltration membranes. Journal of Membrane Science, **342**: 165-172.

Quinlan, P.J., Grishkewich, N., Tam, K.C. 2017. Removal of 2-naphtheoxyacetic acid from aqueous solution using quaternized chitosan beads. The Canadian Journal of Chemical Engineering, **95**: 21-32.

Quinlan, P.J., Tam, K.C. 2015. Water treatment technologies for the remediation of naphthenic acids in oil sands process-affected water. Chemical Engineering Journal, **279**: 696-714.

Richards, H.L., Baker, P., and Iwuoha, E. 2012, Metal nanoparticle modifie polysulfone membranes for use in wastewater treatment: a critical review. Journal of Surface Engineered Materials and Advanced Technology, **2**: 183-193.

Rogers, V.V., Liber, K., and MacKinnon, M. 2002. Isolation and characterization of naphthenic acids from Athabasca oil sands tailing pond water. Chemosphere, **48**: 519-527.

Sabde, A., Trivedi, M., Ramachandhran, V., Hanra, M., and Misra, B. 1997. Casting and characterization of cellulose acetate butyrate based UF membranes. Desalination, **1997**: 223-232.

Sawyer, C.N., McCarty, P.L., and Parkin, G.F. 2003. Chemistry for Environmental Engineering and Science, 5th Edition. McGraw-Hill, New York, N.Y.

Shi, F., Ma, Y., Ma, J., Wang, P., and Sun, W. 2012. Preparation and characterization of PVDF/TiO_2 hybrid membranes with different dosage of nano-TiO_2. Journal of Membrane Science, **389**: 522-531.

Shrestha, N., Chilkoor, G., Wilder, J., Gadhamshetty, V., and Stone, J. 2017. Potential water resource impacts of hydraulic fracturing from unconventional oil production in the Bakken shale. Water Research, **108**: 1-24.

Shu, Z., Li, C., Belosevic, M., Bolton, J.R., and Gamal El-Din, M. 2014. Application of a solar UV/cholorine advanced oxidation process to oil sands process-affected water remediation. Environmental Science and Technology, **48**: 9692-9701.

Small, C., Hashisho, Z., and Ulrich, A.C. 2012. Preparation and characterization of activated carbon from oil sands coke. Fuel, **92**: 69-76.

Sun, N. Chelme-Ayala, P., Klamerth, N., McPhedran, K., Islam, M.S., Perez-Estrada, L., Drzewicz, P., Blunt, B., Reichert, M., Hagen, M., Tierney, K., Belosevic, M., and Gamal El-Din, M. 2014. Advanced Analytical Mass Spectrometric Techniques and Bioassays to Characterize Untreated and Ozonated Oil Sands Process-Affected Water. Environmental Science and Technology, **48**: 11090-11099.

Taylor, J.S., and Wiesner, M. 1999. Membranes. *In* Water Quality and Treatment: A Handbook of Community Water Supplies. *Edited by* R.D. Letterman. McGraw-Hill, New York, N.Y. pp. 11.1-11.71.

Vantanpour, S., Madaeni, S., Morandian, R., Zinadini, S., and Astinchap, B. 2011. Fabrication and characterization of novel antifouling nanofiltration membrane prepared from oxidized multiwalled carbon nanotube/polyethersulfone nanocomposite. Journal of Membrane Science, **375**: 284-294.

Villacanas, F., Pereira, M.F.R., Orfao, J.J.M., and Figueiredo, J.L. 2006. Adsorption of simple aromatic compounds on activated carbons. Journal of Colloid and Interface Science, **293**: 128-136.

Wang, C., Klamerth, N., Huang, R., Elnakar, H., and Gamal El-Din, M. 2016a. Oxidation of oil sands process-affected water by potassium ferrate (VI). Environmental Science and Technology, **50** (8): 4238-4247.

Wang, C., Klamerth, N., Messele, S.A., Singh, A., Belosevic, M., and Gamal El-Din, M. 2016b. Comparison of UV/hydrogen peroxide, potassium ferrate (VI), and ozone in oxidizing the organic fraction of oil sands process-affected water (OSPW). Water Research, **100**: 476-485.

Wang, L., Zhang, J., Zhao, R., Li, C., Li, Y., and Zhang, C. 2010. Adsorption of basic dyes on activated carbon prepared from *Polygonum orientale* Linn: Equilibrium, kinetic and thermodynamic studies. Desalination, **254**: 68-74.

Wang, W., Wang, J., Guo, Y., Zhu, C., Pan, F., Wu, R., and Wang, C. 2018. Removal of multiple nitrosamines from aqueous solution by nanoscale zero-valent iron supported on granular activated carbon: Influencing factors and reaction mechanism. Science of the Total Environment, **639**: 934-943.

Watson, J.S., Jones, D.M., Swannell, R.P.J., and van Duin, A.C.T. 2002. Formation of carboxylic acids during aerobic biodegradation of crude oil and evidence of microbial oxidation of hopanes. Organic Geochemistry, **33**: 1153-1169.

Wei, C.H., Laborie, S., Aim, R.B., and Amy, G. 2012. Full utilization of silt density index (SDI) measurements for seawater pre-treatment. Journal of Membrane Science, **405-406**: 212-218.

Wu, H., Tang, B., and Wu, P. 2013. Optimization, characterization, and nanofiltration properties test of MWNTs/polyester thin film nanocomposite membrane. Journal of Membrane Science, **428**: 425-433.

Wu, Z., and Zhao, D. 2011. Ordered mesoporous materials as adsorbents. Chemical Communications, **47**: 3332-3338.

Xing, W., Ngo, H.H., Kim, S.H., Guo, W.S., and Hagare, P. 2008. Adsorption and bioadsorption of granular activated carbon (GAC) for dissolved organic carbon (DOC) removal in wastewater. Bioresource Technology, **99**: 8674-8678.

Yang, Y., Zhang, H., Wang, P., Zheng, Q., and Li, J. 2007. The influence of nano-sized TiO_2 fillers on the morphologies and properties of PSU UF membranes. Journal of Membrane Science, **288**(1-2): 231-238.

You, S.J., Semblante, G.U., Lu, S.C., Damodar, R.A., and Wei, T.C. 2012. Evaluation of the antifouling and photocatalytic properties of poly(vinylidene fluoride) plasma-grafted poly(acrylic acid) membrane with self-assembled TiO_2. Journal of Hazardous Materials, **237-238**: 10-19.

Young, R.F., Wismer, W.V. and Fedorak, P.M. 2008. Estimating naphthenic acids concentrations in laboratory-exposed fish and in fish from the wild. Chemosphere **73**(4), 498-505.

Young, T.H., and Chen W. 1995. Pore formation mechanisms of membranes from phase inversion process. Desalination, **103**: 233-247.

Yuan, Y., and Lee, T.R. 2013. Contact angle and wetting properties. *In* Springer Series in Surface Science Techniques. *Edited by* G. Bracco and B. Holst. Heidelberg, Springer, pp. 3-34.

Zaidi, A., Simms, K., and Kok, S. 1992. The use of micro/ultrafiltration for the removal of oil and suspended solids from oilfield brines. Water Science & Technology, **25**(10): 163-176.

Zhang, Y., Xue, J., Liu, Y. and El-Din, M.G. 2016. Treatment of oil sands process-affected water using membrane bioreactor coupled with ozonation: A comparative study. Chemical Engineering Journal, **302**: 485-497.

Zhou, J., Wandera, D., and Husson, S. 2015. Mechanisms and control of fouling during ultrafiltration of high strength wastewater without pretreatment. Journal of Membrane Science, **488**: 103-110.

Zhu, S., Li, M., and Gamal El-Din, M. 2017. Forward osmosis as an approach to manage oil sands tailings water and on-site basal depressurization water. Journal of Hazardous Materials, **327**: 18-27.

Zhu, X., Loo, H.E., and Bai, R. 2013. A novel membrane showing both hydrophylic and oleophobic surface properties and its non-fouling performances for potential water treatment applications. Journal of Membrane Science, **436**: 47-56.

Zodrow, K., Brunet, L., Mahendra, S., Li, D., Zhang, A., Li, Q., and Alvarez, P.J.J. 2009. Polysulfone ultrafiltration membranes impregnated with silver nanoparticles show improved biofouling resistance and virus removal. Water Research, **43**(3): 715-723.

Zubot, W., MacKinnon, M.D., Chelme-Ayala, P., Smith, D.W., and Gamal El-Din, M. 2012. Petroleum coke adsorption as a water management option for oil sands process-affected water. Science of the Total Environment, **427-428**: 364-372.

Appendix: Supporting Information

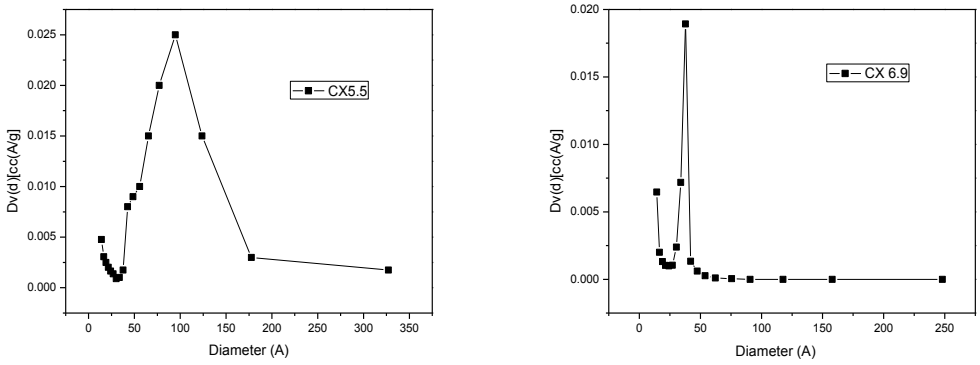

(a) (b)

Figure S1 Pore size distribution for carbon xerogel samples: (a) CX5.5 and (b) CX6.9.

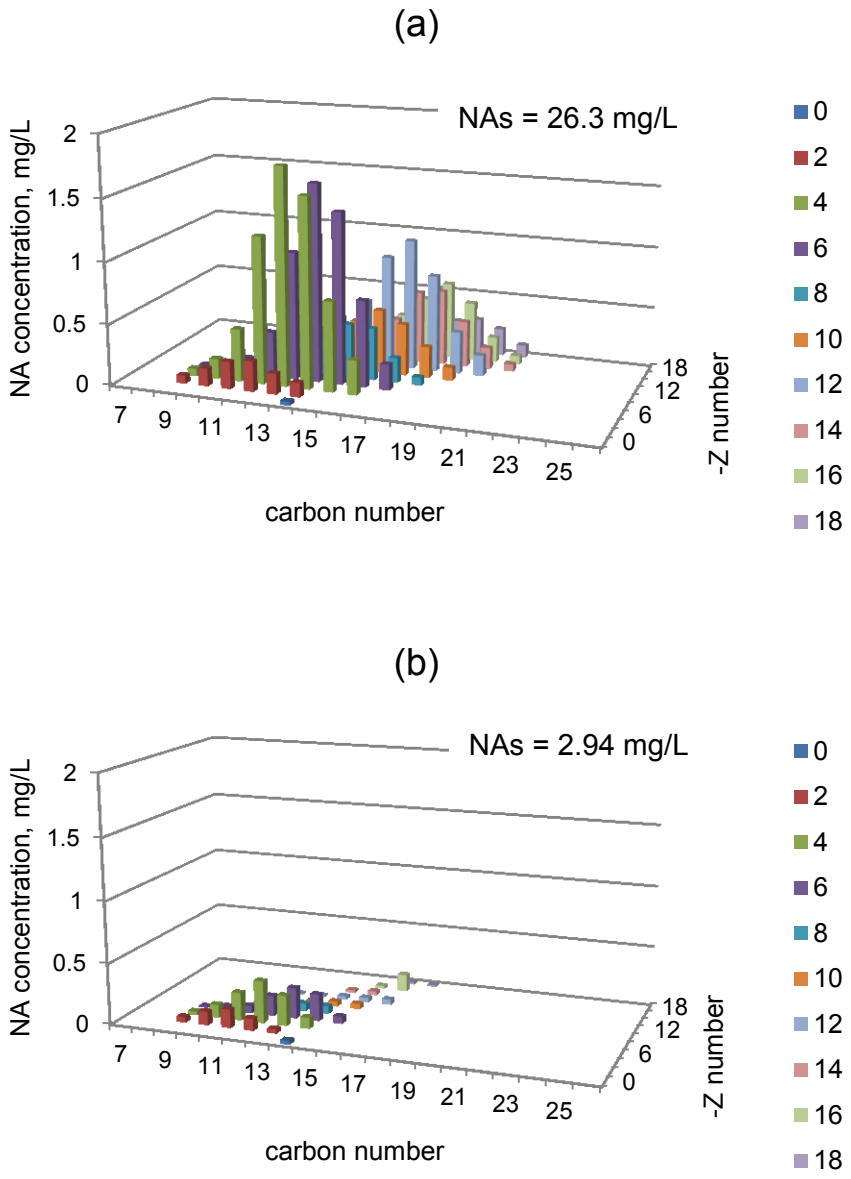

Figure S2 Classical NAs concentration profiles as determined using a high resolution TOF-MS with electrospray in negative mode of (a) raw OSPW and (b) OSPW after adsorption with a 3 g/L dose of Cx5.5 for 24 hours.

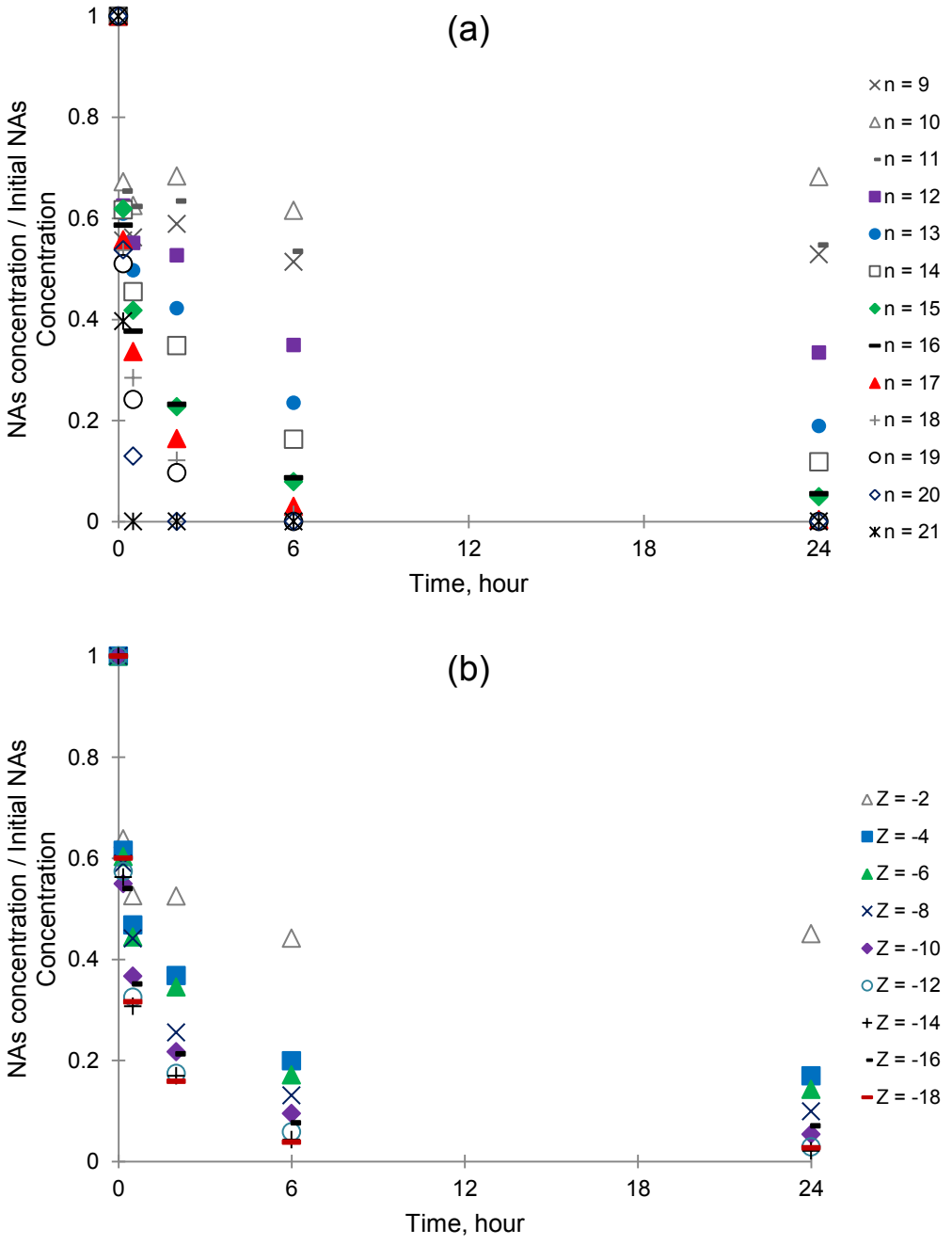

Figure S3 Normalized classical NAs concentration profiles in OSPW subjected to adsorption with 3 g/L of CX5.5 for various time partitioned by (a) different carbon numbers, n, and (b) different -Z numbers .

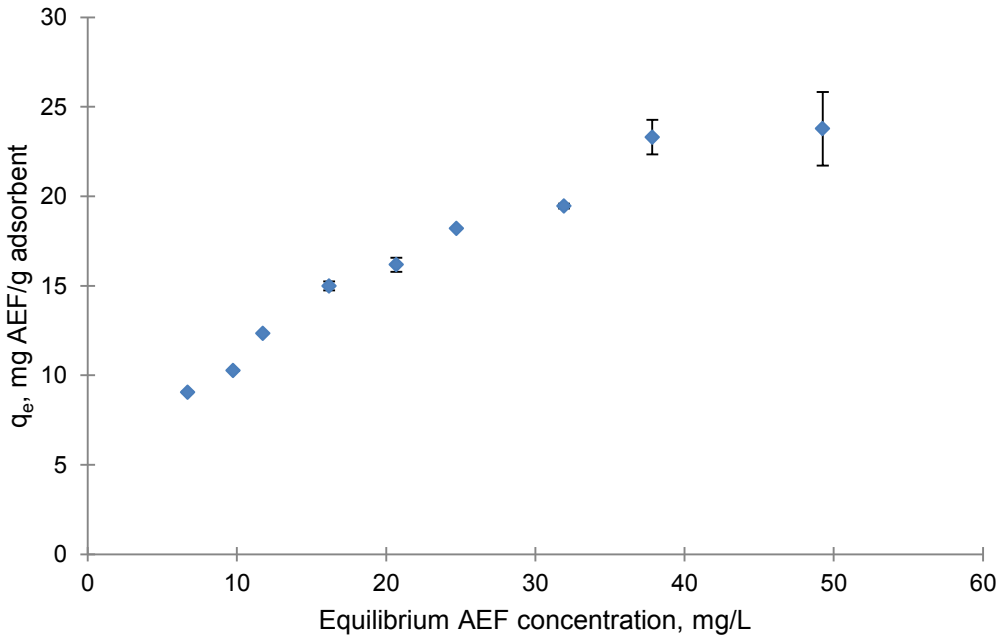

Figure S4 Equilibrium adsorption capacities for CX5.5 as a function of AEF equilibrium concentration in OSPW for adsorbent load from 6 g/L to 0.5 g/L.

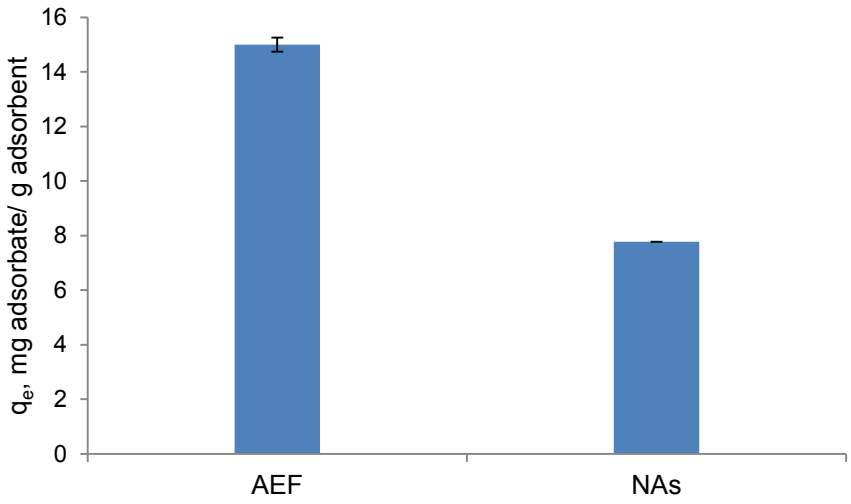

Figure S5 Equilibrium adsorption capacities for AEF and classical NAs by CX5.5 (3 g/L dose) used to treat OSPW (initial concentration of 61.2 mg AEF/L or 26.3 mg NAs/L) for 24 hours obtained by FT-IR AEF concentration data and by overall MS-TOF classical NAs concentration data.

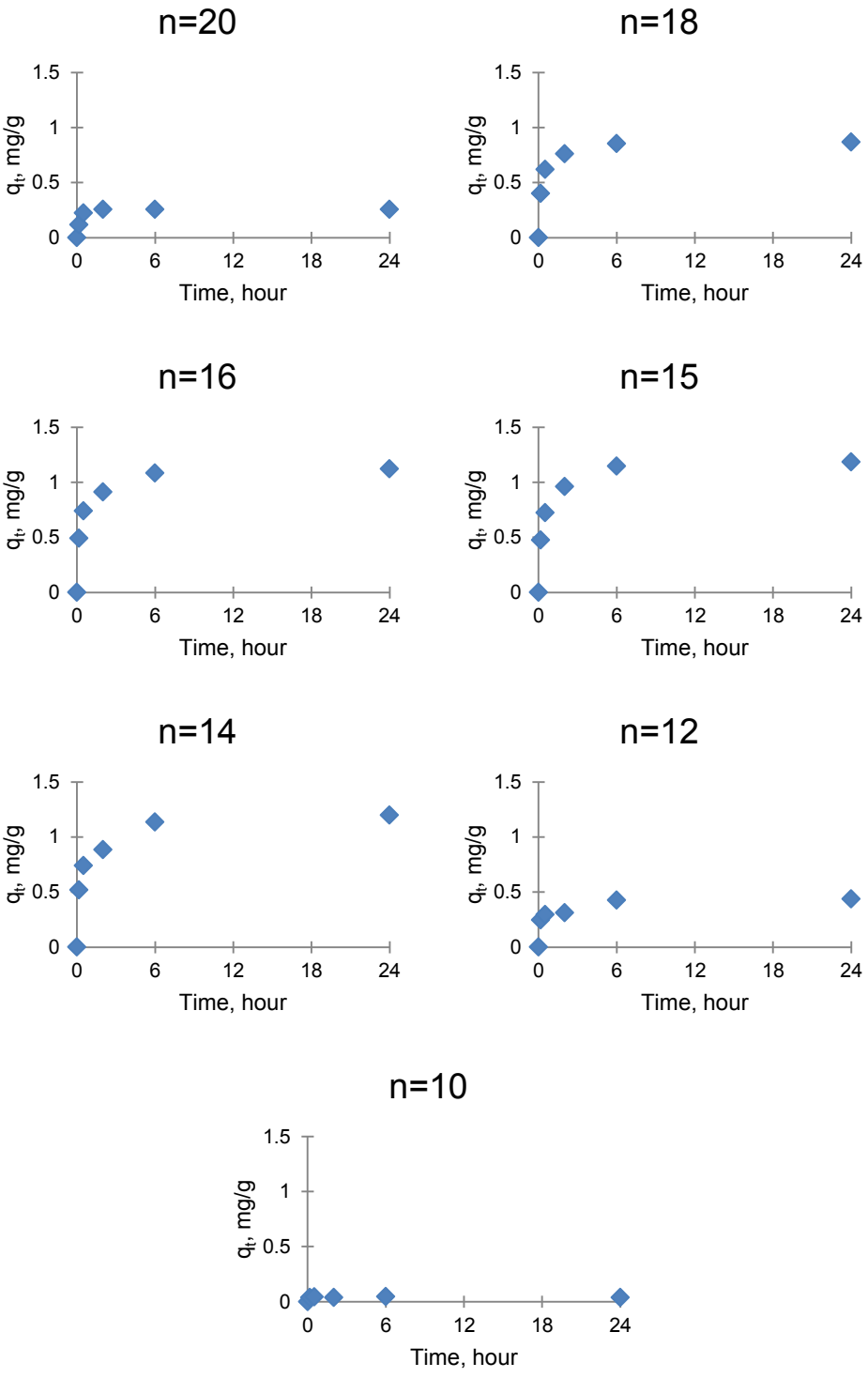

Figure S6 Classical NAs adsorbed onto CX5.5 (qt) as a function of time and carbon number for 3 g/L dose of CX5.5.

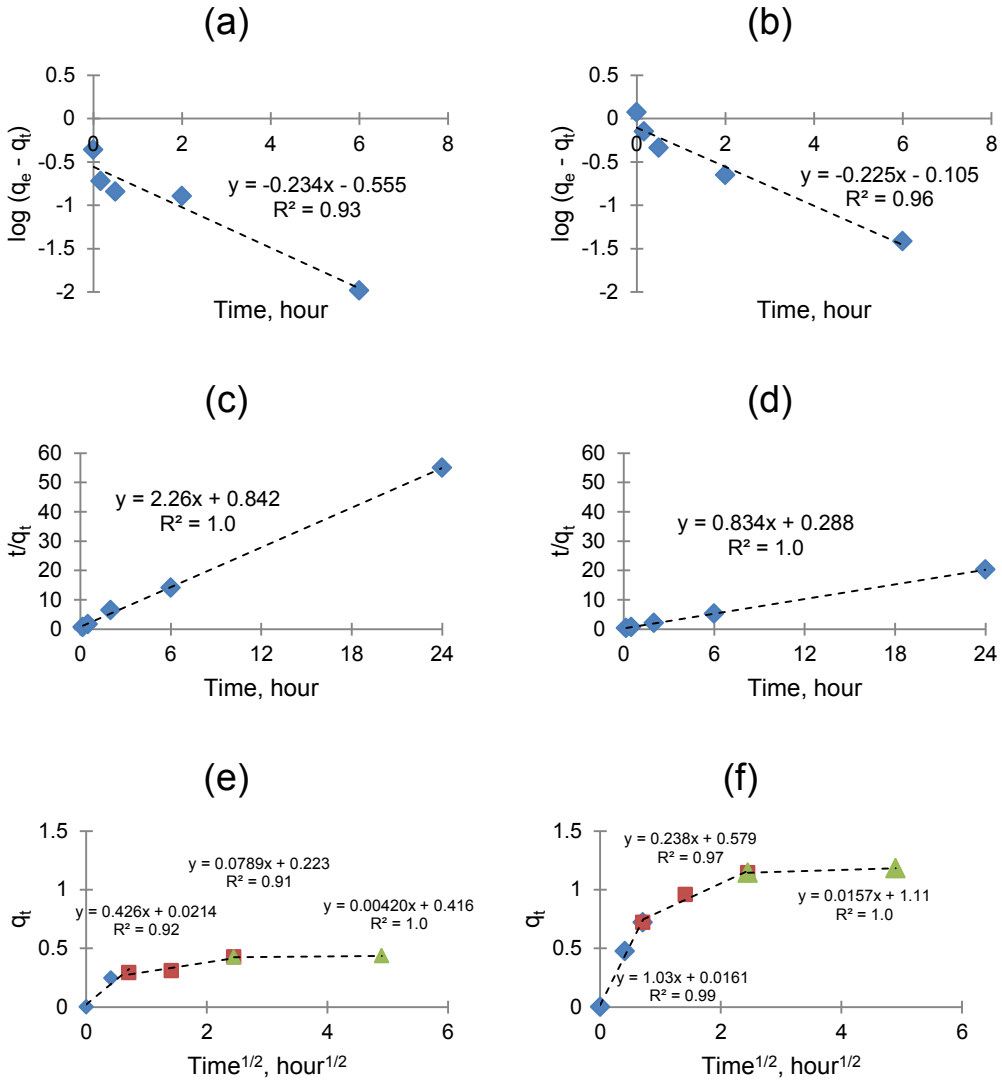

Figure S7 Kinetics and diffusion modeling for the adsorption of NAs onto Cx5.5 at a dose of 3 g/L for various adsorption times for carbon # 12 and 15. Pseudo-first order kinetic model for carbon # (a) 12 and (b) 15. Pseudo-second order kinetic model for carbon # (c) 12 and (d) 15. Intraparticle diffusion model for carbon # (e) 12 and (f) 15.

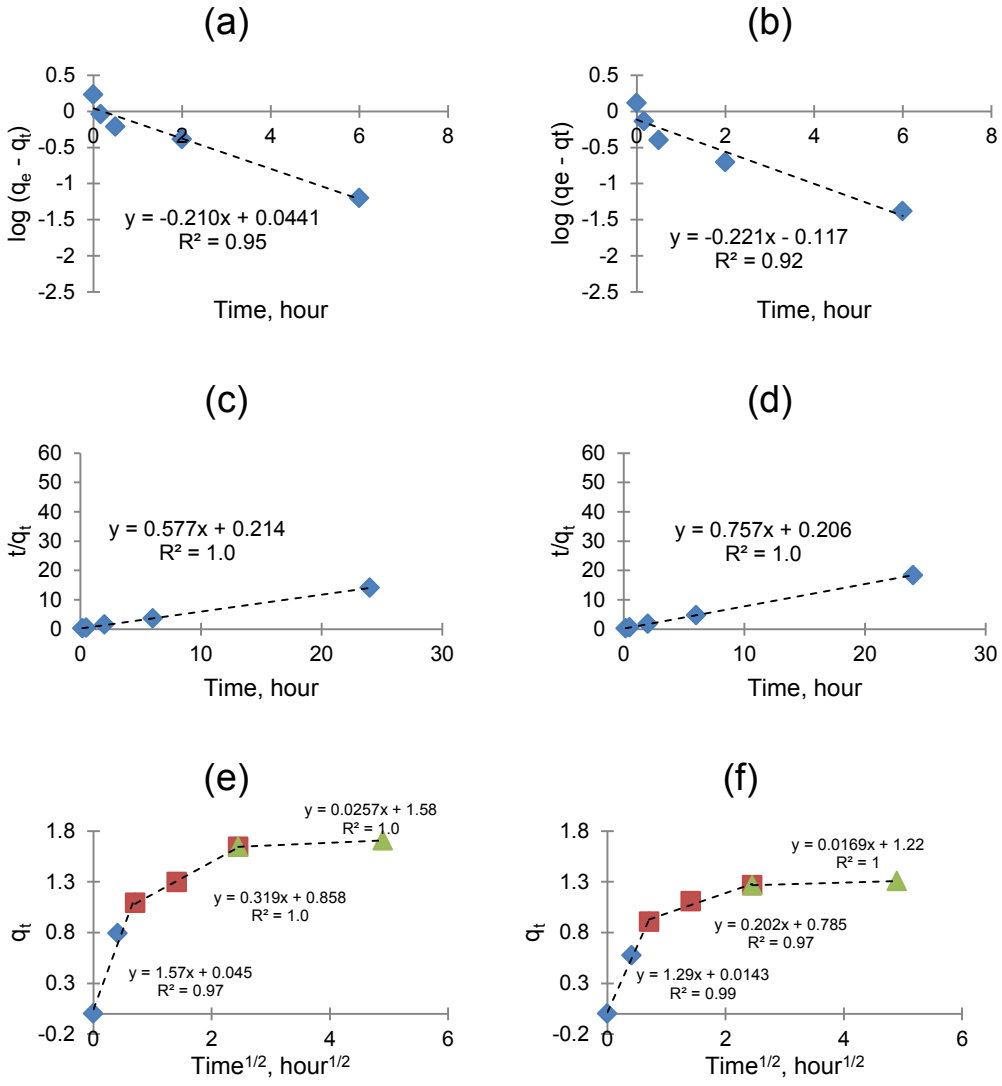

Figure S8 Kinetics and diffusion modeling for the adsorption of NAs onto Cx5.5 at a dose of 3 g/L for various adsorption times for Z # 4 and 12. Pseudo-first order kinetic model for –Z of (a) 4 and (b) 12. Pseudo-second order kinetic model for –Z of (c) 4 and (d) 12. Intraparticle diffusion model for –Z of (e) 4 and (f) 12.